7-6-2021

Studying Complex Aquifer Systems from Large-Scale Stratigraphy Development to Local Aquifer Storage and Recovery

Hamid Vahdat Aboueshagh
Louisiana State University

STUDYING COMPLEX AQUIFER SYSTEMS FROM LARGE-SCALE STRATIGRAPHY DEVELOPMENT TO LOCAL AQUIFER STORAGE AND RECOVERY

A Dissertation

Submitted to the Graduate Faculty of the
Louisiana State University and
Agricultural and Mechanical College
in partial fulfillment of the
requirements for the degree of
Doctor of Philosophy

in

The Department of Civil and Environmental Engineering

by
Hamid Vahdat-Aboueshagh
B.S., University of Tabriz, 2010
M.S., University of Tehran, 2013
August 2021

Table of Contents

List of Tables

List of Figures

Abstract

Hydrostratigraphy model is an essential component of building valid groundwater models. Many challenges are associated with constructing hydrostratigraphy models which include geological complexities such as faults, domes, and angular unconformities. Developing a method with an emphasis on capturing big data to thoroughly inform large-scale models is one of the challenges addressed in the first part of this study. The method is predicated upon discretization of the study domain into tiles based on the geological dip direction and faults. The application of the method in the state of Louisiana with the utilization of more than 114000 well logs demonstrates promising results including identification of hydrostratigraphic characteristics for different aquifers, connections between the Mississippi River and the Red River and their alluviums, connections between state's surface waters and aquifers, and identification of recharge zones. The Louisiana model also demonstrated two different sand patterns in southeast Louisiana which might have been caused by two depositional environments. Employment of the method in a groundwater flow modeling framework to build a flow model for the Chicot aquifer system in southwest Louisiana revealed the complexity of the aquifer system that contains highly interconnected aquifer sands. The groundwater flow analysis of the Chicot aquifer is of great importance because it is the most heavily pumped aquifer in the state as a part of the Coastal Lowland Aquifer System. The modeling results show that the storage loss due to groundwater pumping is offset by inflows from surficial recharge, rivers, and boundaries. The two large cones of depression created by the agricultural pumping in the east and by the industrial pumping in the west represent the key feature in the Chicot aquifer system. As the final goal of this study, an aquifer storage and recovery operation in south of the Chicot aquifer was studied. The focus of this part was on optimal scheduling of an aquifer storage and recovery (ASR) operation while

addressing parameter uncertainty for one cycle where an injection season is followed by a pumping season. This end was achieved via utilization of a supervised learning method for surrogated modeling and use of an evolutionary optimization method. The results indicate that artificial neural network (ANN) is a promising tool for evaluation of ASR efficiency. The hydraulic conductivity and longitudinal dispersivity were found to be the most significant parameters which affect ASR.

Chapter 1. Introduction

1.1. Importance and scope of study

The groundwater resources are not abundant and yet threatened by human activities. The coastal aquifers are notable when it comes to study groundwater systems. Groundwater level decline and consequent saltwater intrusion into majority of aquifers along the U.S. contiguous coastline are becoming more concerning (Jasechko et al.; 2020). Hence, rigorous study of coastal groundwater systems and effective management of them are of paramount importance. The study of groundwater systems in not possible without the aid of a robust hydrostratigraphy model. Construction of a valid hydrostratigraphy model in large scales is a formidable challenge and has not been practiced so often in the past. Incorporation of big dataset into large-scale hydrostratigraphy model needs to be considered in order to capture geological complexities. In addition, integration of geological data with hydrogeological data is inevitable when it comes to groundwater flow model development. Finally, exploitation of computational resources may be a concern when constructing such models. Therefore, the developed methodological framework must take into the account all of aforementioned considerations.

As a coastal state, the state of Louisiana is not an exception to coastal aquifer studies. Although the state has the advantage of having access to aquifers with high portion of sand thank to historical depositional processes of the Mississippi River, the freshwater aquifers along its coastal line suffer from heavy pumping activities. The Chicot aquifer system in southwest Louisiana as a precious source of groundwater is the most heavily pumped aquifer in the state and supplies water mostly for agriculture sector. Overdrafting groundwater for growing rice in the eastern part of the aquifer domain and industrial overuse of groundwater in the Lake Charles area in west have lowered groundwater levels which reportedly have created cones of depression in

different sands of the aquifer system (Fendick and Nyman, 1987; Lovelace et al., 2004). Although recharged mostly by precipitation water in north of the aquifer domain, the Chicot aquifer may still be threatened by unbalanced groundwater flow in their sands. To further combating saltwater intrusion in the coastal area and better use the groundwater resources, aquifer storage and recovery (ASR) may be practiced as an additional solution. The extent of the ASR project is limited and normally applies to local scale aquifers.

1.2. Research questions

This dissertation attempts to address the following technical and scientific questions:

- Is it possible to integrate a set of well log data and geological knowledge, such as dip directions, dip angles, and fault traces, into a methodology in order to construct a geologically-sound hydrostratigraphic architecture?
- How does such an architecture help better understand the hydrostratigraphic characteristics of an area under study?
- How can the developed methodology be brought into groundwater flow modeling to identify complex aquifer characteristics?

The following specific questions are also addressed to a certain extent:

- What is the groundwater flow dynamics in the Chicot aquifer system, Southwest Louisiana?
- Must different sand units in the Chicot aquifer system be considered as significant components in the groundwater storge analysis for better understating of the aquifer system or the budget analysis of the Chicot aquifer system as a single unit would be sufficient?
- Is “the water budget myth” true for the Chicot aquifer? In other words, is the natural recharge merely balanced by pumping activities or there must be more components to the

analysis of the groundwater budget in the subject of sustainable development for the Chicot aquifer system?

- Can we speculate about saltwater intrusion into the Chicot aquifer system from underneath saline aquifers and the Gulf of Mexico?
- How may supervised learning techniques and optimization algorithms be incorporated into an ASR operation scheduling problem to address uncertainty and to be an efficient substitute for traditional simulation-optimization approaches?

1.3. Objectives

Based on the scope discussed in the previous section, the following objectives are defined for this study:

The first objective of the present dissertation is to develop a methodology to construct hydrostratigraphy model for large-scale domains. The emphasis of the methodology is on groundwater resources. The developed methodology must have three important characteristics of being applicable to complex geological structures, computationally effective, and easy to use for the sake of reproducibility. The simple yet very effective solution to these problems utilized in this study was tessellation of the study domain based on geological features. The tessellated areas are named tiles. In addition to horizontal tessellation into tiles, each tile may also be split in vertical direction to address the complexity of the angular unconformity between alluvial formations and steeper formations. The method also allows for grid refinements wherever necessary for obtaining higher accuracy. The grid-based modeling approach of this method also allows for extraction of results and interpretation of results for a desired hydrogeological feature such as an aquifer. The parallelization of the modeling process based on the horizontal tessellation was achieved which saved a lot of computational effort. Due to its simplicity, the methodology is straightforwardly

applicable to other study areas and geological configurations. In order to validate the method, the state of Louisiana was picked as a study domain. More than 114000 well log data, including electric logs, drillers logs, and groundwater screens, were collected, digitized, and processed. The geological complexities addressed in the hydrostratigraphy model for the state of Louisiana were faults, geological domes, and angular conformities. The computational source for the statewide model was the High Performance Computing (HPC) center at the Louisiana State University. The outputs of this study were promising and helped better fathom the geological and hydrostragraphic characteristics of the study domain. A prospective goal for future studies will be developing a statewide groundwater model.

The second objective of this work is to develop groundwater flow model for complex aquifer system using the proposed method for hyrostratigraphy modeling. Integration of geological data and hydrological data into an aquifer model is not a common practice and normally avoided due to complexity and high dimensionality of the problem. The compilation of well log data into binary data was accomplished through a word recognition technique. The hydrogeological data including observation data, recharge data, pumping data, and relevant parameters were acquired from different sources. The calibration of the groundwater flow model was another challenging issue which was accomplished through adaptation of the Covariance Matrix Adaptation Evolutionary Strategy (CMA-ES) (Hansen et al., 2003). The application of the framework to the Chicot aquifer in southwest Louisiana and subsequent interpretation of the results helped better understand the dynamics in the aquifer system. The possibility of saltwater intrusion into different sands of the aquifer system is investigated. The pumping patterns and how they affect the groundwater levels as well as the existence of cone of depressions are also assessed. The developed framework to study the Chicot aquifer system may lay a foundation for future groundwater related

studies in the region and may also serve as a tool for constructing any other complicated aquifer system.

The final objective of this study is to schedule an ASR operation and addresses multiple issues regarding optimal solution and uncertainty stemmed from lack of knowledge on parameters. The optimal schedule obtained for the ASR operation includes one ASR cycle. That is one injection season, which could be a wet season, is followed by a pumping season, which could be a dry season. The objectives of the study are to maximize the amount of injected water (injectate) into the aquifer during the injection season and to maximize the ASR efficiency that involves both injection season and pumping season. In each season the operation of injection or pumping may be halted in certain stress periods. This converts the optimization problem into a mixed integer nonlinear programming (MINLP) which requires a special formulation for the optimization problem and a suitable solver. To address the uncertainty issue, many model runs are demanded due to specifics of the Monte Carlo approach employed in this study. Therefore, a solution is needed to alleviate the computational cost and yet not to sacrifice the accuracy of the models. A surrogate modeling approach with the aid of a supervised learning method was adopted to build predictors for groundwater levels and concentration of freshwater injected into the aquifer. The supervised learning method utilizes artificial neural network models as means to replace high fidelity groundwater models and solute transport models. The computational time saved owing to utilization of such an approach is very significant and accuracy of the developed model is completely acceptable as reported in the literature.

1.4. Organization

The present dissertation is organized in five chapters. The studies conducted in Chapter 2, Chapter 3, and Chapter 4 rank in order of the study area scale, from a largest to smallest scale.

Chapter 1 is an introductory chapter explaining the scopes of different studies in Chapter 2 to Chapter 5. Chapter 2 elaborates on the methodology of constructing large-scale hydrostratigraphy models which may also be employed to develop small scale models. The framework presented in Chapter 3 utilizes the method in Chapter 2 to develop a groundwater model for a regional aquifer system which has geological complexities. The methods for building a complex aquifer system is used to study an ASR operation in a local scale in Chapter 4. Chapter 5 includes concluding remarks out of this study and feature study research topics.

Chapter 2. Constructing Large-Scale Complex Aquifer Systems with Big Well Log Data: Louisiana Model

2.1. Introduction

Modeling geological stratigraphy over large-scale domains becomes achievable owing to large data storage and high computing power, especially for applications in the field of hydrogeology (D'Agnese et al., 1999; Döll et al., 2014) with either simplified or conceptual models (de Graaf et al., 2015; Goderniaux et al., 2009; Maxwell et al., 2015; Sutanudjaja et al., 2011). There has been an increased uptake of 3D mapping and modelling methods at geological survey organizations (GSOs). MacCormack et al. (2019) highlights the recent successes, accomplishments, and challenges experienced by GSOs in the development and deployment of their 3D modelling programs. Stratigraphy models play an important role in understanding geological formations for groundwater studies, sustainable resource development, environmental protection, and public safety.

Various methods were developed to model stratigraphy. Conceptual methods such as sequence stratigraphy (Haq, 1991; Posamentier and James, 1993; Posamentier and Allen, 1993; Yoshida et al., 2007; Catuneanu et al., 2011; Catuneanu, 2019) identify chronostratigraphic surfaces based on spatial patterns of depositions within the geological timeline of sedimentary processes. Geostatistics-based methods provide detailed facies variation, including occurrence probability (Dowd, 1991; Chilès and Delfiner, 2009; Wackernagel, 2013). Among various geostatistical approaches are multi-point simulation (Strebelle, 2002; Liu et al., 2004; Hu and Chugunova, 2008), transition probability simulation (Journel and Alabert, 1989; Weissmann et al., 1999; Lee et al., 2007; He et al., 2014), and two-point variogram methods (Johnson and Dreiss,

This chapter was previously published as Vahdat-Aboueshagh, H. and Tsai, F.T.-C., 2021. Constructing large-scale complex aquifer systems with big well log data: Louisiana model. Computers & Geosciences, 148, p.104687. https://doi.org/10.1016/j.cageo.2021.104687. Reprinted by permission of Elsevier.

1989; Johnson, 1995). The geostatistical methods are robust at integrating different sources of information; however, they are very sensitive to input datasets and can be computationally exhaustive for large-scale modeling with abundant data. The conceptual models in large scales can be combined with geostatistical methods in finer scales to create a detailed stratigraphy for a large domain. Another class of stratigraphy modeling methods is the horizon method (Lemon and Jones, 2003; Wu et al., 2005; Caumon et al., 2009; Gallerini and De Donatis, 2009; Touch et al., 2014) which interpolates upper and lower limits of stratigraphic units using lithologic bed data at borehole locations and cross sections. The simplicity and computational efficiency in dealing with abundant data make the horizon method a suitable approach for large-scale facies modeling.

In developing stratigraphy models, collecting data and processing data are very challenging (Chang and Park, 2004). A big volume of data introduces a computational burden as well as complexity (Katal et al., 2013; Sivarajah et al., 2017). Lithological data may be integrated from different sources such as lithologic logs and electric logs. Cognitive geological knowledge may be also used to inform the model (Royse, 2010). Various types of well log information, distribution and density of well logs in a study domain, and frequent variation of lithofacies in boreholes add to the complexity of lithofacies modeling (Wycisk et al., 2009; Chesnaux et al., 2011; Zhu et al., 2012; Jørgensen et al., 2015; Song et al., 2020). Unifying different sources of well log data into the same classes is the key mechanism to deal with big data complexity. In this study the term "big well log data" refers to a large volume of well log dataset.

This study introduces a lithofacies modeling method utilizing lithologic information in a big well log dataset to build a large-scale complex lithofacies model. The modeling processes include tessellation, discretization, translation, and interpolation to cope with geological complexities such as structural dips, domal uplifts, angular unconformities, and faults. The

lithofacies modeling method is demonstrated through the development of a Louisiana lithofacies model. This study does not intend to find correlation among well logs. Instead, the correlation and stratigraphic units in Louisiana have been established by the USGS studies (Hosman 1996; Weiss 1990) that determine the dip directions and dip angles. These stratigraphic units are coarse. This study introduces the proposed method and a vast amount of well logs to construct detailed sand-clay facies structures along the dip directions and dip angles. The modeling processes working together with big well log data present an appealing approach.

2.2. Methodology

2.2.1. Well logs

Well logs are the key source of data in understanding the dipping geological structure. Well logs include drillers' logs, geotechnical borings, and wireline electric logs. Geotechnical borings have high-quality lithologic descriptions using the Unified Soil Classification System (ASTM, 2017), but are usually shallow (less than 10 m). Electric logs provide more accurate bed boundaries for lithofacies (Hilchie, 1982) compared to other types of well logs. However, electric logs are usually not abundant and often miss information for top 30 m to 40 m due to the well casing. Drillers' logs are produced by drillers during drilling. Lithologic descriptions in drillers' logs are sometimes ambiguous or unrecognizable. Drillers' logs with unrecognizable lithological descriptions shall be discarded.

2.2.2. Model domain tessellation and discretization

In order to cope with changes in structural dip direction (e.g., domes) and discontinuity (e.g., faults), this study tessellates the model domain into a collection of tiles. Geological formations in each tile are assumed to have the same dip direction, but dip angle can vary in depth.

Different tiles may have different dip directions. Therefore, a region of changing strikes is made of many tiles. A tile is further discretized into a number of computational cells in order to build a lithofacies model. The size of computational cells depends on the desired accuracy. For example, areas surrounding fault traces may be given finer discretization in order to capture the discontinuity at faults.

The proposed method uses lithological data, well location, dip direction, and slopes of the upper and lower inclined planes in geological formations as input data to generate lithofacies for computational cells. Consider a dipping geological structure for a tile shown in Figure 2.1. The dip direction α is the same within a tile, which results in a constant strike. The slope represents the tangent value of a dip angle. This study assumes linear slope increase from slope s_1 to slope s_2. In the plan view (Figure 2.1.a), the tile is discretized into a number of computational cells. A pivot point (x_P, y_P) is at the southwest corner of the tile, where a pivot strike passes. The pivot strike is perpendicular to the dip direction. The pivot strike divides the tile into an updip domain and a downdip domain. A pivot plane is a vertical plane passing the pivot strike.

Given a vertical well location Q in the tile, a fold line AA′ passes Q and intersects the pivot strike at location B. The cross-sectional view of the fold line is shown in Figure 2.1.b. At location B, the slope at elevation z_1 is s_1 and at elevation z_2 is s_2. The inclined plane E_1 passes elevation z_1 with slope s_1 and the inclined plane E_2 passes elevation z_2 with slope s_2. Elevations above the plane E_1 have the same slope as s_1. Elevations below the plane E_2 have the same slope as s_2. Plane E_1 and plane E_2 intercept at the line O. The inclined plane E between the plane E_1 and the plane E_2 passes elevation z_Q at the vertical well location Q and elevation $z_{Q'}$ at the location B or the pivot plane. Elevations z_1, z_2 and, $z_{Q'}$ are vertically beneath the location B. In what follows, the key parameters s_1, s_2, z_1 and z_2 are used to determine a dipping stratigraphy.

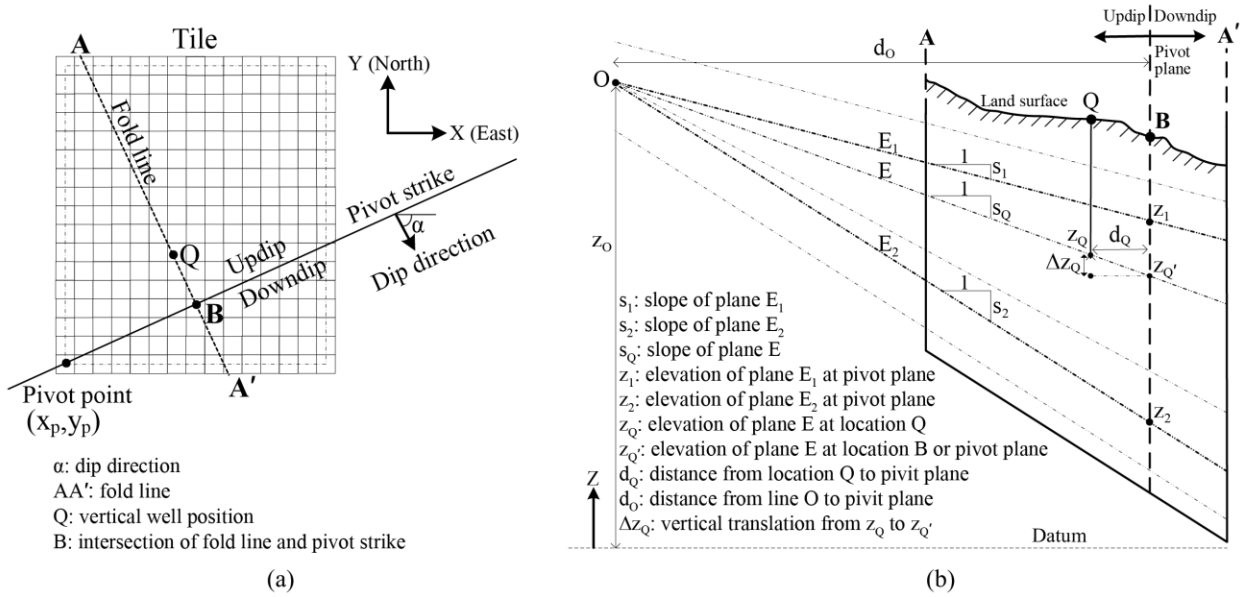

Figure 2.1. (a) The plan view of a discretized tile, and (b) the cross-sectional view of the fold line AA′.

2.2.3. Domain transformation: From dipping domain to non-dipping domain

Using well logs to directly construct a stratigraphy of varying slopes of dips in a dipping domain can be difficult. Instead, translating all well log data into a non-dipping domain and performing lithofacies modeling in horizontal planes is much easier than directly interpolating lithofacies modeling in the dipping domain. A similar concept was suggested by Mallet (2004, 2014), which transforms horizons from a curvilinear system to a rectilinear system. Lithofacies modeling is performed in the rectilinear system. The domain transformation in this study is made simpler than Mallet (2004) by tessellating a non-linear domain (changing dip direction and slope) into a number of semi-linear domains (tiles) with constant dip direction, but varying slope in each tile. For each tile, well log data are translated from a dipping domain to a non-dipping domain, and then are interpolated to computational cells on horizontal planes. The resulting lithofacies distribution is then back-translated to the dipping domain.

To translate well log data at location Q to a non-dipping domain, the vertical translation for elevation z_Q (Figure 2.1.b) is calculated based on the horizontal distance (d_Q) from the location Q to the pivot plane and the slope (s_Q) at elevation z_Q:

$$\Delta z_Q = d_Q s_Q \tag{2-1}$$

where Δz_Q is the vertical translation at elevation z_Q. The greater the distance d_Q, the larger the vertical translation. The horizontal distance d_Q is calculated by (Spiegel, 1986)

$$d_Q = \left(x_Q - x_P\right)\cos\alpha + \left(y_Q - y_P\right)\sin\alpha \tag{2-2}$$

where x_Q and y_Q are the coordinates of the well location Q. d_Q is negative if the well location Q is in the updip domain and is positive if the well location is in the downdip domain.

Given the slope s_1 and slope s_2, where $s_2 > s_1$ in Figure 2.1.b, a slope at any elevation z_Q vertically beneath location Q is determined as follows:

$$s_Q = \begin{cases} s_1 & \text{if } z_{Q'} > z_1 \\ \frac{z_O - z_Q}{d_O - d_Q} & \text{if } z_2 \le z_{Q'} \le z_1 \\ s_2 & \text{if } z_{Q'} < z_2 \end{cases} \tag{2-3}$$

where s_Q is the slope at elevation z_Q. $z_{Q'}$ is the translated elevation of z_Q, z_O is the elevation of the line O. Elevations above the inclined plane E_1 have the same slope s_1, which is defined at elevation $z_1$in the pivot plane. Elevations below the inclined plane E_2 have the same slope s_2, which is defined at elevation z_2 in the pivot plane. Based on the trigonometry, the slope s_Q is $\frac{z_O - z_Q}{d_O - d_Q}$ for any elevation between the planes E_1 and E_2. d_O is the horizontal distance from line O to the pivot plane. d_O is calculated by

$$d_O = \frac{z_1 - z_2}{s_2 - s_1} \tag{2-4}$$

Therefore, $z_{Q'}$ is calculated as

$$z_{Q'} = z_Q + \Delta z_Q \tag{2-5}$$

If the formations have the same dip angle (i.e. $s_1 = s_2$) throughout the depth, the slope at elevation z_Q is s_1 (i.e. $s_Q = s_1$).

2.2.4. Lithofacies modeling on non-dipping domain

This study adopted the lithofacies modeling approach from Pham and Tsai (2017) to construct a stratigraphy on a non-dipping domain. Binary values are assigned to sand facies and clay facies. Well log data are mapped to a non-dipping domain. Sand and clay facies at well log locations are interpolated on horizontal planes at different depths via indictor natural neighbor interpolation method (Tsai, 2009)

$$\hat{I}\left(\mathbf{x}_0\right) = \sum_{i=1}^{N} w_i I_i \tag{2-6}$$

where $\hat{I}$ is the estimated indicator value at unsampled location $\mathbf{x}_0$, I_i is the indicator value at well log *i*, w_i is the natural neighbor weight for well log i, and N is the number of well logs. *I*=1 refers to sand facies. *I*=0 refers to clay facies. The weights are calculated by the natural neighbor interpolation method (Green and Sibson, 1978; Sukumar et al., 2001). Further details about the natural neighbor method can be found in Boissonnat and Cazals, (2002) and Watson (1999). A Fortran program – Tile (Green and Sibson, 1978) was used to calculate the natural neighbor weights in Eq. 2-6. A cutoff value that determines $\hat{I}$ to be either a sand or a clay facies can be approximated based on the sand facies fraction of the well log data in a tile (Elshall et al., 2013).

Similar to the indicator kriging, Tsai (2009) derived conditional estimation variance for using non-kriging weights in Eq. 2-6. It is noted that the indictor natural neighbor interpolation method is one of many interpolation methods but is computationally efficient. A three-

dimensional stratigraphy model in the non-dipping domain is resulted by stacking up all horizontal planes.

2.2.5. Back-translating non-dipping stratigraphy to dipping domain

After a stratigraphy is determined in a non-dipping domain, estimated lithofacies at any location Q at elevation $z_{Q'}$ is back-transformed to corresponding depth z_Q in the dipping domain by:

$$z_Q = z_{Q'} - \Delta z_Q \tag{2-7}$$

where Δz_Q is calculated by Eq. 2-1.

The geometry of a non-dipping domain is changed after the translation from its dipping domain. Figure 2.2.a illustrates transformation of a dipping formation to a non-dipping formation. The lithofacies in the non-dipping domain are stretched due to increasing slope with depth and lie horizontally. To cope with an angular unconformity in a tile as shown in Figure 2.2.b, the mildly dipping stratum (younger) is separated from the steeply dipping stratum (older). As a result, lithofacies estimation is conducted separately in two non-dipping domains. Then, the estimated lithofacies are transformed back and merged to the same tile. Figure 2.2.b illustrates the Louisiana geology that the Holocene-Pleistocene alluvial deposits eroded and replaced partial Tertiary deposits. Because each tile can be modeled independently from the other tiles, the modeling can be efficiently performed by parallel computing.

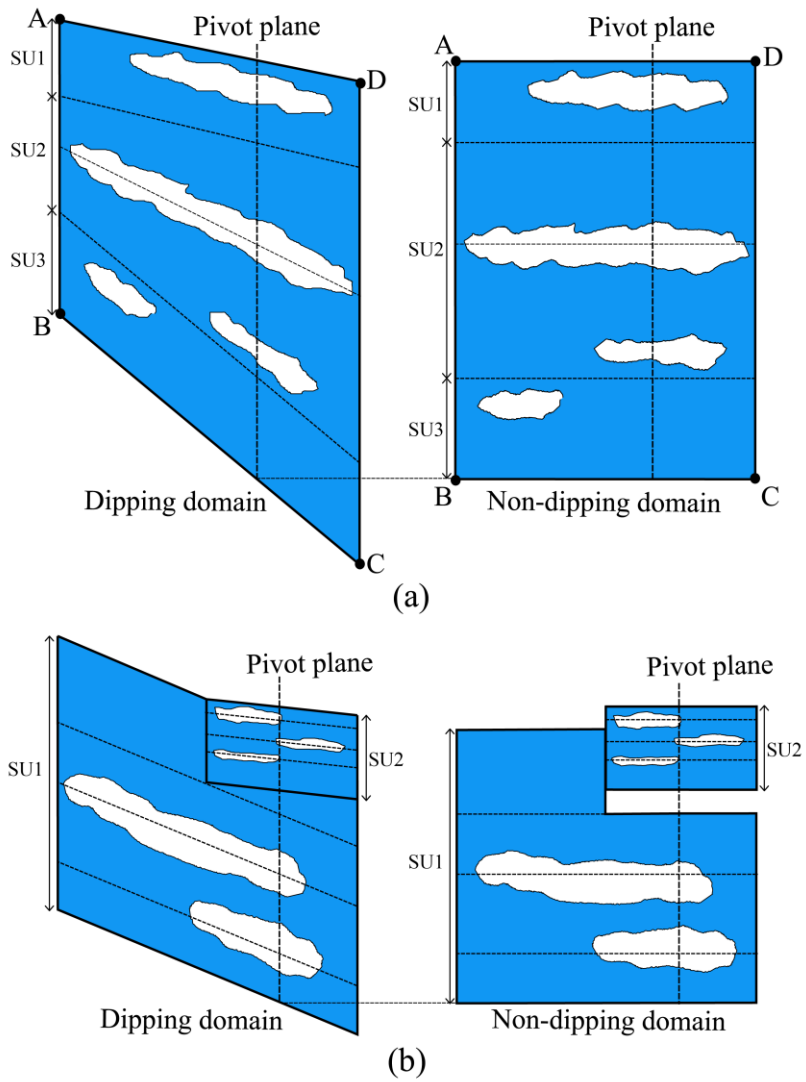

Figure 2.2. Translation from dipping domains to non-dipping domains: (a) three stratigraphic units with increasing slope in depth, and (b) two stratigraphic units with angular unconformity. Blue and white colors represent two different lithofacies. SU: Stratigraphic Unit.

One caveat in tessellating the domain is unavoidably creating interpolation discontinuity in dip direction and dip angle across tile boundaries, which may result in lithofacies discontinuity at tile boundaries. Other factors contributing to boundary discontinuity include a lack of deep wells in a tile and non-uniform well depth. The interpolation discontinuity can be minimized by refining the tile size and incorporating more well logs outside the tile of interest. However, the interpolation discontinuity issue arising from deep well scarcity and non-uniform well depth is difficult to

resolve and artifacts around tile boundaries may remain. If a tile boundary is formed by a fault line, then the well logs across the fault line are not included for interpolation in order to maintain lithofacies discontinuity at the fault line.

2.3. Study area: State of Louisiana (USA)

The proposed methodology was employed to develop a state lithofacies model for Louisiana, USA. The state covers an area of about 135,000 km^2 (U.S. Census Bureau, 2010). Topography decreases from the upland terraces in the north to the relatively flat Chenier Plain and the Mississippi River Delta Plain in the south adjacent to the Gulf of Mexico. Figure 2.3 shows the major rivers, lakes, coastal plains, fault traces and the Sabine Uplift area in Louisiana. The Eocene-Pleistocene formations are partly overlain by the Holocene sediments mainly from the alluvial depositions of the Red River, the Ouachita River, and the Mississippi River (Horton, 2017).

There are a few major geological structures in Louisiana: dips, faults, and domes. The dip angle and dip direction are not constant over the entire state. There are also angular unconformities formed by flat-lying alluvial deposits over steep-dipping formations (Hosman, 1996). In addition, there are families of faults in the southern Louisiana, of which the Baton Rouge fault system is the most distinct fault system (McCulloh and Heinrich, 2012). The Sabine Uplift is an important Cretaceous basement block, which extends from easternmost Texas to northwestern Louisiana (Halbouty and Halbouty, 1982).

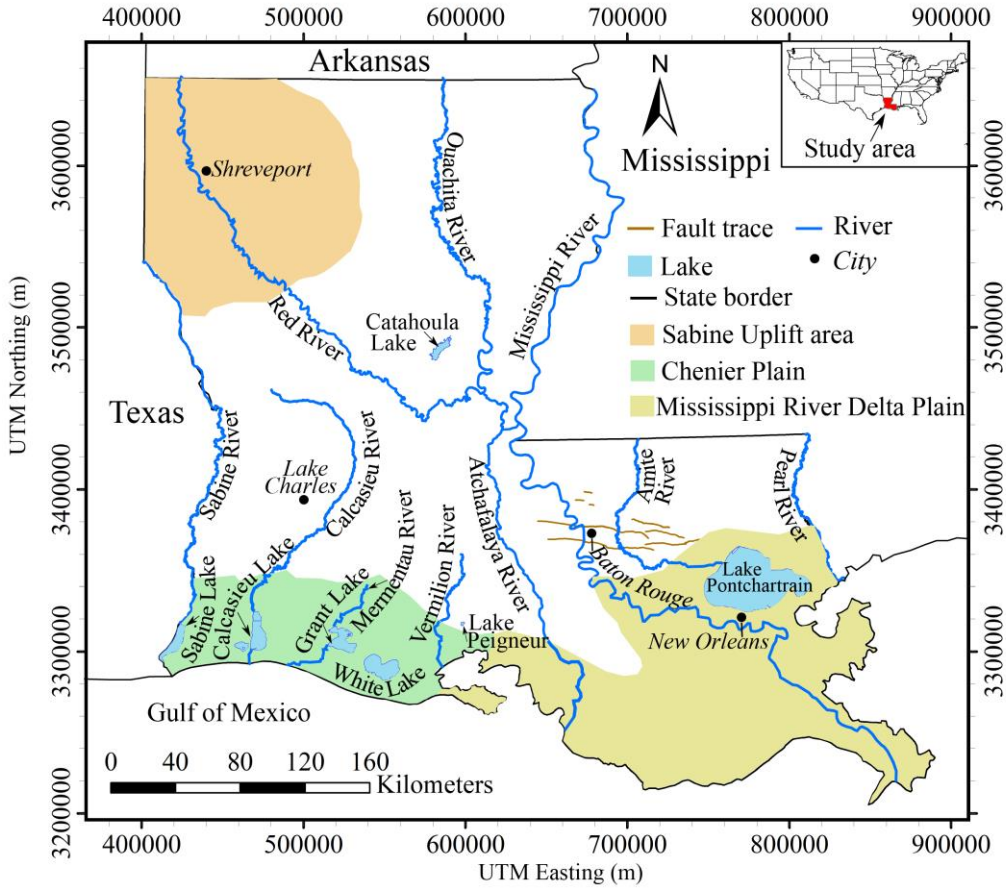

Figure 2.3. Study area (Louisiana) that includes major rivers, lakes, coastal plains, fault traces in the southeast, and Sabine Uplift in the northwest. The coordinates are in NAD83 / UTM zone 15N.

The areal extent of 13 major freshwater aquifer systems and their vertical sequence in Louisiana are shown in Figure 2.4 (Smoot, 1986). The Paleocene-Eocene Carrizo-Wilcox and Sparta aquifers are overlain by the Pleistocene-Holocene Red River alluvial aquifer (RRAA) and the Upland Terrace aquifer in the northwest. The Eocene Cockfield aquifer is above the Sparta aquifer and is overlain by the Mississippi River alluvial aquifer (MRAA) of Pleistocene-Holocene age. The Oligocene-Miocene Catahoula aquifer underlies the MRAA, the RRAA, and the Upland Terrace aquifer in the central Louisiana and underlies the Miocene Jasper aquifer in the western Louisiana. In the southwest, the Evangeline aquifer of Miocene-Pliocene age overlies the Jasper aquifer and is overlain by the Pleistocene Chicot aquifer system. The Jasper Equivalent aquifer,

Evangeline Equivalent aquifer, and Chicot Equivalent aquifer in the southeast are from the Miocene to the Pleistocene (Weiss, 1990; Renken, 1998). These three aquifers together are also known as the Southern Hills regional aquifer system (Buono, 1983). Both the Southern Hills regional aquifer system and the Chicot aquifer system are designated as the Sole Source Aquifers (SSA) by the U.S. Environmental Protection Agency.

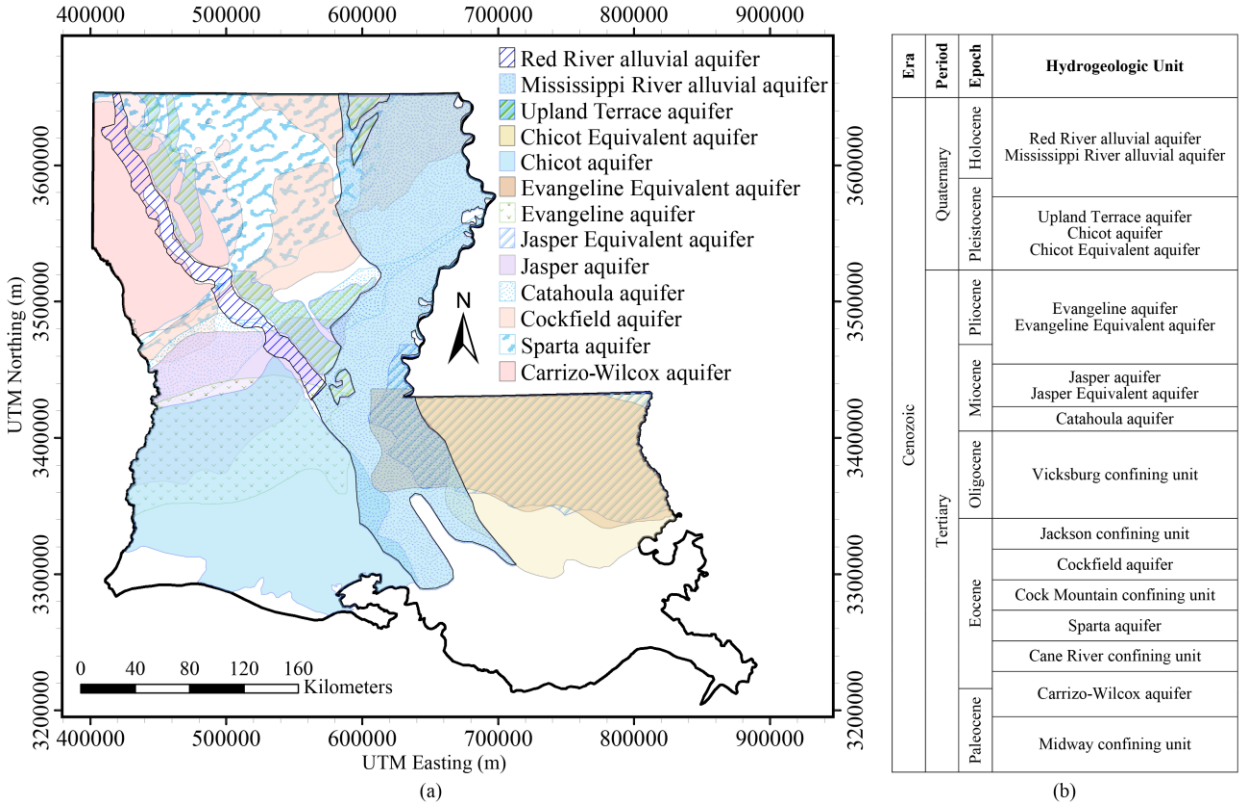

Figure 2.4. (a) Areal extent of the freshwater quifers in Louisiana, and (b) vertical sequence of the hydrogeologic units of Louisiana, modified from Smoot (1986).

More than 90% of groundwater use in Louisiana is for agriculture, industry and public supply. 66% of the total groundwater withdrawal are from the Chicot aquifer system and MRAA (Collier and Sargent, 2018). Although groundwater is an abundant source, there are concerns regarding aquifers in Louisiana, such as declined groundwater level due to heavy pumping,

contamination from agricultural chemicals, hazardous-waste sites and surface disposals, and saltwater encroachment (Stuart et al., 1994).

2.3.1. Big well log data

The number of drillers' logs are much greater than the number of geotechnical borings and electric logs. Drillers' logs can provide good lithologic information for shallow depths (e.g., less than 100 m). For the lithofacies modeling drillers' logs, geotechnical borings, and electric logs were interpreted into either sand facies or clay facies. Sand facies represents a group of relatively coarse-grained sediments (e.g., gravel and sand) that have relatively high hydraulic conductivity and form aquifers. Silt, clay, and shale represent a group of relatively fine-grained sediments that have relatively low hydraulic conductivity and form aquitards and aquicludes.

More than 12,000 electric logs and more than 102,000 drillers logs and geotechnical borings (Figure 2.5) in Louisiana were collected from the Louisiana Department of Natural Resources, the U.S. Geological Survey (USGS), and the Louisiana Geological Survey. There are more than 355,000 sand and clay facies intervals in the well log data. While the well data distribution is not uniform, on average one well log covers about 1 km^2. Well logs were digitized and interpreted into sand facies and clay facies following the method in Elshall et al. (2013) and Pham and Tsai (2017). Lithologic information in drillers' logs was considered only down to a depth of 107 m (350 feet) while electric logs of water wells can be as deep as 914 m (3,000 feet). The number of lithofacies intervals identified in well logs varies from 1 to 76. About 6% of the well logs in Eocene-Pleistocene formations have surficial sand records. 23% of the well logs cover the alluvial formations of the Mississippi River and the Red River.

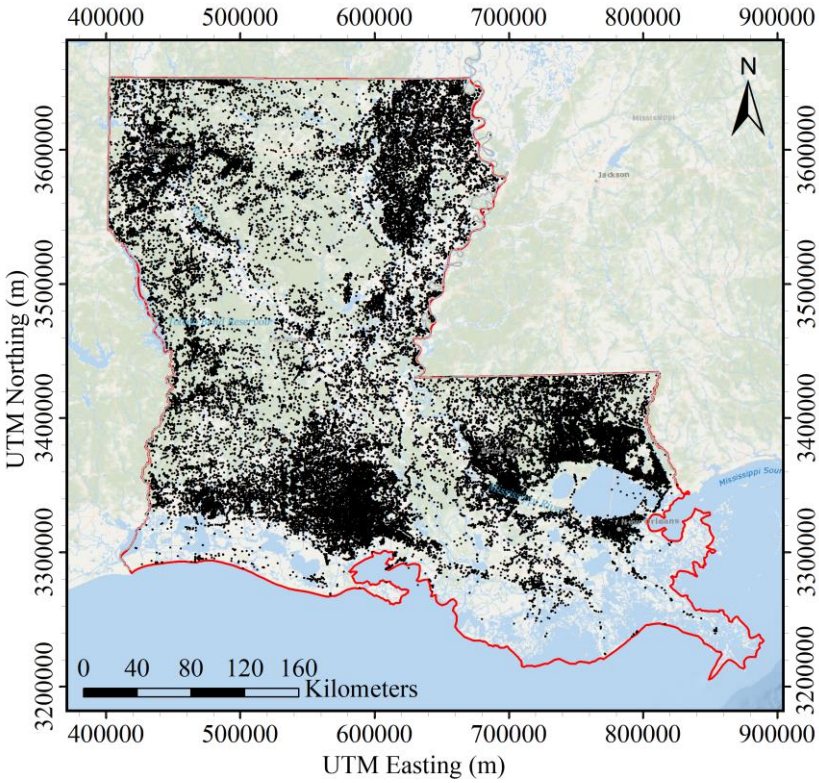

Figure 2.5. Location of well logs (black dots) used for lithofacies modeling.

2.3.2. Tessellation

Dip directions and dip angles in Louisiana were derived from USGS' regional stratigraphy studies in the south-central United States (Hosman, 1996; Weiss, 1990). Accordingly, this study tessellated Louisiana into 375 tiles shown in Figure 2.6 Each tile size is 20 km. The tiles with irregular shape in the southeast were generated to fit fault traces. The tile size is subjective, so is the tile geometry. If needed, the tiles can be refined to account for rapid change in dip direction. Nevertheless, the tessellation in Figure 2.6 sufficiently captures the regional dip directions and fault lines. Dip direction and slope in each tile are represented by a vector and its magnitude. In general, formations in the north-central Louisiana dip east toward the axis of the Mississippi embayment (Hosman, 1996). Formations in South Louisiana are dipping south uniformly, better known as the homocline of the Gulf Coast (Granata, 1963). The truncated Sabine Uplift domal

shape indicates that the overlying formations extend outward from the center of the dome and the formation slope increases when moving away from the center (Ewing, 2009). The southern extent of the Sabine Uplift dips south towards the Gulf of Mexico.

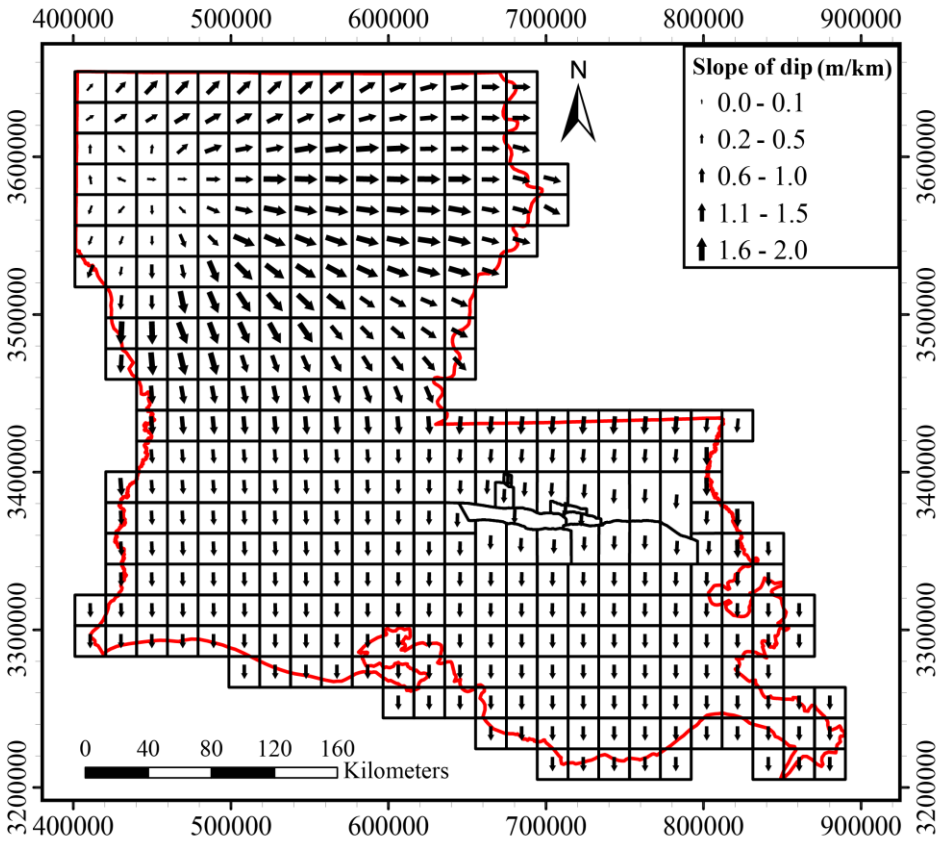

Figure 2.6. Tile configuration for the lithofacies model of Louisiana. The vectors show the dip direction for each tile. Thickness of vectors represents the magnitude of the slope. The MRAA and RRAA slope and dip direction are not included.

It was considered that slopes of dips start from zero at the center of the Sabine Uplift and smoothly increase to 2 m/km (0.002) outward (Ewing, 2009). The slope of Gulf Coast homocline is considered to be 1.5 m/km (0.0015) (Jones et al., 1956). The transition between 1.5 m/km and 2.0 m/km was obtained through vector interpolation. For simplicity, the slope remains the same in depth. The dip direction to the south with a gentle slope of 0.1 m/km (0.0001) is considered for

the MRAA and the RRAA. Angular unconformities occur between the alluvial formations and their underneath steeper formations.

2.3.3. Surface discretization

Each tile was discretized into computational cells of 1 km. However, special refinement around the Baton Rouge fault system was made by nested quadtree grid cells as shown in Figure 2.7. Nested quadtree structures were created based on recursive bisectional decomposition of the parent grid (Lien et al., 2015). The cell size gradually decreases from 1 km to 50 m at fault traces. The total number of computational cells at land surface for the Louisiana model is more than 174,000. The vertical resolution for the non-dipping domain is about 3 m (10 feet). The vertical extent is about 900 m, which yields 300 horizontal planes.

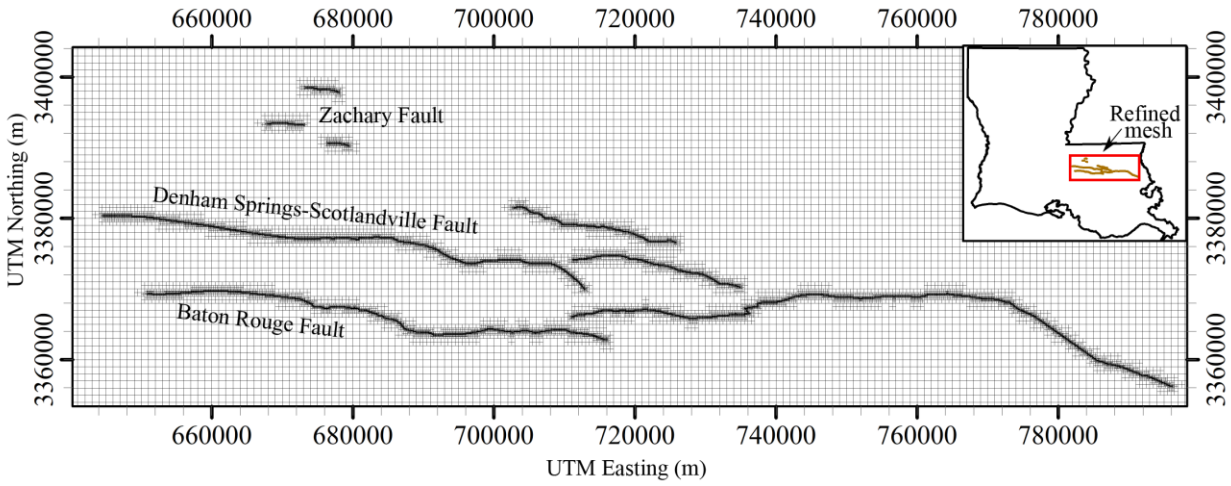

Figure 2.7. Computational cells around the Baton Rouge fault system. Base grid resolution is 1 km. Cell size along the fault traces is 50 m.

2.4. Results and discussions

2.4.1. Computation time

The lithofacies model for Louisiana was set up and run on a supercomputer at the High Performance Computing (HPC) center at the Louisiana State University. The computation time was around 14 hours without parallel computing and was reduced to less than 1 hour with the parallel code for computing 375 tiles. The computation time for larger tiles was longer than small tiles.

2.4.2. Surficial characteristics

Surficial distributions of sand facies and clay facies shown in Figure 2.8 suggest 12.4% of land in Louisiana to be potential outcrops of high-permeability facies. The result confirms the outcrop zones of the Southern Hills regional aquifer system in southeastern Louisiana (Buono, 1983), outcrop zones of the Chicot aquifer system and the Evangeline aquifer in west-central Louisiana (Jones et al., 1956), and outcrop zones of the Sparta aquifer in northwestern Louisiana (Ryals, 1982). Figure 2.8 also shows potentially limited superficial recharge to the MRAA, which accords with Ackerman (1989), and the RRAA. Southern Louisiana is mostly covered by low-permeability facies. The lithofacies model reveals that the Chenier Plain is mostly fine-grained at surface with a few lenticular sands dispersed across the plain (Byrne et al., 1959; Owen, 2008).

Depth to the topmost sands has tremendous implications on surficial groundwater recharge and groundwater accessibility. The topmost sands in this study are considered to have thickness 6.1 m (20 feet) or greater and are shown in Figure 2.9.a. The topmost sands for the MRAA and RRAA areas refer to their alluvial sands. By defining a high recharge zone as an area with no surficial confining layer, the Chicot aquifer system has high recharge zones of 283 km^2 in its north. The Southern Hills regional aquifer system has high recharge zones of 268 km^2. The Sparta aquifer

has high recharge zones of 200 km^2 in its west. No high recharge zone is recognized for the Cockfield aquifer in the north-central region and for the Carrizo-Wilcox aquifer in the northwestern region.

The effect of well log data density is showing in Figure 2.9.a and the later figures. The modeling results in the coastal zone have relatively large mosaic pattern due to the low data density. As a result, the estimated lithofacies in the coastal zone have relatively large uncertainty.

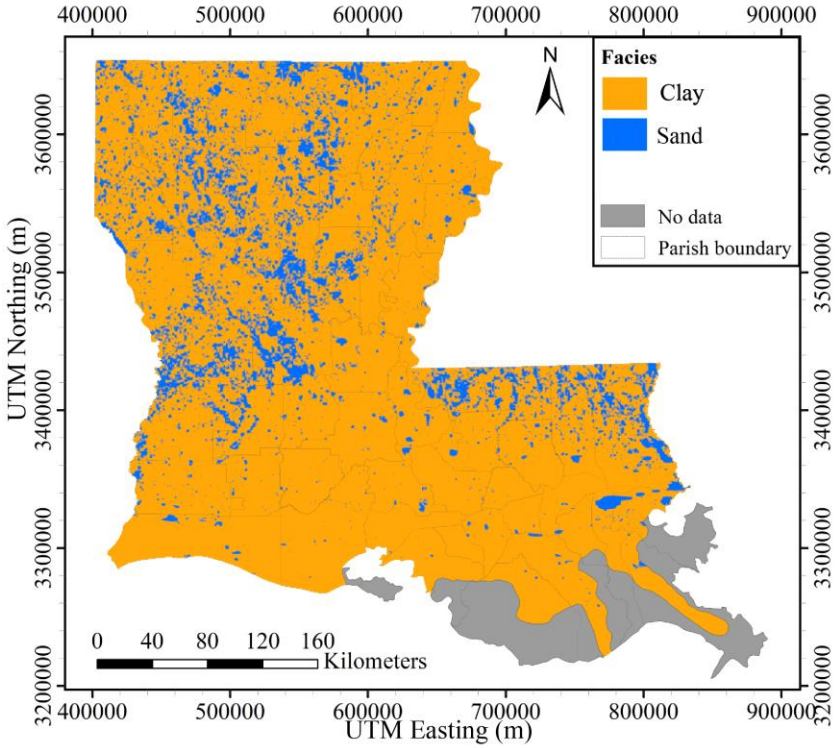

Figure 2.8. Distributions of surficial sand facies and surficial clay facies. The gray zones have no well log data in the coastal zone.

Depth to the topmost sands is a useful index to evaluate the accessibility to shallow groundwater. It is evident in Figure 2.9.a that the Chicot aquifer system, MRAA and RRAA are highly accessible by agricultural and industrial wells. The Southern Hills regional aquifer system is also highly accessible by domestic wells in the north of the Baton Rouge Fault. The dense well logs in these regions (Figure 2.5) reflect the high aquifer accessibility at relatively shallow depths.

The Chicot aquifer system has much thicker topmost sands than other aquifer systems (Figure 2.9.b). Topmost sands as thick as 200 m are recognized in the central and eastern areas of the Chicot aquifer where extensive groundwater is extracted for the irrigation purpose. The thickness of the MRAA in the northern area is as high as 60 m and increases towards the south. The northern and central areas of the Southern Hills regional aquifer system have thick topmost sands as well. In contrast, the RRAA and the topmost sands in the Sparta aquifer are thin.

The statistics of top confining units and topmost sands for important aquifers are shown in Table *2.1*. The MRAA has the most uniform top confining unit, whereas the thickness of confining unit of the Sparta aquifer spatially varies the most. Comparing the average values of the depth to the topmost sands, the MRAA and the Sparta aquifer have the best and worst groundwater accessibility, respectively. The range and average of the topmost sand thickness for the Chicot aquifer system indicate that this aquifer has the thickest shallow aquifer sands. On the other hand, the RRAA is thin compared to the other aquifers.

Table 2.1. Statistics of topmost sands for different aquifers or aquifer systems

Aquifer	Depth to topmost sand (m)			Topmost sand thickness (m)		
	Range	Average	Standard deviation	Range	Average	Standard deviation
Sparta	0-420	70	54	6-140	18	13
Chicot	0-328	36	33	6-326	74	61
Southern Hills	0-424	38	36	6-265	32	27
MRAA	0-91	18	14	6-91	40	19
RRAA	0-91	20	23	6-90	16	8

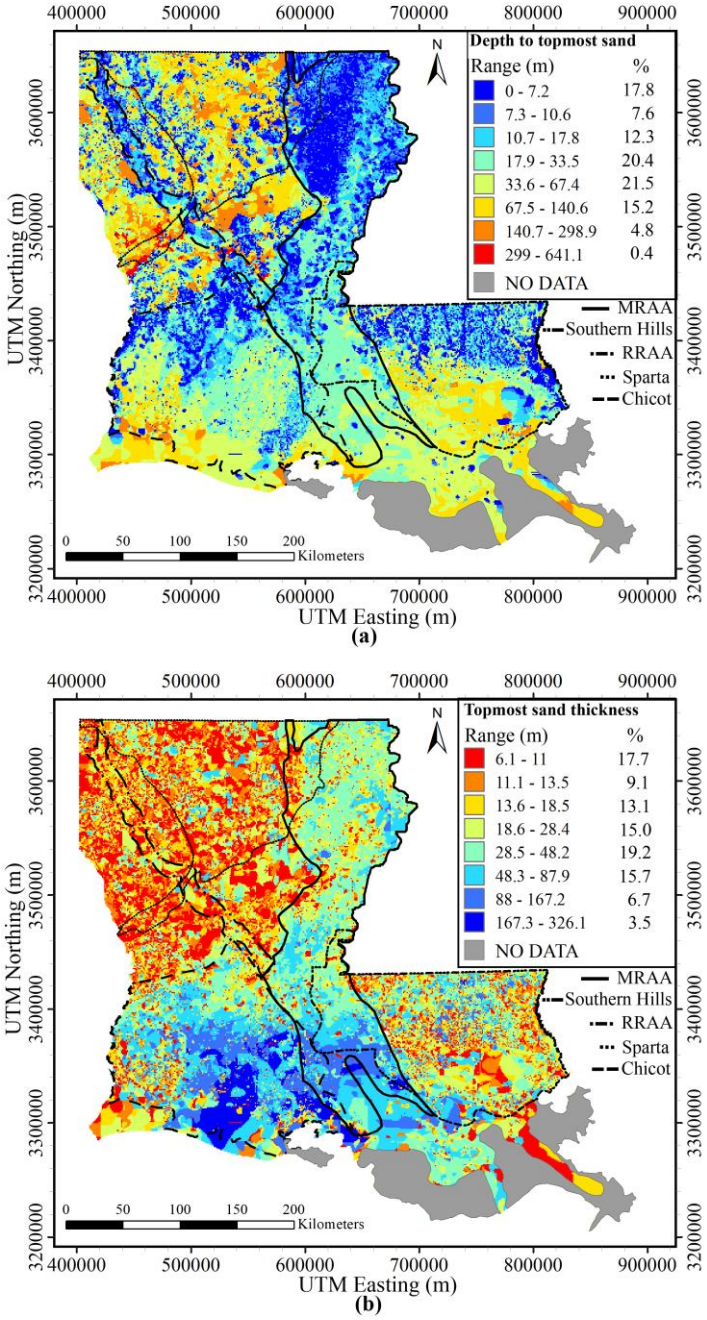

Figure 2.9. Maps of topmost sands that have thicknesses greater than 6.1 m (20 ft): (a) depth to topmost sand, and (b) topmost sand thickness.

More than 50% of Louisiana is covered with clays thicker than 9.1 m and thinner than 71.1 m (Figure 2.10). Thick surficial clays mostly appear in southern Louisiana and in the coastal zone.

Figure 2.10 is similar to Figure 2.9a, where areas with shallow depth to the topmost sands also have thin surficial clay.

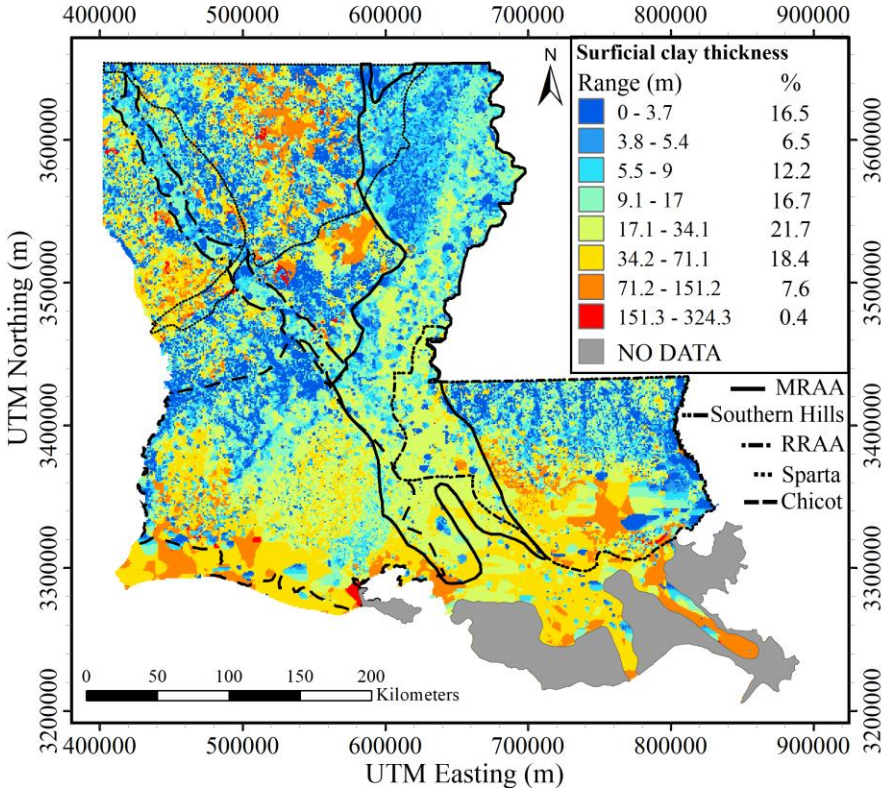

Figure 2.10. Map of surficial clay thickness.

2.4.3. Connections with rivers and lakes

Connections between rivers and lakes and their underlying aquifers were identified. Figure 2.11 shows the thickness variation of topmost sands that are connected to the major rivers. The Mississippi River and the Red River are connected to their alluvial sands through around 50% of their river length. Most of the connections along the Mississippi River are identified along its northern extent (Figure 2.12). The average sand thickness is higher in the north of the Mississippi River. The decrease in sand thickness from the north to the south of the Mississippi River is probably due to different depositional environments (Saucier, 1994) and reduction in sediment load as the river approaches the Gulf of Mexico (Bentley et al., 2016). In addition, the Atchafalaya

River captures around 30% of the Mississippi River flow which causes additional sediment reduction (Roberts, 1997). The Amite River, the Calcasieu River, and the Atchafalaya River are connected to their topmost sands majorly in outcrop zones. The northern reach of the Calcasieu River is connected to the Chicot aquifer system, where the thickness of the topmost sands can be up to 100 m. However, the connection length is very limited to only 14 km. Very limited connection was also found for the Vermilion River. No direct connection was identified between the Mermentau River and its topmost sands as well as the Pearl River and its topmost sands. The Ouachita River and the Sabine River were not analyzed due to the lack of bathymetric data.

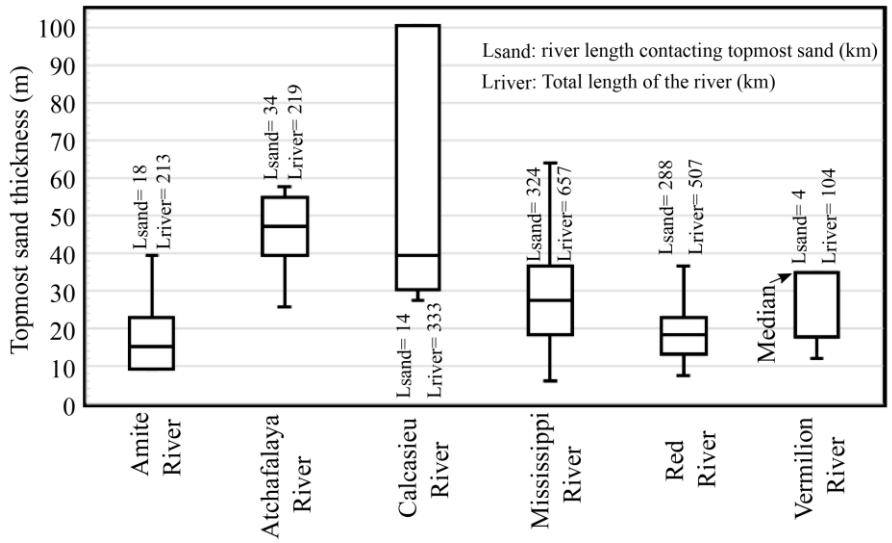

Figure 2.11. Thickness of topmost sands contacted by major rivers.

Eleven percent (11%) of Lake Catahoula is connected to the MRAA, where the thickness of sand is from 28 to 38 m (Figure 2.13). The connection area appears in the southwest of the lake (Figure 2.12). Lake Pontchartrain is strongly connected to the topmost sands in the southeast. The lake also reaches the Pleistocene sands in the north and Holocene sands in the southwest (Kindinger et al., 1997). No direct connection could be found between other major lakes and their topmost sands. In general, the surface waters in South Louisiana are less likely to be connected to the topmost sands.

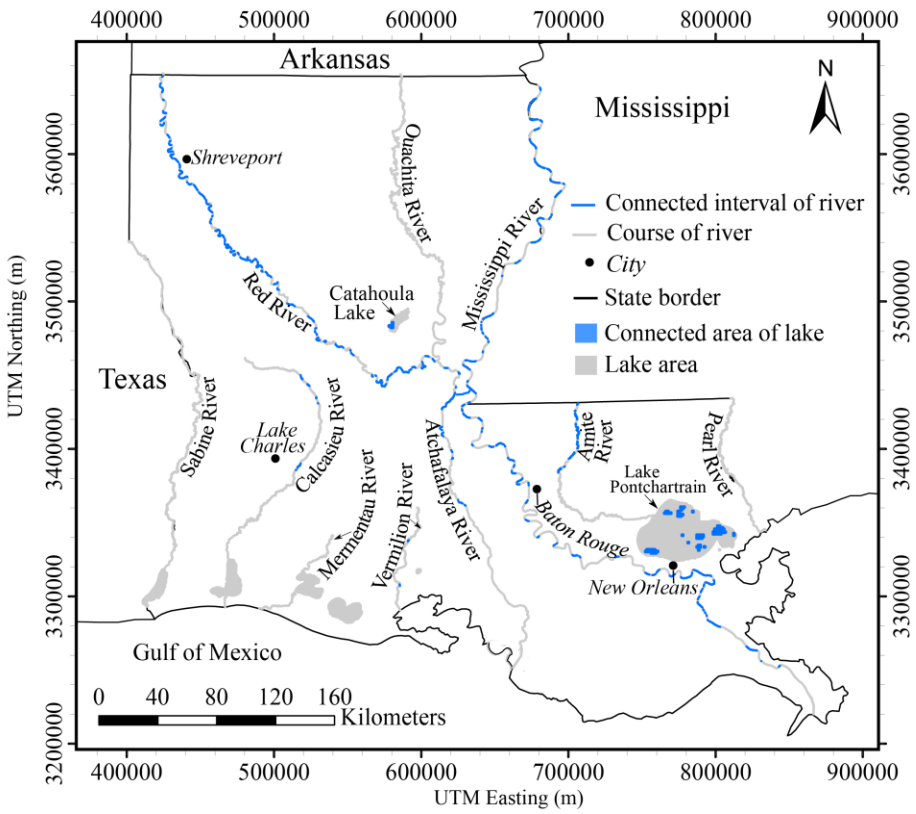

Figure 2.12. The connection intervals of the rivers and lakes with their underneath topmost sands.

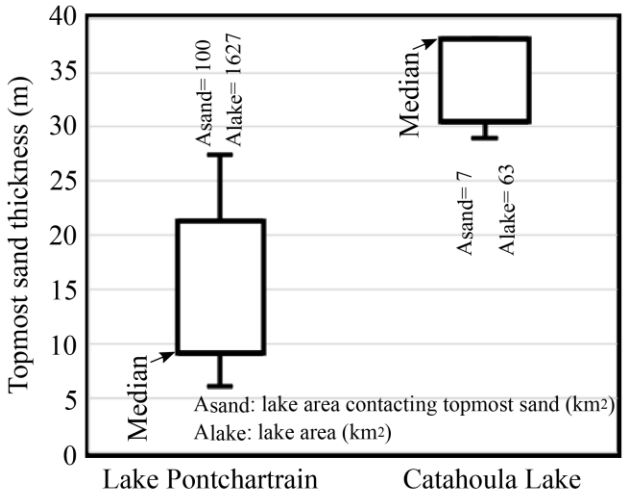

Figure 2.13. Thickness of topmost sands contacted by major lakes.

2.4.4. Hydrostratigraphy of Western Louisiana

Further analysis is conducted at three north-south cross sections AA′, BB′, and CC′. The cross section AA′ (Figure 2.14) along with deep well logs illustrates the location of the named aquifers in western Louisiana as well as the domal shape of the Sabine Uplift in the northwest, centered at Bienville Parish. Well logs are relatively shallow in the northwest and deeper in the southwest resulting in greater modeling depths in the southwestern parishes. The names of the hydrogeologic units are referred to Figure 2.4.b. The cross section AA′ shows outcrops of the Upland Terrace sand in the northwest, which is underlain by the Carrizo-Wilcox aquifer formed from deposits of the Wilcox Group and Carrizo Sand Formation (Ryals, 1982). The Carrizo-Wilcox aquifer extends southward to Sabine Parish. The Sparta aquifer outcrops in Webster and Bienville Parishes and is separated from the underlying Carrizo-Wilcox aquifer by the Cane River confining unit (Hosman, 1996). The shallow RRAA is hydraulically connected to the Red River. The Catahoula aquifer outcrops in the southern Sabine Uplift, and is overlain by the Jasper aquifer in Vernon Parish. The Jasper aquifer outcrops in Vernon Parish and is overlain by the Evangeline aquifer in Beauregard parish. The Chicot aquifer system outcrops in Vernon and Beauregard Parishes. The Chicot aquifer system includes three named aquifers (200-foot sand, 500-foot sand and 700-foot sand) in the Lake Charles area (Nyman et al., 1990) and in the western Cameron Parish. The Chicot aquifer system overlies the Evangeline aquifer.

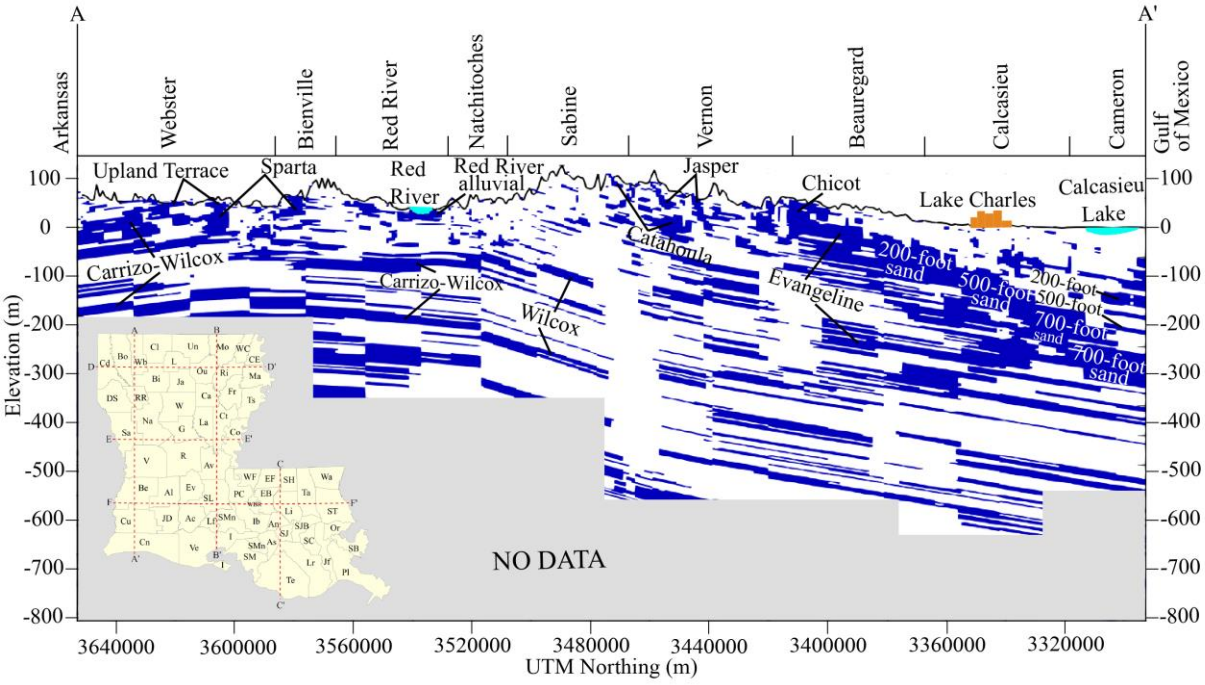

Figure 2.14. Sand distributions (blue color) at cross section AA′ at UTM zone 15N Easting 465000 m.

Lithofacies discontinuities shown in Figure 2.14 and other cross sections appears in deep depths at some tile boundaries are due to the tessellation effect that creates discontinuous dip direction and dip angle across tile boundaries. The lack of deep wells makes the interpolation discontinuities more pronouncing. Estimated lithofacies at upper depths exhibit less interpolation discontinuities at tile boundaries because of abundant shallow wells. Lithofacies discontinuities occurring within a tile are the result of abrupt lithofacies change in neighboring well logs and the use of the natural neighbor interpolation method. Currently, it is not known whether these are natural lithofacies limits or the results of undiscovered faults.

2.4.5. Hydrostratigraphy of Central Louisiana

Geological characteristics from the north-central Louisiana to the south-central Louisiana are shown in cross section BB′ (Figure 2.15). The MRAA stretches from Morehouse Parish to St.

Landry Parish. The alluvial aquifer is underlain by the Cockfield aquifer in the north-central parishes. The stratigraphy model reveals connections between the MRAA and the Cockfield aquifer in the north (Hosman, 1996). The Cockfield aquifer is separated from the underlying Sparta aquifer by the Cook Mountain confining unit. An angular unconformity is clearly visible in the south-central parishes, where the relatively flat MRAA lies on the top of the relatively steep Chicot aquifer. The Chicot aquifer system includes two named aquifers (Upper Chicot and Lower Chicot) in the east of the aquifer system. The MRAA has an extensive contact (around 1000 km^2) with the Upper Chicot aquifer from St. Landry Parish to Iberia Parish (Weiss, 1990). This contact implies that groundwater exchange between the MRAA and the Upper Chicot aquifer may occur (Nyman et al., 1990). The MRAA is also referred to as the Atchafalaya River alluvial aquifer in this region because of the presence of the Atchafalaya River. The Upper Chicot aquifer can be as thick as 275 m. The average sand thickness in the contact area is 113 m.

2.4.6. Hydrostratigraphy of Southeast Louisiana

Geological characteristics in southeastern Louisiana exhibit two interesting depositional environments as shown in Figure 2.16. The closely interbedded deposit of sand and clay occurs to the north of the Baton Rouge fault, whereas relatively continuous sands occur to the south. Many freshwater aquifers have been named in the St. Helena and Livingston Parishes down to the Catahoula aquifer. The area to the south of the Baton Rouge fault has four named aquifers: the Gramercy aquifer, the Norco aquifer, the Gonzales-New Orleans aquifer, and the 1,200-foot sand, all of which are part of the Chicot Equivalent aquifer.

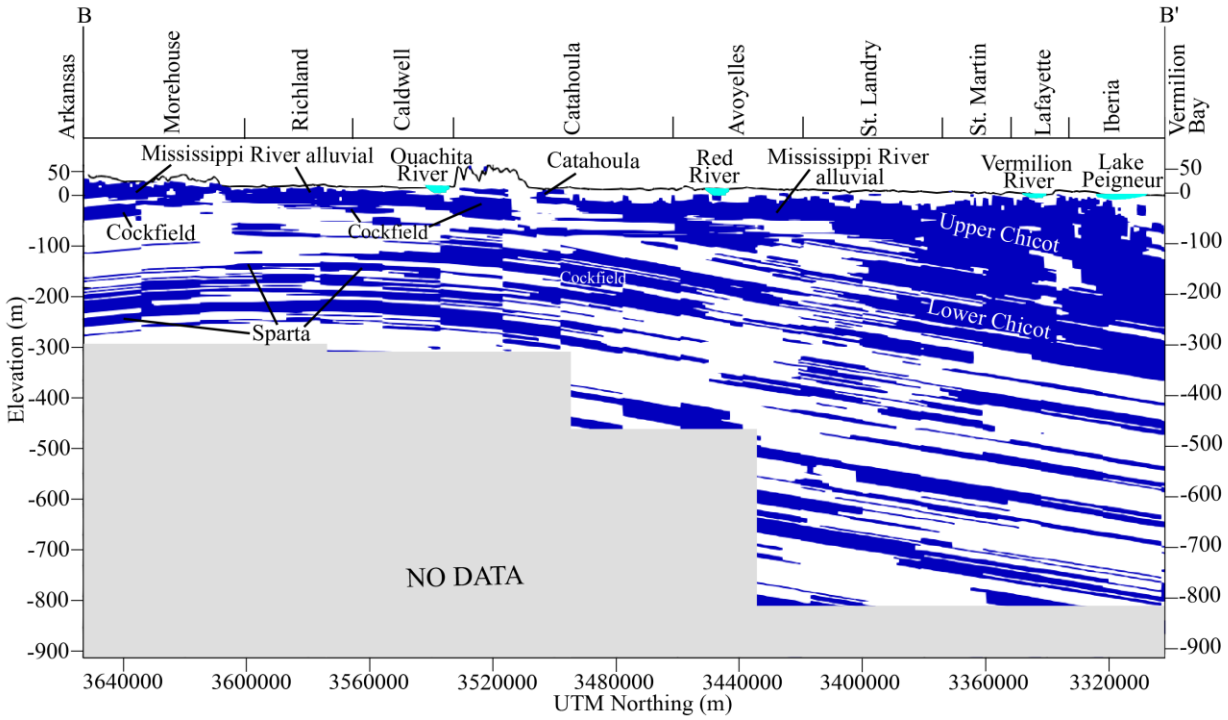

Figure 2.15. Sand distributions (blue color) at cross section BB′ at UTM zone 15N Easting 600000 m.

The two different depositional environments may either be related to undiscovered faults in the north creating the disturbed sand beds, or to the source of progradation of Louisiana's coastal plain. There are two substantial hypotheses on the source of progradation (Bentley et al., 2016). Saucier (1994) suggested that the Mississippi River is the only one major fluvial axis, to which all other tributaries join. However, Galloway et al. (2011) suggested the existence of multiple fluvial axes, such as the Mississippi River and the Tennessee River. Saucier's hypothesis would result in a single depositional pattern like the one to the south of the Baton Rouge fault in Figure 2.16. However, the multi-axis hypothesis much better complies with the modeling result. The closely interbedded deposit of sand and clay may be further elucidated by the lenticular depositional pattern in the Citronelle Formation (Matson, 1916). Post-depositional faults might have further amplified the close interbedding. The Citronelle Formation is buried by the Pleistocene river

terraces where the close interbedding is less conspicuous. More research is necessary to prove that multiple faults in the north of the Denham Springs-Scotlandville fault do exist.

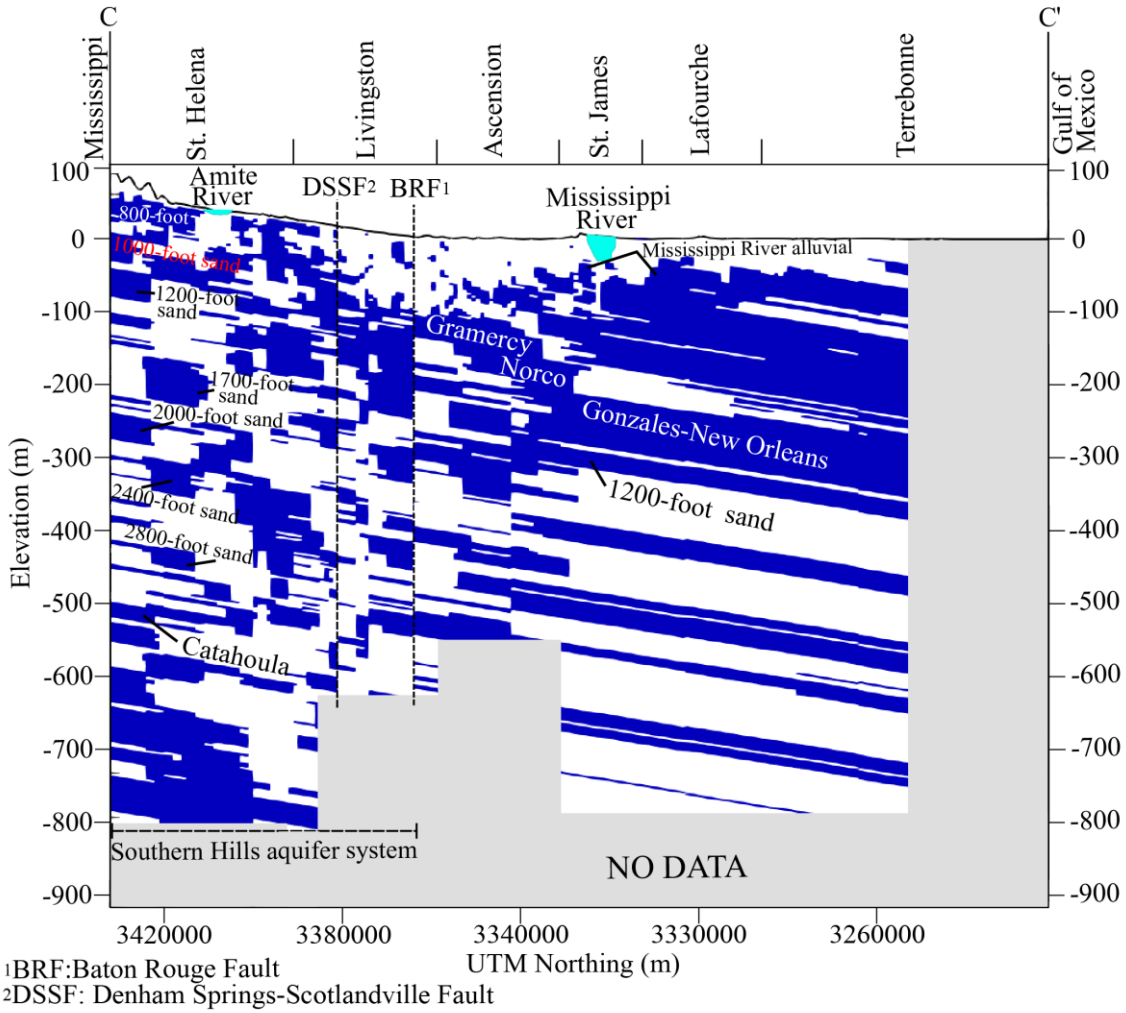

Figure 2.16. Sand distributions (blue color) at cross section CC′ at UTM zone 15N Easting 707000 m.

The east-west extents of lithofacies in Louisiana shown in cross sections DD′, EE′, and FF′ are illustrated in Figure 2.17, Figure 2.18, and Figure 2.19, respectively. The additional cross sections help the understanding of the hydrogeology in Louisiana.

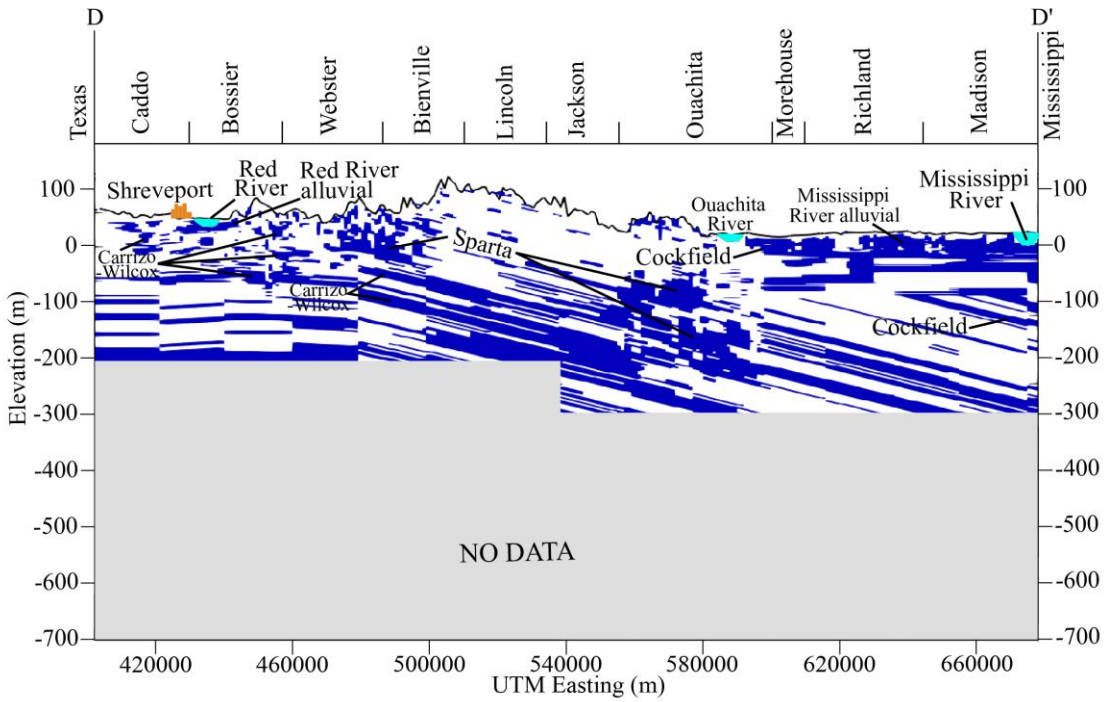

Figure 2.17. Sand distributions (blue color) at cross section DD′ at UTM zone 15N Northing 3600000 m.

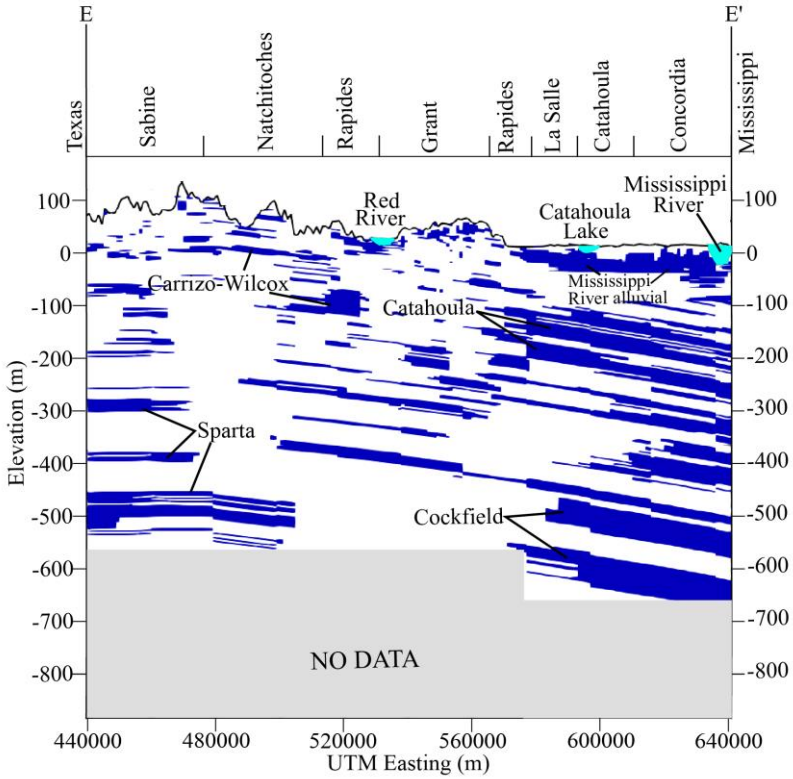

Figure 2.18. Sand distributions (blue color) at cross section EE′ at UTM zone 15N Northing 3480000 m.

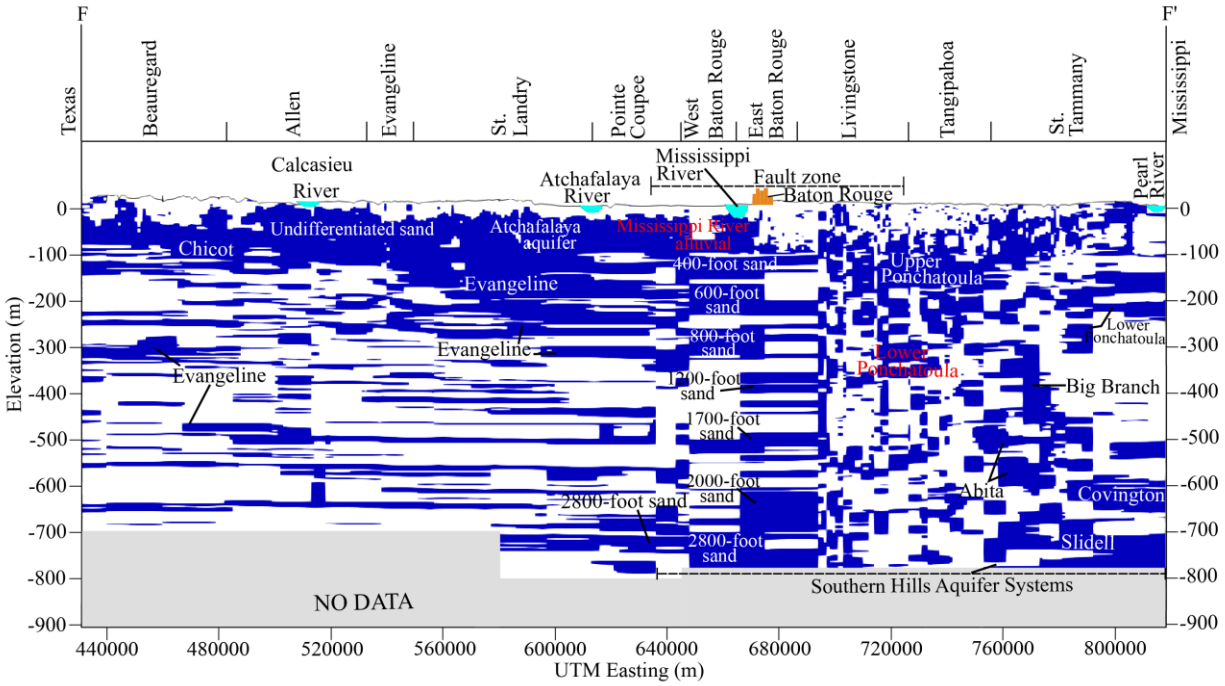

Figure 2.19. Sand distribution (blue color) at cross section FF′ at UTM zone 15N Northing 3375000 m.

2.4.7. Major alluvial aquifers

A 3D plot of the sand distribution of the RRAA and the MRAA is shown in Figure 2.20. The sand distribution of the RRAA has lenticular characteristics. The vertical extent of the alluvial aquifers is based on the USGS Fact Sheets (USGS, 2020). Less than 29% of the Red River alluvial deposits are composed of sand. The lower interconnections are the results of downcutting, erosive actions of the Red River. Sand units in northwestern Louisiana on the other hand are well connected and occur close to land surface (Figure 2.9.a), indicating potentially strong interactions of the Red River and its alluvial aquifer. The average sand thickness is around 8 m. The total sand volume in the RRAA is approximately 600 million m^3. The RRAA and the MRAA merge in Rapides Parish. 51% of the Mississippi River alluvial deposits are composed of sand. The MRAA is thick and extensive. A relatively thin top confining unit in the north (Figure 2.9.a) provides

favorable conditions for accessing groundwater. The average sand thickness of the MRAA increases from an average of 17 m in the north to an average of 42 m in the south. The total sand volume of the MRAA is around 3,900 million m^3.

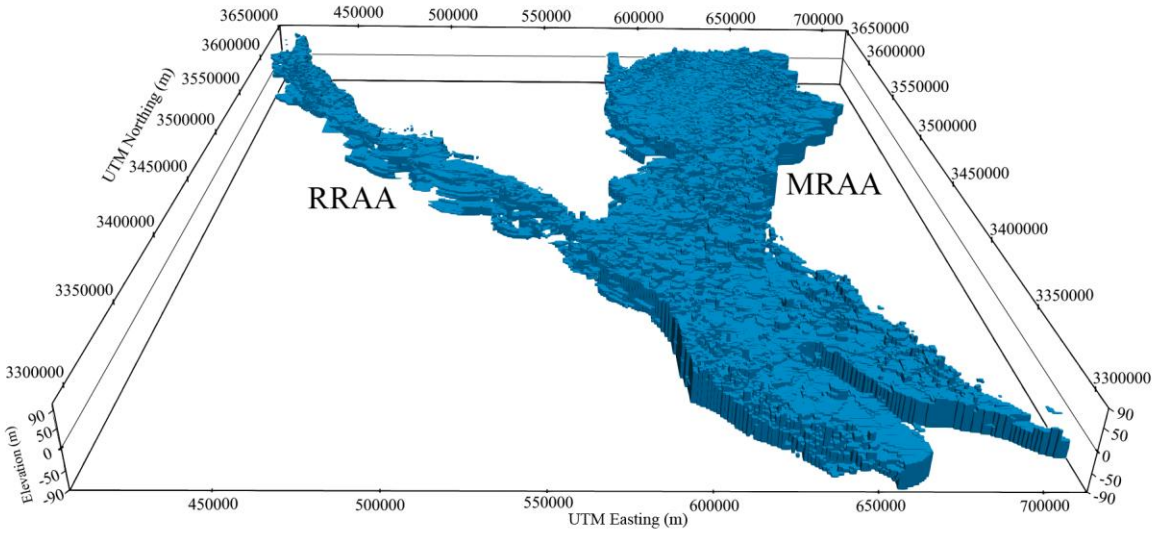

Figure 2.20. Sand distributions of the MRAA and the RRAA.

2.5. Conclusions

The proposed lithofacies modeling method is simple, but efficient to deal with a vast amount of well logs over a very large region. The method accounts for the geologic information (dip direction, dip angle, strike) from the structural geology and transforms the structural information into a non-dipping domain for lithofacies interpolation. The method has been successfully demonstrated to handle distinct geological features in Louisiana (such as angular unconformities, domes, and faults) through domain tessellation, tile discretization, vertical translation, and lithofacies interpolation.

Hydrogeological characteristics were identified for the state of Louisiana through developing a complex lithofacies model. There are three major outcrop zones in northwestern,

southeastern, and west-central Louisiana, through which precipitation and surface water recharge the aquifer systems. Southern Louisiana is mostly covered by low-permeability sediments. The average thickness of the top confining layers for the MRAA and the RRAA is around 20 m, which indicates high accessibility to groundwater in these aquifers. The stratigraphy model also reveals that the Mississippi River alluvial aquifer has a strong connection to the sands of both the Upper Chicot and Lower Chicot aquifers.

Assessing the connections between the major rivers and the aquifers reveals that the Mississippi River and the Red River are strongly connected to the MRAA and the RRAA, respectively. The connections between the Mississippi River and its sands mostly occur in the northern reach of the river, whereas the connections become weaker in the Mississippi River Delta. The Calcasieu River, the Atchafalaya River, and the Amite River are all mostly connected to their underlying aquifer systems in the outcrop zones. Catahoula Lake connects to the MRAA. Lake Pontchartrain have connections with shallow sands in many areas.

Sand formations in southeastern Louisiana show two different patterns. The closely interbedded deposit of sand and clay is identified to the north of the Baton Rouge fault while the sand formations to the south of the fault are continuous. The modeled difference between these two patterns of sand formations corresponds well with the hypothesis of multi-axis depositional patterns of the ancestral Mississippi River and Tennessee River. The close interbedding has also been confirmed through the studies on the Citronelle Formation in southeastern Louisiana.

This study does not include uncertainty analysis. The sources of error in the facies modeling results likely come from well log quality, well log interpretation, domain tessellation, tile discretization, interpolation methods, etc. Uncertainty quantification for such a large-scale complex lithofacies model remains a challenging future work.

Chapter 3. Irrigation-Intensive Groundwater Modeling of Complex Aquifer Systems through Integration of Big Geological Data

3.1. Introduction

Groundwater resource management of coastal aquifers has become a focal center of interest for many studies (Bocanegra et al., 2010; Custodio, 2010; Christelis and Mantoglou, 2016; Quintana et al., 2018). Overdrafting coastal aquifers has reportedly caused significant change in pre-development flow patterns leading to saltwater intrusion (Barlow and Reichard, 2010; Parizi et al., 2019; Azizi et al., 2019) and land subsidence (Eggleston and Pope, 2013; Guo et al., 2015). Hence, sustainable management of the aquifers plays an important role in counteracting the negative impacts (Abd-Elhamid and Javadi, 2011; Sreekanth and Datta, 2015). A key to understand the sustainability of aquifer systems is the analysis of influxes and outfluxes, which is elaborated in the concept of sustainable yield (Bredehoeft, 2002; Alley and Leake, 2004). As previous researches have emphasized, measuring the contributions of different inputs and outputs to a groundwater system is not a straightforward task for complex aquifer systems and flow modeling could help to overcome this issue (Loucks, 2000; Cao et al., 2013). The Chicot aquifer system in the southwestern Louisiana, as a very important groundwater resource in the Coastal Lowland aquifer system (Weiss, 1990), has been exploited mostly for irrigation during the past decades (Sargent, 2011). Understanding groundwater dynamics in the Chicot aquifer system is the primary step for its future sustainable development.

Understanding the groundwater dynamics in complex aquifers needs the assistance of stratigraphy models as well as groundwater models with different hydrogeologic properties (Zhang et al., 2006; Lee et al., 2007; Berg and Illman, 2015). Selecting an appropriate stratigraphic

This chapter was previously published as Vahdat-Aboueshagh, H., Tsai, F.T.-C., Bhatta, D. and Paudel, K.P., 2021. Irrigation-Intensive groundwater modeling of complex aquifer systems through integration of big geological data. Frontiers in Water, 3, p.29. https://doi.org/10.3389/frwa.2021.623476. Reprinted by permission of Frontiers.

modeling method mainly depends on data availability, computational resources, and adequacy of results reflecting the reality. Geostatistical methods have been extensively applied to developing stratigraphy models (Johnson and Dreiss, 1989; Soares, 1990; Marinoni, 2003; Kostic et al.; 2005). However, computational expenses with a very large dataset are among the limitations of using kriging methods (Pardo-Iguzquiza and Dowd, 1998; Tartakovsky et al., 2007; Cheng, 2013). Non-geostatistical interpolation methods such as the natural neighbor interpolation method (Watson, 1999) and the triangulated irregular networks (Clevis et al., 2006) avoid covariance matrix calculations and are computationally efficient.

One of the challenges associated with constructing stratigraphic structure for large-scale models is processing a huge volume of geological data. Several attempts have been made in organizing well log records and geological information by using Geographic Information System (GIS) tools (Chang and Park, 2004; Ross et al., 2005; Chesnaux et al., 2011). However, how to process raw well log data has not received enough attention. Prioritizing data from different well log sources based on their reliability (Ross et al., 2005) and selecting the most reliable piece of information are solutions to reduce errors in stratigraphy models. Another way to increase the model reliability is to consider an effective depth, to which a given well log includes proper stratigraphic information (Danielsen et al., 2007).

Model calibration is very challenging for an expensive groundwater model. Due to high dimensionality of parameters in a large-scale, complicated aquifer system, it is impossible to tune parameters without the aid of automatic calibration through optimization. Global search optimization methods such as the genetic algorithm (Kumar et al., 2010), the simulated annealing algorithm (Aarts and van Laarhoven, 1987), the ant colony optimization (Dorigo and Di Caro, 1999), and the particle swarm optimization (Poli et al., 2007) have the advantage of being

derivative-free (Rios and Sahinidis, 2013) over derivative-based local search optimization methods but require a large number of model runs. The Covariance Matrix Adaptation Evolutionary Strategy (CMA-ES) (Hansen et al., 2003) has proven to be an efficient method to calibrate expensive groundwater models with parallel computing (Elshall et al., 2015). This study adopted the CMA-ES for model calibration.

The goal of this study is to address the two aforementioned modeling challenges: (1) building a complex stratigraphy structure with large, non-uniform well log data, and (2) calibration of a high dimensional groundwater model, while investigating the groundwater dynamics of the Chicot aquifer system in Southwest Louisiana. The Chicot aquifer system has been known for its intensive use of groundwater for irrigation (Konikow, 2013) and its complex aquifer structure is largely ignored. This study adopted a lithofacies modeling method and a parallel optimization method for model calibration to improve groundwater modeling. Moreover, to the authors' best knowledge, there is no such a detailed large-scale groundwater model been built to advance hydrogeological knowledge in the Gulf of Mexico region and other coastal areas. The study presents an important worked example to bridging the gap between research and professional practice. In section 2, the Chicot aquifer system is introduced. Section 3 discusses data and methods to develop a Chicot groundwater model. Section 4 shows results and discussion. Section 5 draws the conclusions.

3.2. Chicot aquifer system

The Chicot aquifer system is part of the Coastal Lowlands aquifer system (Weiss, 1990). It covers Southeast Texas and Southwest Louisiana (Weiss, 1990). Nominally, the Chicot aquifer system only refers to its extent in Southwest Louisiana (Jones et al., 1956; Nyman et al., 1990; Sargent, 2004). The annual precipitation is about 1,473 mm (58 inches). The Chicot aquifer system

is the most heavily pumped aquifer in Louisiana, accounting for 41% of the state's groundwater use (Sargent, 2011). 72% of groundwater withdrawals are for the agriculture sector (including aquaculture). The Chicot aquifer system is also a sole source aquifer (USEPA, 2019), providing the major water supply to the public in the region. Figure 3.1 shows the study domain, major rivers, lakes, the Chenier Plain, and 2,709 pumping wells. The Chicot aquifer boundaries are determined by the USGS (Smoot, 1986) covering parishes of Acadia, Allen, Beauregard, Calcasieu, Cameron, Evangeline, Iberia, Jefferson Davis, Lafayette, St. Landry, St. Martin, St. Mary, and Vermillion. About 87% of total pumping wells have depth less than 120 m, which are generally irrigation wells. Deep wells are usually public supply wells and industrial wells. More than 2,400 irrigation wells are in the east-central area. Monthly pumping rates for irrigation were estimated based on cultivation area, crop type, growing seasons of crops, and pumping capacity of wells. The pumping wells in the west-central area are mostly industrial wells. The major public supply wells are located in or around municipalities. The pumping rates for the industrial use, public supply, and power generation were obtained from the U.S. Geological Survey (USGS).

The Chicot aquifer system is the uppermost hydrogeological unit in southwest Louisiana and encompasses seven aquifers (Nyman et al., 1990). The aquifer system gently dips southward at an angle of 0.06° (Jones et al., 1956). Figure 3.2 displays the location of well logs and geological fault traces. The fault traces are part of the Tepetate fault system (McCulloh and Heinrich, 2013). Well log data include 29,107 drillers' logs and 811 electrical logs that were collected from the Louisiana Department of Natural Resources (LDNR) and the USGS. Well logs are sparse in the Chenier Plain at the south and in the Atchafalaya River Basin at the east. The drillers' logs are mostly shallow (less than 120 m), accounting for 93% of total well logs. The electrical logs are primarily deep. 70% of electrical logs have depth deeper than 120 m. The well logs show about

40% of lithological information to be sand facies, indicating a sizable amount of permeable formations for storing groundwater.

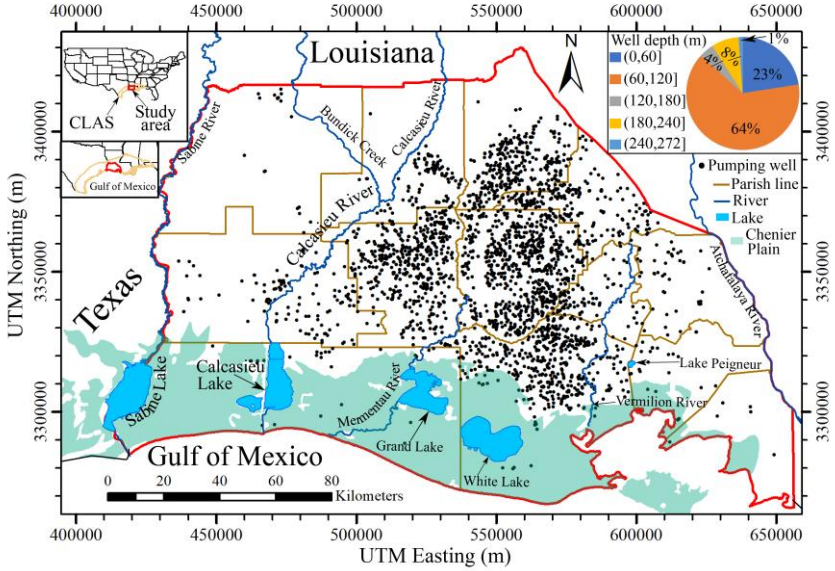

Figure 3.1. Chicot aquifer domain (red line). Black dots are pumping wells. Blue lines show the major rivers in the Chicot aquifer domain. The pie chart shows the fractions for depth ranges of pumping wells. The coordinates are in NAD83 / UTM zone 15N.

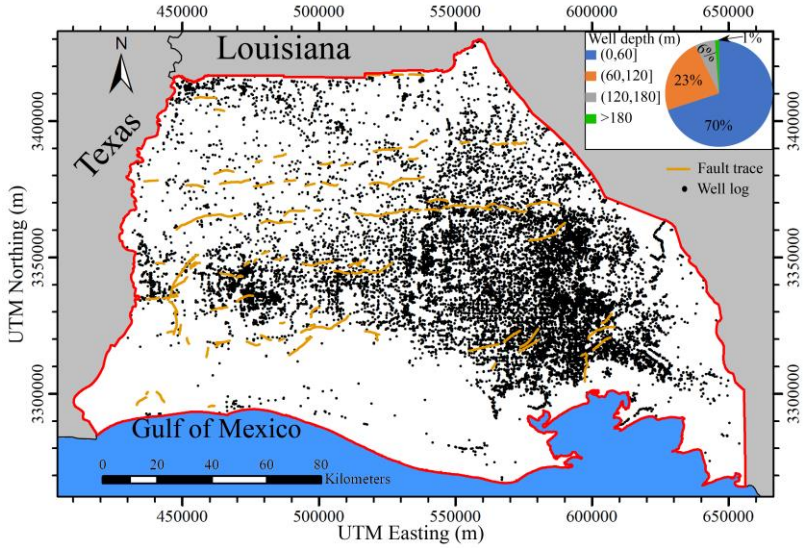

Figure 3.2. Location of well logs and fault traces in the study area. The pie chart shows the fractions for depth ranges of well logs.

3.3. Data and methods

3.3.1. Well logs for stratigraphy model development

This study employed two types of well logs to develop a stratigraphy model: electrical logs and drillers' logs. Electrical logs show the electrical properties of strata along a borehole, where in general high resistivity and low resistivity indicate sand facies (high-permeability facies) and clay facies (low-permeability facies), respectively (Archie, 1942; Galloway, 1977). The gamma ray and spontaneous potential curves when available were also used to assist sand picks in the electrical logs. The 811 electrical logs were analyzed. Each electrical log was interpreted as a sequence of sand facies and clay facies. Since electrical logs usually start at a deeper depth below land surface and contain stratigraphic information for deeper formations, they were employed to build the deeper portion of the stratigraphy model.

The drillers' logs contain useful lithologic descriptions along boreholes. Since drillers' logs normally begin at land surface, they provide important lithologic information for the top portion of the stratigraphy model. Lithologic descriptions in all 29,107 drillers' logs were interpreted as a sequence of sand facies and clay facies. Logs with ambiguous descriptions, depths and locations were disregarded. This study used lithologic descriptions of drillers' logs down to 152 m (500 ft). Since some of electrical logs and drillers' logs may be available at the same location, we prioritized geological information of electrical logs over drillers' logs. Moreover, screen intervals of pumping wells were assumed at permeable formations and provided sand facies interval information. Figure 3.3 shows a composite well log data out of an electrical log, a drillers' log, and two well screens at the same location.

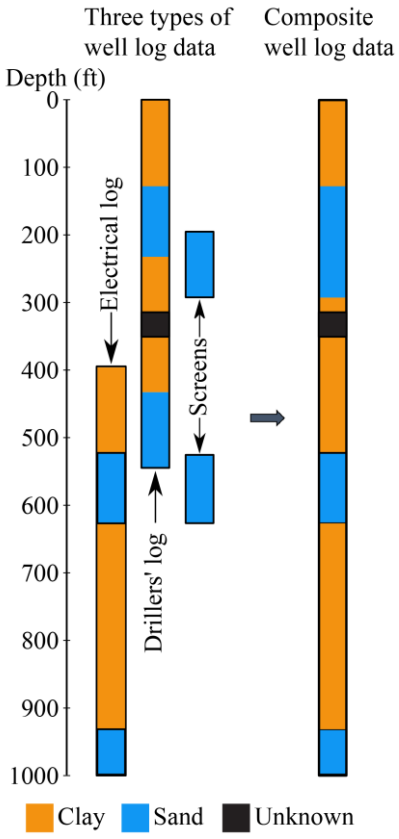

Figure 3.3. Integration of different well log data.

3.3.2. Lithofacies modeling

This study adopted the lithofacies modeling technique in Vahdat-Aboueshagh and Tsai (2021) to construct a complex stratigraphy model shown in Figure 3.4. Lithofacies modeling involves domain translation and facies interpolation. In general, strata in Louisiana have changing dips (Vahdat-Aboueshagh and Tsai, 2021). However, the Chicot aquifer system appears to be homoclinal and dip south. Therefore, the lithofacies model was constructed with the same dip direction and dip angle.

Consider a cross section in the coordinate system (x,y,z) with a changing dip angle and a number of well logs that are interpreted and labeled as a sequence of sand facies and clay facies (Figure 3.4.A). The well logs in the dipping cross section are translated to a non-dipping domain

(Figure 3.4.B) with respect to the pivot plane in a new coordinate system (x,y,w):

$$f_{(x,y,z)} \rightarrow g_{(x,y,w)} \tag{1}$$

where $f_{(x,y,z)}$ is the facies label data from well logs in the dipping domain, and $g_{(x,y,w)}$ is the facies label data of well logs in the non-dipping domain. The updip area with respect to the pivot plane is translated down and stretched from the projection top to the projection base. The downdip area with respect to the pivot plane is translated up and squeezed between the projection top and the projection base. An indicator interpolation method is performed to generate a non-dipping facies model (Figure 3.4.C):

$$\hat{g}_{(x,y,w)} = \sum_i \lambda_i g_{i\,(x,y,w)} \tag{2}$$

where $\hat{g}_{(x,y,w)}$ is the estimated facies label in the non-dipping domain, $g_{i\,(x,y,w)}$ is the facies label data from well log i in the non-dipping domain, and λ_i in the weighting coefficient for an interpolation method. Finally, the non-dipping facies model is translated back to the dipping domain (Figure 3.4.D).

$$\hat{g}_{(x,y,w)} \rightarrow \hat{f}_{(x,y,z)} \tag{3}$$

where $\hat{f}_{(x,y,z)}$ is the estimated facies label in the dipping domain.

An indicator natural neighbor interpolation method (Tsai and Li, 2009) was utilized to construct a stratigraphy model using the 29,918 well logs, the dip direction of 270° (southward), and the structure dip angle of 0.06° (Jones et al., 1956). The indictor value for sand facies is 1 and for clay facies is 0 (Pham and Tsai, 2017). A cutoff value was suggested based on the proportion of sand facies in well logs (Elshall et al., 2013). In this study, the cutoff value was 0.4 for the Chicot aquifer system. The stratigraphy model started at the land surface and extends to a depth of about 305 m (1000 ft). The study area was discretized into 56 layers. Each layer had 40,755 cells with a resolution of 1 km with varied layer thickness. A MODFLOW-2005 grid (Harbaugh, 2005)

was developed based on the stratigraphy model. Readers are referred to Pham and Tsai (2017) for the detailed MODFLOW-2005 grid generation techniques.

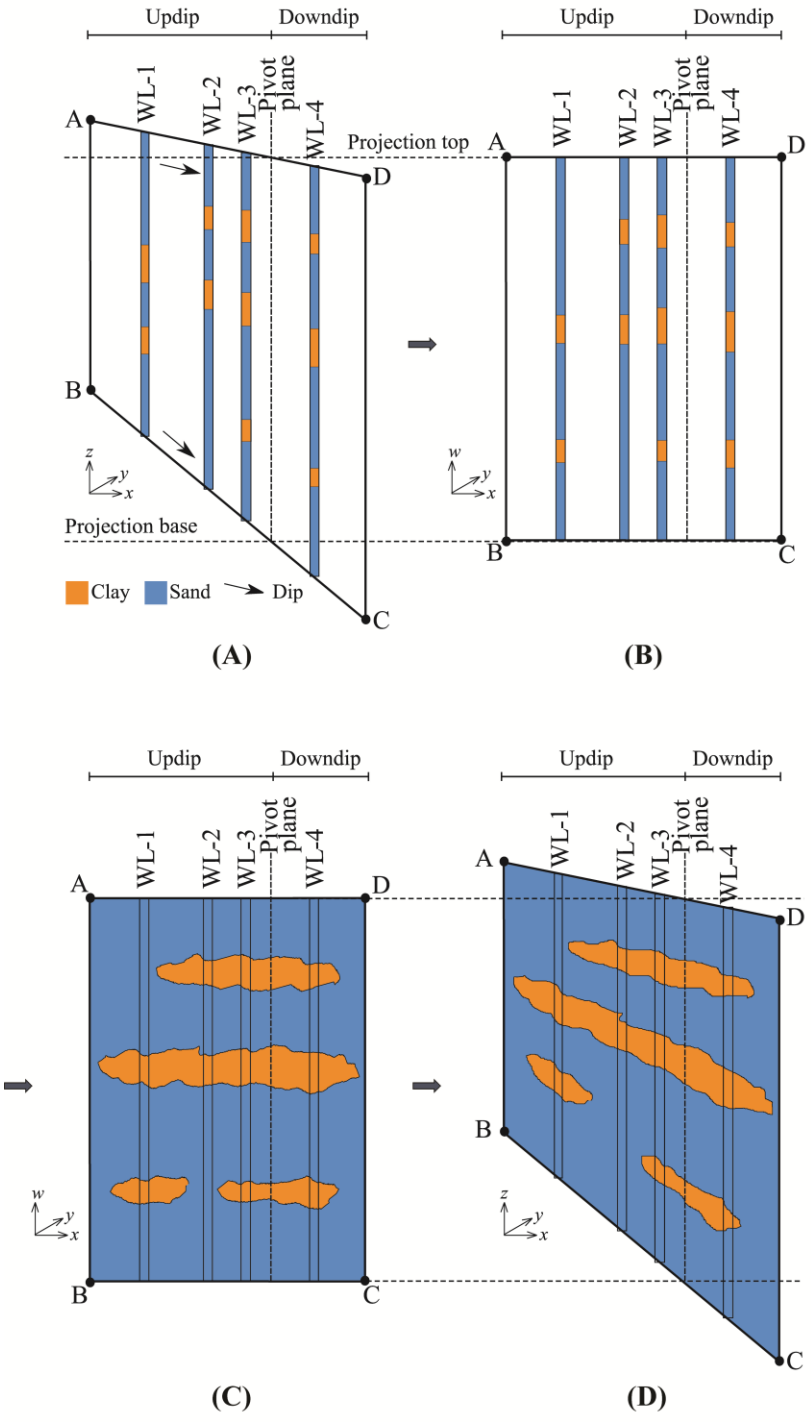

Figure 3.4. A schematic of lithofacies modeling with domain translation and facies interpolation: **(A)** well logs in a dipping domain, **(B)** well logs in a non-dipping domain, **(C)** lithofacies modeling in the non-dipping domain, and **(D)** the stratigraphy model in the dipping domain.

3.3.3. Chicot groundwater model development

Different MODFLOW-2005 packages were set up in order to develop a MODFLOW model with monthly stress periods. A River package was used to include river reaches and temporal river stages. The location of USGS stream gages is shown in Figure 3.5. A Recharge package was created based on a fraction of monthly surficial recharge rates provided by the USGS from January 2004 to December 2014 (Reitz and Sanford, 2019a). The USGS recharge rates were estimated as the residuals between water supply and the rest of water budget components (Reitz and Sanford, 2019b). A Well package was developed to include agriculture, industry, and public supply wells. A Horizontal Flow Barrier package was developed to simulate the Tepetate fault system. The lakes were not included in the groundwater model because of very limit hydraulic connection to the Chicot aquifer system (Vahdat-Aboueshagh and Tsai, 2021).

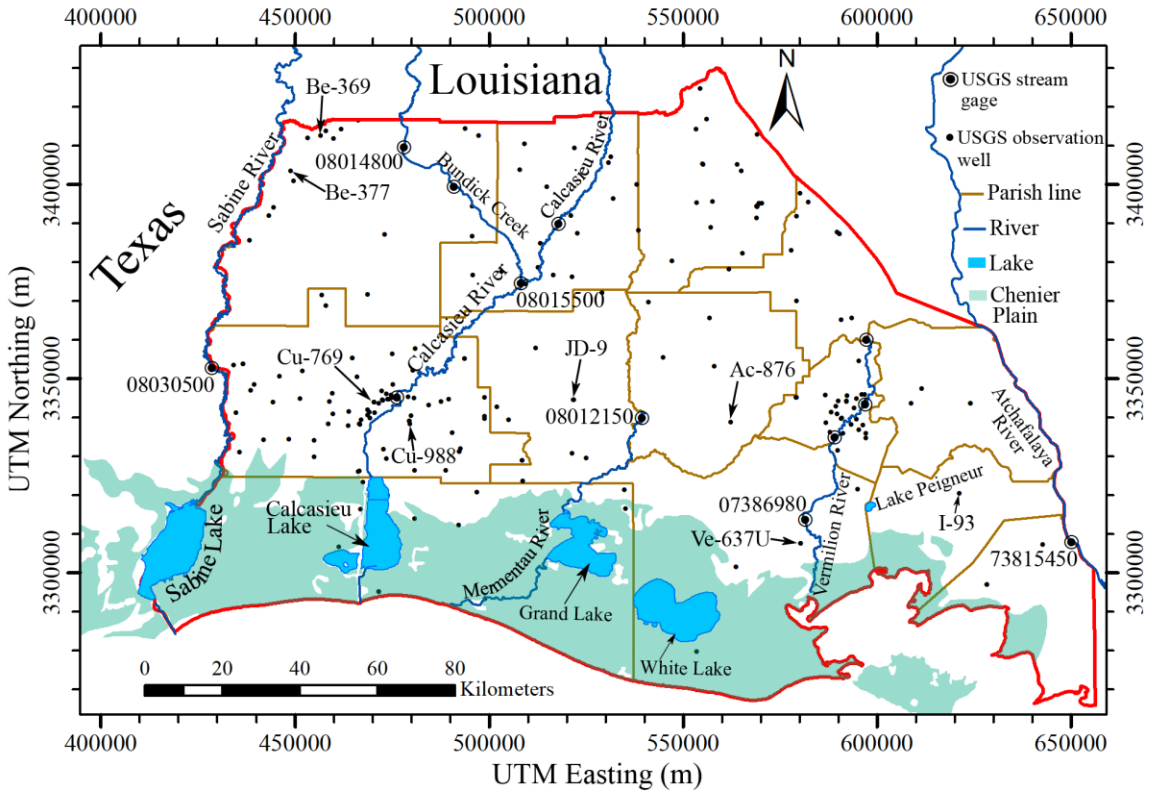

Figure 3.5. Locations of USGS stream gages and groundwater observation wells. Measured and simulated groundwater levels in the wells with well name are shown in Figure 3.6.

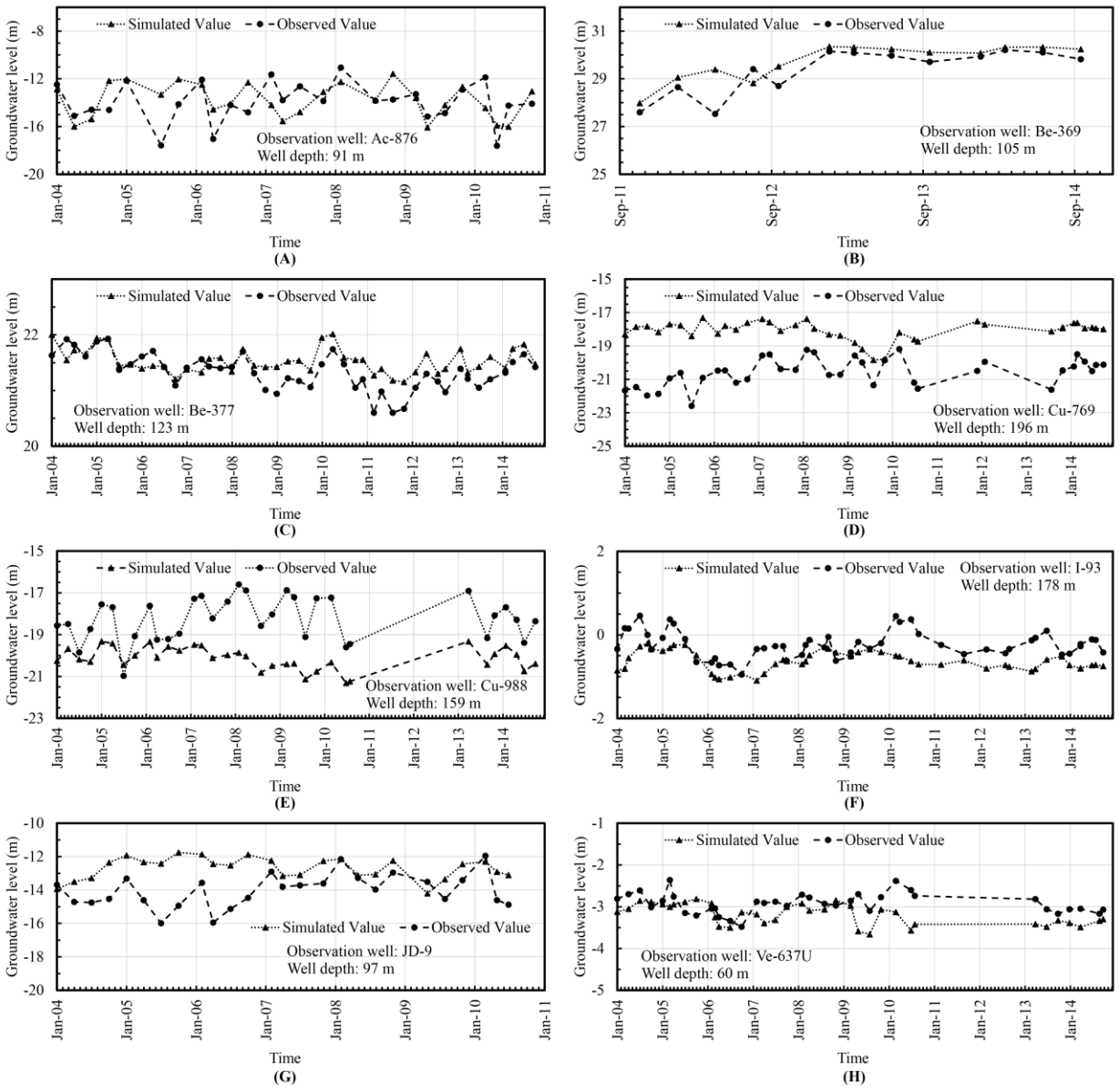

Figure 3.6. Observed and simulated groundwater levels at selected wells (see Figure 3.5 for well locations).

Historical groundwater data were prepared for the simulation period from January 1, 2004 to December 31, 2014. There were 211 USGS wells with 2,161 groundwater level data. The location of USGS observation wells is shown in Figure 3.5. The groundwater data of January 2004 were employed to determine the initial condition for the groundwater model by spatial interpolation. Groundwater observation wells close to the model boundaries were used for the

time-variant specified-head boundaries. The values of groundwater level from observation were interpolated spatially and temporally to obtain groundwater levels at different layers of the model. The temporal river stage data of Sabine River and Atchafalaya River were also used to estimate the boundary values at the stream portions. A total of 132 monthly stress periods were used in the MODFLOW model.

USGS water wells and Borrok and Broussard (2016) indicate that salt water is limited to the southern part of the Chicot aquifer system. The majority of the study region is not impacted by denser groundwater flows. Therefore, the effect of density-dependent flows was assumed insignificant. A future study may include the density effect in the vicinity of the Gulf of Mexico.

3.3.4. Model calibration with parallel computing

Model parameters to be estimated were hydraulic conductivity (K) of sand, specific storage (S_s) of sand, hydraulic conductivity of clay, specific storage of clay, river conductance for 4 rivers, a fraction of USGS surficial recharge rates, and fault hydraulic characteristic (fault permeability per unit width of a fault). This study considered heterogeneous K and S_s for sand. Other parameters were considered to be homogeneous for the purpose of simplicity. The study assumed that the USGS recharge data is only applicable to surficial sand facies that directly link to deep aquifers. Recharge to surficial clay is negligible due to very low K. We applied the pilot point approach (Doherty et al., 2010) to estimate K and S_s of sand at 57 locations of the USGS groundwater observation wells. The natural neighbor interpolation method (Watson, 1999) was used to derive spatial distribution of K and S_s of sand. In total, there were 124 model parameters to be estimated through optimization. The ranges of model parameter values in optimization are shown in Table 3.1.

Table 3.1. Ranges and estimated parameter values for the Chicot groundwater model

Parameter	Range	Estimated value
Sand hydraulic conductivity (m/day)	5 ~ 700 [1]	5 ~ 300
Sand specific storage (1/m)	$10^{-6} \sim 10^{-3}$ [2]	$10^{-6} \sim 9.56\times10^{-4}$
Clay hydraulic conductivity (m/day)	$10^{-7} \sim 10^{-2}$ [3]	10^{-4}
Clay specific storage (1/m)	$10^{-5} \sim 10^{-1}$ [4]	10^{-3}
Mermentau River conductance (m^2/day)	$5 \sim 10^4$ [5]	50
Bundick Creek conductance (m^2/day)	$5 \sim 10^4$ [5]	50
Vermilion River conductance (m^2/day)	$5 \sim 10^4$ [5]	810
Calcasieu River conductance (m^2/day)	$5 \sim 10^4$ [5]	330
Fault hydraulic characteristic (1/day)	$10^{-6} \sim 10^{-4}$ [6]	5×10^{-4}
Fraction of USGS surficial recharge rate	0.0 ~ 1.0	0.30
Sand specific yield	0.15 ~ 0.35 [7]	0.30
Clay specific yield	0.00 ~ 0.07 [7]	0.05

[1]Rahman et al. (2008), [2]Nyman et al. (1990), [3]Daniel, (1984), [4]Younger (1993), [5]Cousquer et al. (2017), [6]Elshall et al. (2015), [7]Johnson (1967).

The Chicot groundwater model was calibrated using the parallel CMA-ES (Elshall et al., 2015) approach to minimize the root mean square error (RMSE) (Chai and Draxler, 2014) between the 2,161 observed and simulated groundwater levels:

$$\min_{\boldsymbol{p}} \text{RMSE} = \sqrt{\frac{1}{L}\sum_{i=1}^{L}[h_i(\boldsymbol{p}) - h_i^{obs}]^2} \tag{4}$$

where h_i and h_i^{obs} represent the i^{th} simulated groundwater level and the i^{th} observed data, respectively, L is the number of observed data, and $\boldsymbol{p}$ is a set of model parameters.

The Nash–Sutcliffe model efficiency coefficient (NSE) was used to evaluate the model calibration result.

$$\text{NSE} = 1 - \frac{\sum_{i=1}^{L}(h_i - h_i^{obs})^2}{\sum_{i=1}^{L}(h_i^{obs} - \bar{h}^{obs})^2} \tag{5}$$

where $\bar{h}^{obs}$ is the mean of the observed groundwater data.

Parallel computation was performed on a supercomputer that has 380 nodes. Each node has 16 processors. A population size of 1,240, a tenfold size of unknown parameters recommended by Pham and Tsai (2017), was used. The computation time for each model run was about 50

minutes on a 2.6 GHz Xeon 64-bit Processor. To maximize the computational efficiency, this study ran the parallel CMA-ES code on 1,240 processers. The data-model processes are presented in the flowchart, Figure 3.7.

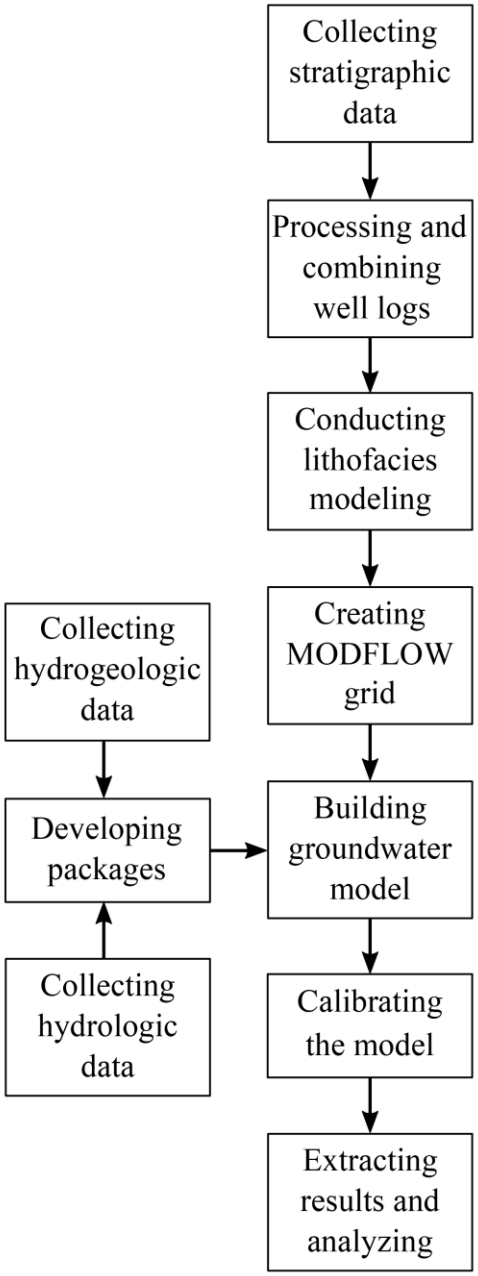

Figure 3.7. A flowchart of groundwater model development with stratigraphy data, hydrogeologic data and hydrologic data.

3.4. Results and discussions

3.4.1. Stratigraphy reconstruction

A stratigraphy model of 56 non-uniform model layers was constructed for the Chicot aquifer system. The layer thickness varied from 2.2 m to 10.4 m. The distributions of surficial sand facies and surficial clay facies at land surface are shown in Figure 3.8.A. Around 7% of the model domain is covered by the surficial sand facies. The surficial sand facies appear to the northern area, which is the essential recharge zone for the Chicot aquifer system (Jones et al., 1956). The surficial sand facies are also seen in the vicinity of the Sabine River in the northwest.

The north-south cross sections AA′, BB′, and CC′ (Figure 3.8.B-D) show the surficial clay thickening toward the Gulf of Mexico. Most of the surficial sand facies in the north connect to the Chicot aquifer system, where precipitation and streams recharge the aquifer system. The Chicot aquifer system encompasses seven aquifers (Nyman et al., 1990): the Upper Chicot and the Lower Chicot aquifers in the east, the Undifferentiated sand in the central area, and the Shallow sand, the "200-foot" sand, the "500-foot" sand and the "700-foot" sand in the west. The late Pleistocene-Holocene Shallow sand in the west (AA′ and EE′ cross sections) is underlain by the Pleistocene "200-foot" sand, the "500-foot" sand, and the "700-foot" sand (Nyman et al., 1990). The Shallow sand is sparsely interbedded in the top confining clay layer and has limited spatial extent, implying that the Shallow sand is not as productive as the other sand aquifers. The three sands grade from a fine-medium sand to coarse gravel (Nyman et al., 1990). They are separated by interbedded clays in a few areas, but are connected in the most areas.

The "200-foot" sand, the "500-foot" sand, and the "700-foot" sand (EE′ and FF′ cross sections) merge into the late Pleistocene Undifferentiated sand in the center of the aquifer system (Nyman et al., 1990). The Undifferentiated sand links to the Upper Chicot aquifer and Lower

Chicot aquifer in the central and south of the aquifer domain. The Undifferentiated sand is much thicker than other sands in the aquifer system. The Pleistocene Upper Chicot and Lower Chicot aquifers are separated by clay beds as thick as 30 m (100 ft) in a few areas. The clay beds are not extensive (Williams and Duex, 1995). In general, sands in the north are relatively shallow and often interbedded with clays. Sands thicken and clays pinch out from the north to the south.

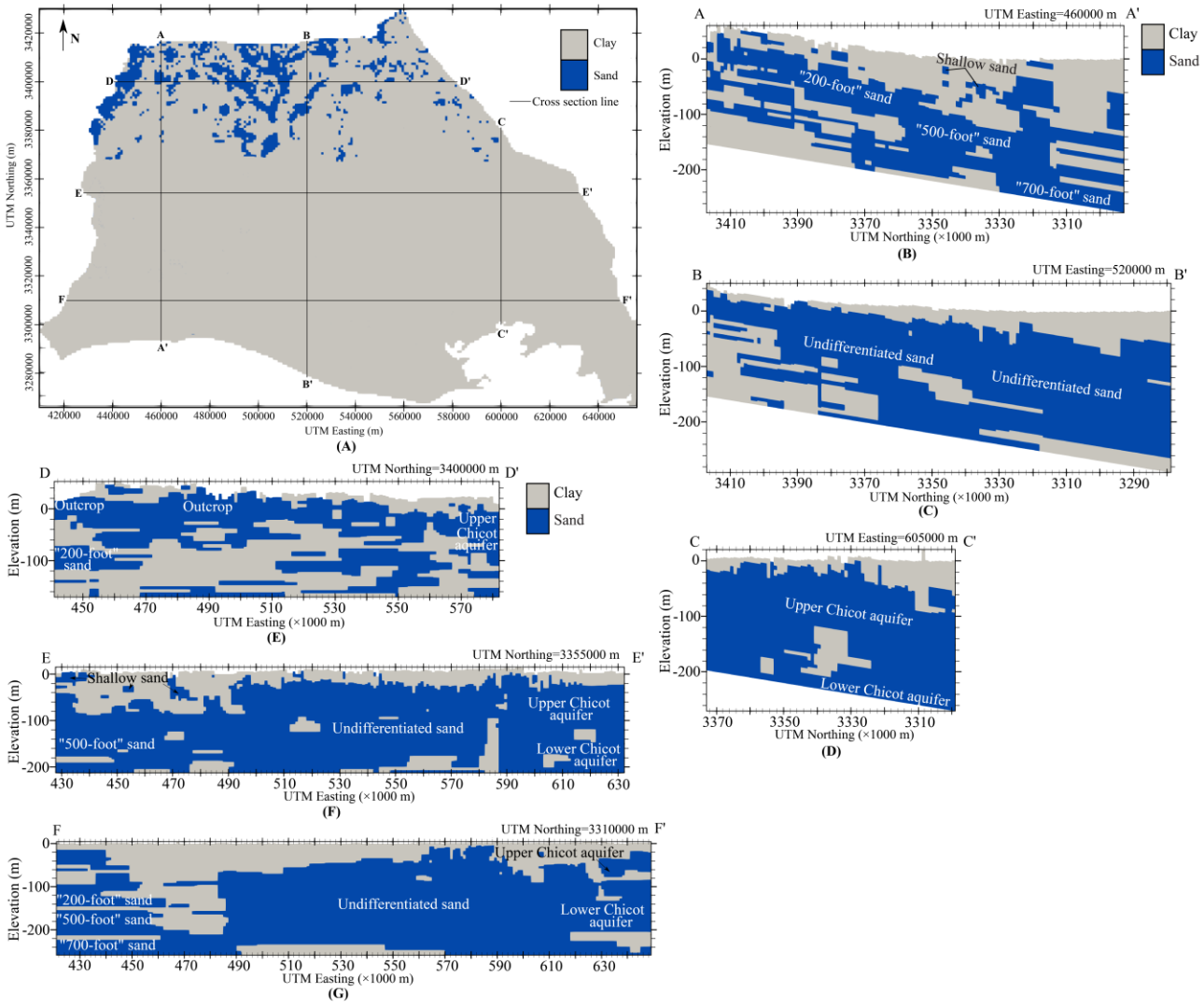

Figure 3.8. The Chicot stratigraphy model: **(A)** distributions of surficial sands and surficial clays, **(B)-(D)** north-south cross sections, and **(E)-(G)** east-west cross sections. The cross sections are magnified 50 times in vertical direction. The vertical datum is NAVD 88.

3.4.2. Model calibration result

The model calibration was completed in 300 hours with the parallel CMEA-ES code and 1,240 processors. The estimated model parameter values are shown in Table 1. In general, the simulated groundwater levels show good agreement in terms of value, trend, or pattern with respect to the observed groundwater levels (Figure 3.9). The root mean square error is 2.14 m. The Nash–Sutcliffe model efficiency coefficient (NSE) of 0.98 indicates a good calibration result. However, it is understood that data uncertainty and model error do exist. The groundwater model could not perform satisfactorily at few observation wells. Comparisons of observed and simulated groundwater levels at selected wells (Figure 3.5) with long records are shown in Figure 3.6. The model calibration result shows that 30% of the USGS surficial recharge amounts (Reitz and Sanford, 2019b) became groundwater recharge to the Chicot aquifer system. The mean monthly surficial recharge rates to the outcrop zone for each quarter in a year are shown in supplementary Figure 3.10.

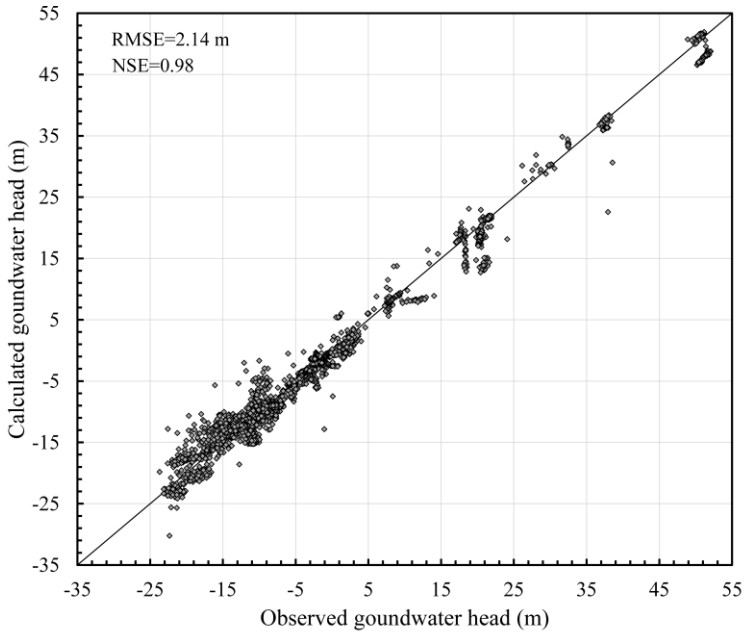

Figure 3.9. Scatter plot of observed groundwater levels versus calculated groundwater levels in 2004-2014. The groundwater level datum is NAVD 88.

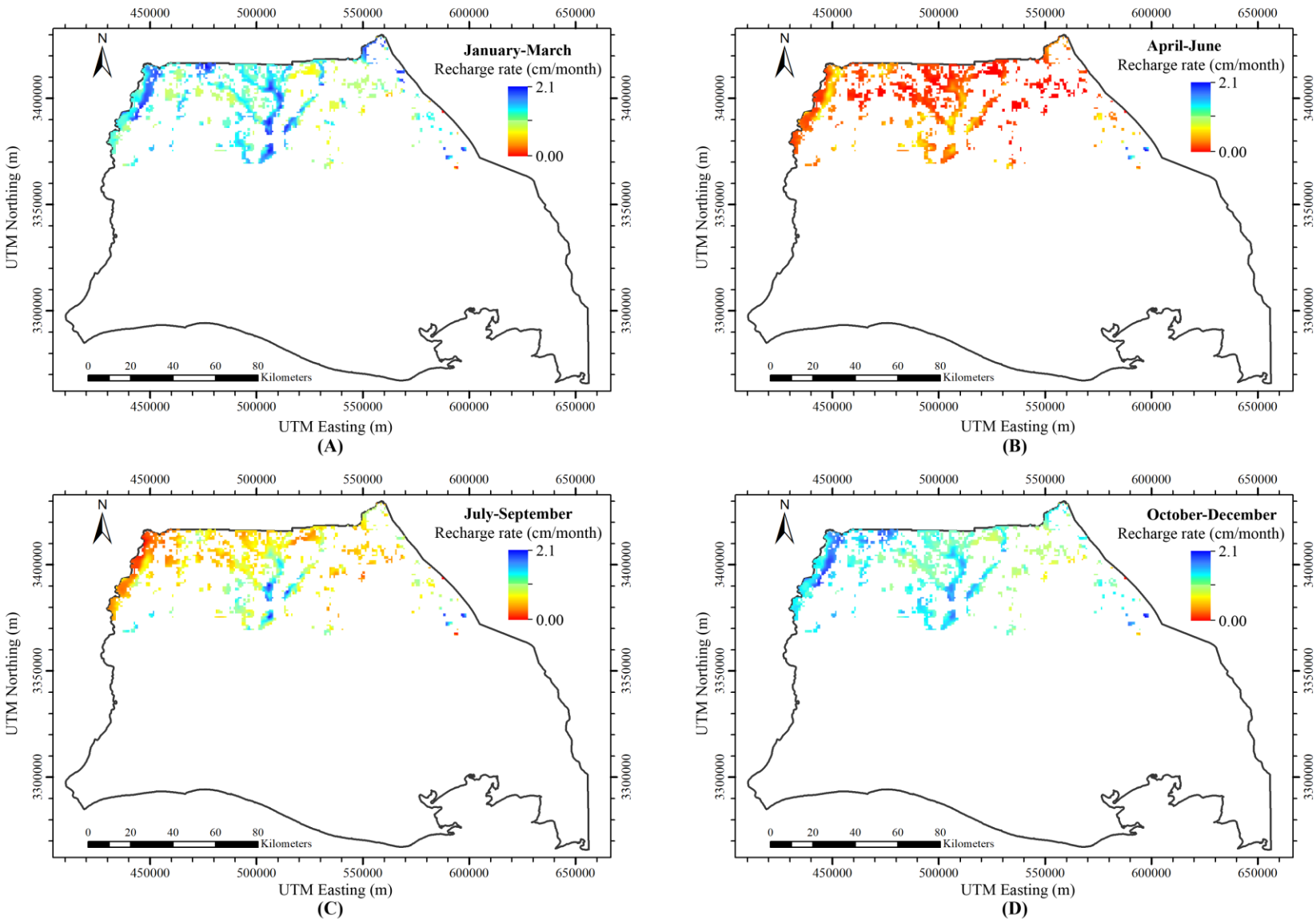

Figure 3.10. Spatial distributions of averaged surficial recharge rates (cm/month) for each quarter of a year.

3.4.3. Temporal water budget analysis

The water budget of the Chicot aquifer system was analyzed by investigating the storage change from January 2005 to December 2014 with respect to the initial storage in January 2005. The model data prior to 2005 was not analyzed in order to skip the influence from the initial condition. Figure 3.11.A shows the cumulative storage change, the monthly storage change, and the monthly pumpage. The average monthly net gain in aquifer storage was estimated about three million m^3. By the end of 2014, groundwater storage gain was estimated 350 million m^3 with respect to the initial storage in January 2005. However, this storage gain was not significant, on average about 1-mm groundwater level increase across the entire domain per year. The storage increase is likely attributed to groundwater recharge increase and pumping decrease. Groundwater recharge to the Chicot aquifer in 2004-2015 (Reitz and Sanford, 2019b) was estimated about 2.4 times greater than that in 1951-1980 (Wolock, 2003). In addition, groundwater pumping decreased from year 2000 to year 2010 by 18% according to Sargent (2011). The model shows slight decrease in storage during the March-July period due to pumping activities in the rice growing season. The aquifer system is quickly replenished during the non-irrigation season owing to the high transmissivity in the pumping areas (Hartono, 2005). The analysis of annual net groundwater inflows and outflows (Figure 3.11.B) shows that the effect of pumping is virtually counteracted by inflows from boundaries, surficial recharge, and rivers.

The concept of safe yield or sustainable yield, where groundwater withdrawals do not exceed surficial recharge rate, has been criticized (Alley et al., 2002) and may not be applicable to the Chicot aquifer system. Instead, the concept of “capture” may be proper to explain the sustainability of the Chicot aquifer, where all the contributing factors to the storage change should be taken into account (Bredehoeft, 2002; Zhou, 2009).

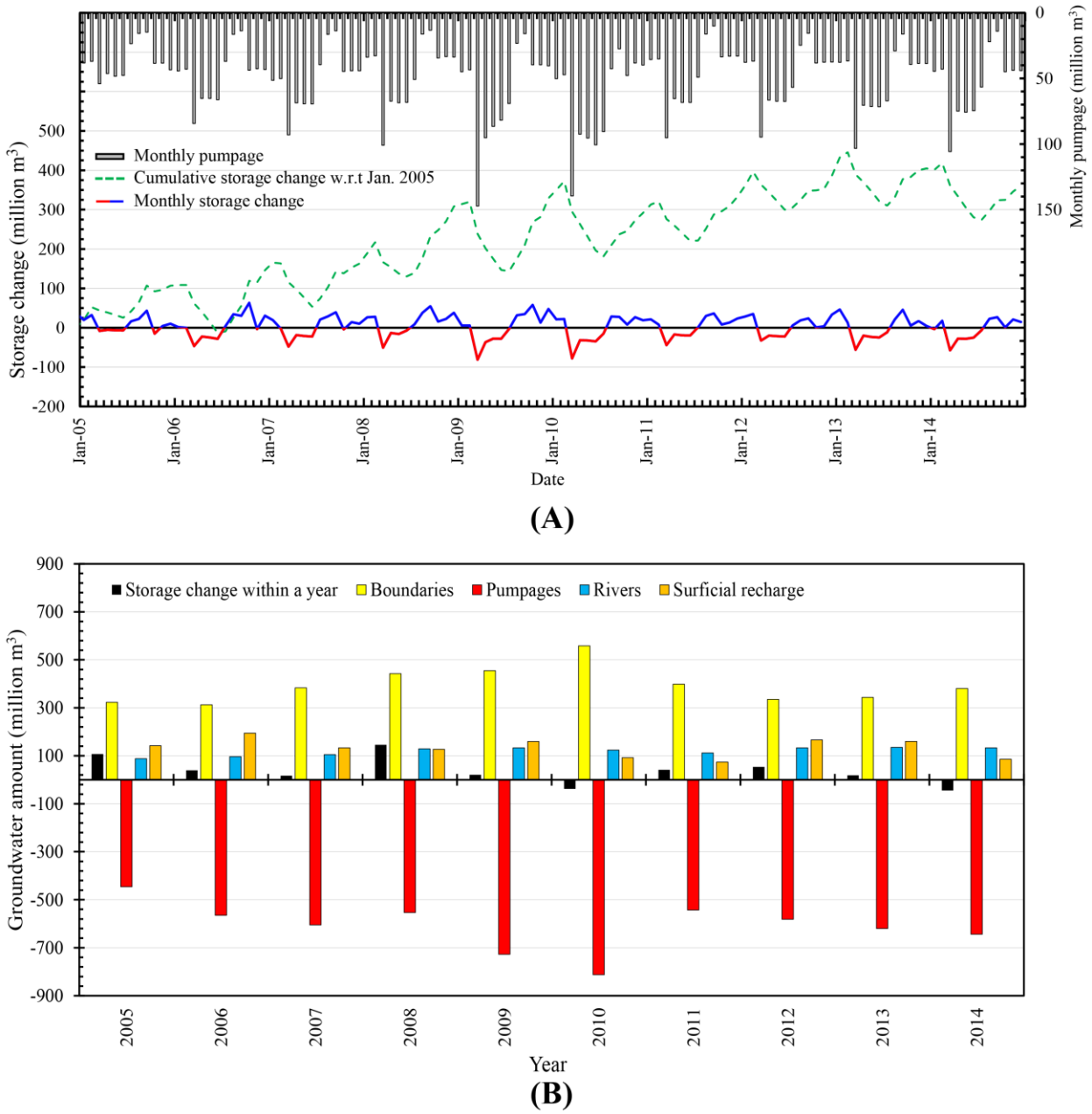

Figure 3.11. Estimated groundwater budget for the Chicot aquifer system: **(A)** monthly pumpage (million m^3), monthly storage increase/decrease (million m^3), and cumulative groundwater storage change (million m^3) with respect to January 2005, and **(B)** annual net groundwater inflow/outflow (million m^3) from the model boundaries, the pumping wells, the rivers, and the surficial recharge along with annual groundwater storage change (million m^3).

3.4.4. Groundwater level analysis

The contour map of groundwater levels in 4-m intervals at the end of December 2014 is shown in Figure 3.12.A. The values were calculated by averaging groundwater levels vertically along different model layers. The groundwater level varies from 40 m above the vertical datum NAVD 88 in the north to 20 m below the NAVD 88 in the industrial area. There are two cones of depression. One is in the agricultural area in the east and the other is in the industrial area in the west. The groundwater level distribution pattern in Figure 3.12.A aligns well with the USGS reports (Fendick and Nyman, 1987; Lovelace et al., 2004).

In order to better understand how the pumping activity has altered the groundwater flow in the predevelopment condition, the groundwater model was run without pumping. Figure 3.12.B shows the contour map of groundwater levels at the end of December 2014. The groundwater level pattern resembles the predevelopment groundwater levels according to Martin and Whiteman (1989). The differences between Figure 3.12.A and Figure 3.12.B imply that the pumping activity has reversed the groundwater flow from a gulfward direction to a landward direction. As Jasechko et al. (2020) has shown, the saltwater intrusion in Southwest Louisiana can be connected to groundwater level decline in inland areas. However, the origin of the salt water is not the Gulf of Mexico as they argued. Indeed, since the sand beds of the Chicot aquifer system dip at a greater angle than the Continental Shelf slope, a direct connection between the aquifer system and Gulf of Mexico is not possible (Martin and Whiteman, 1989). The salt water in the Chicot aquifer system is of ancient origin when the sea level rose and resulted in landward deposition of marine environments (Weiss, 1990).

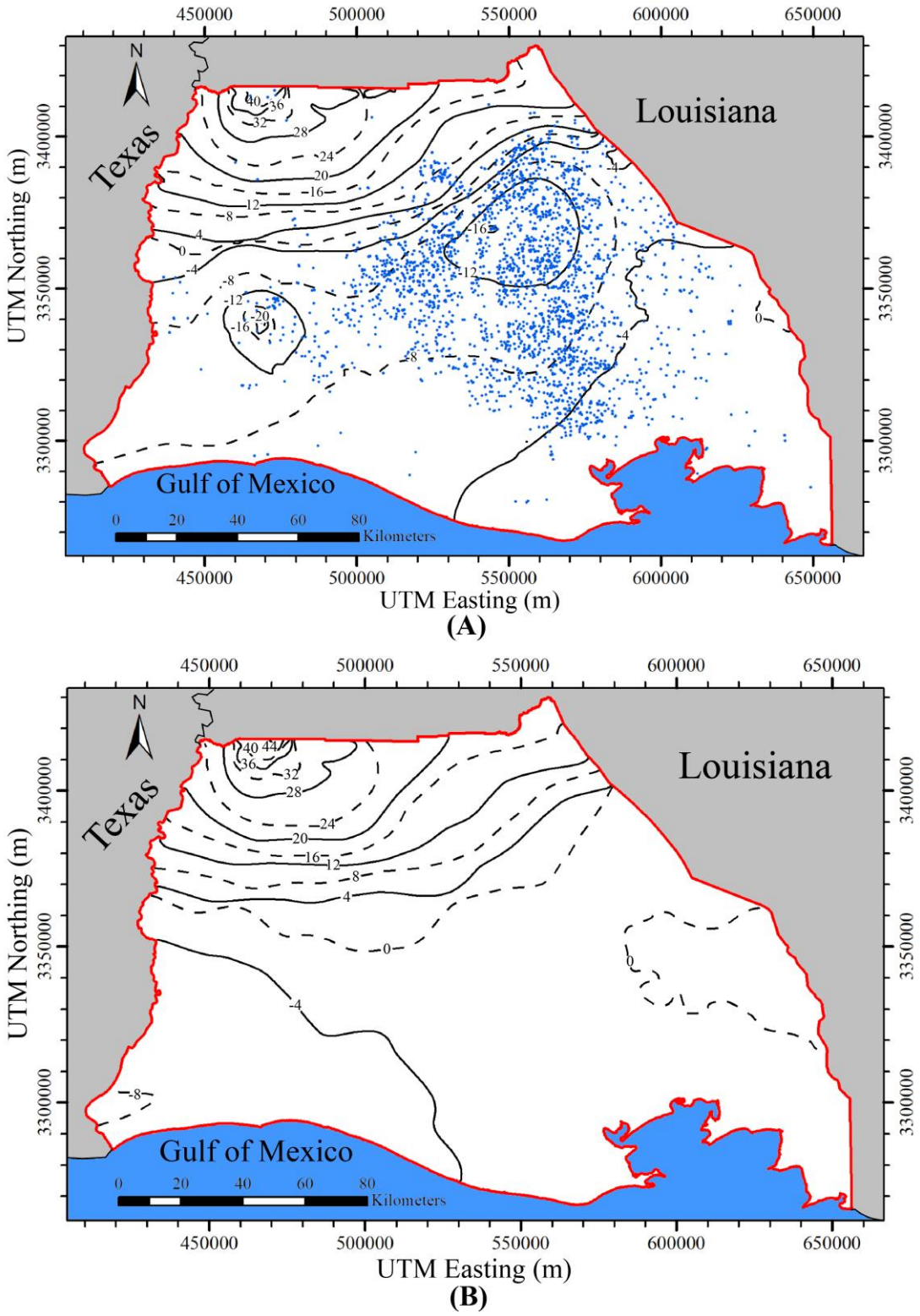

Figure 3.12. Groundwater level map of December 31, 2014 for the Chicot aquifer domain: **(A)** with pumping, and **(B)** without pumping. The groundwater level datum is NAVD 88.

To further analyze the groundwater flow pattern in the Chicot aquifer system, the average groundwater levels were obtained in three zones shown in Figure 3.13. The zones were defined based on the stratigraphy model and groundwater level variations in different model layers. Zone 1 includes the "200-foot" sand, the "500-foot" sand, and the "700-foot" sand in the west. Zone 2 is for the Undifferentiated sand in the central area. Zone 3 includes the Upper Chicot aquifer and Lower Chicot aquifer in the east.

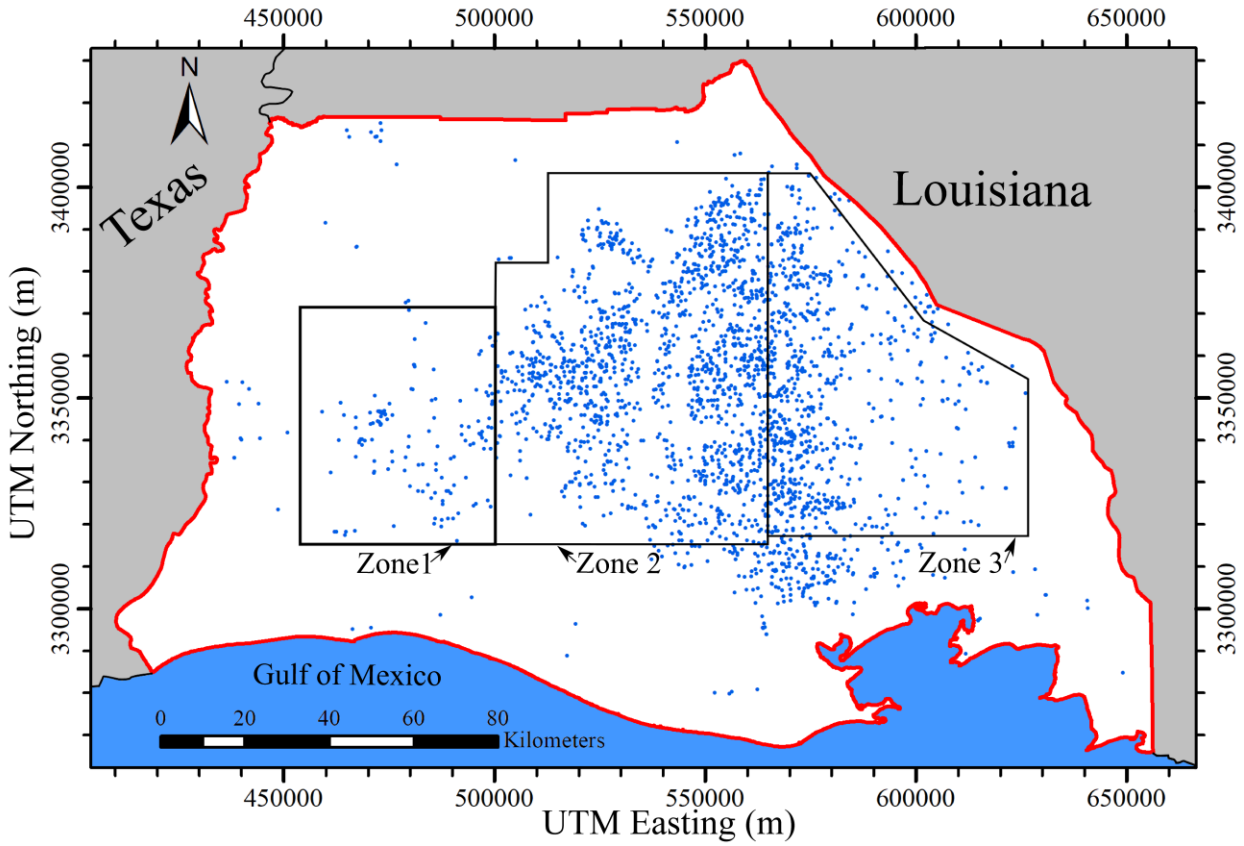

Figure 3.13. Delineation of three zones, where Zone 1 includes the "200-foot" sand, the "500-foot" sand, and the "700-foot" sand, Zone 2 includes the Undifferentiated sand, and Zone 3 includes the Upper Chicot aquifer and Lower Chicot aquifer. Blue dots are pumping wells.

Monthly average groundwater levels in 2005-2014 in different sand systems are shown in Figure 3.14.A. The average groundwater level in the Undifferentiated sand is always less than that in the Upper Chicot and Lower Chicot aquifers, indicating that groundwater generally flows from

the Upper Chicot and Lower Chicot aquifers into the Undifferentiated sand. The heavier pumping in the Upper Chicot sand made the average groundwater level in the Upper Chicot aquifer lower than that in the Lower Chicot aquifer. The seasonal groundwater level decline and recovery in the Upper Chicot aquifer, the Lower Chicot aquifer, and the Undifferentiated sand correspond to the seasonal agriculture pumping. Figure 3.14.A shows fast groundwater level recovery during the non-irrigation season. The low groundwater level variation in the "200-foot" sand, the "500-foot" sand, and the "700-foot" sand shows that groundwater levels in the west are mildly affected by the agricultural pumping. Figure 3.14.A shows downward gradients from the "200-foot" sand to the 500-foot sand and slight upward gradients from the "700-foot" sand to the "500-foot" sand. This verifies the fact that the "500-foot" sand is the most pumped sand in the west.

Groundwater depletion in the Chicot aquifer system (Konikow, 2013) mainly occurs in the agricultural zones as shown in Figure 3.14.B, which reflects the groundwater level decline in Figure 3.14.A. By the end of 2014, groundwater storage depletion was estimated about 45 million m^3 in the Undifferentiated sand and about 35 million m^3 in the Upper Chicot aquifer and the Lower Chicot aquifer with respect to the beginning of 2005. Groundwater storage depletion by the industrial pumping is insignificant during 2005-2014.

A schematic view of flow directions and average flowrates between different sands in 2005 to 2014 is shown in Figure 3.15. The highest vertical groundwater flows occur between the Upper Chicot aquifer and the Lower Chicot aquifer, and between the "500-foot" sand and the "700-foot" sand. The dominant vertical flow directions indicate that potential salt water may vertically migrate from deep brackish formations to the Upper Chicot in the east and to the "500-foot" sand in the west. The highest horizontal groundwater flows are westward from Zone 3 to Zone 2. The overall horizontal flow is westward.

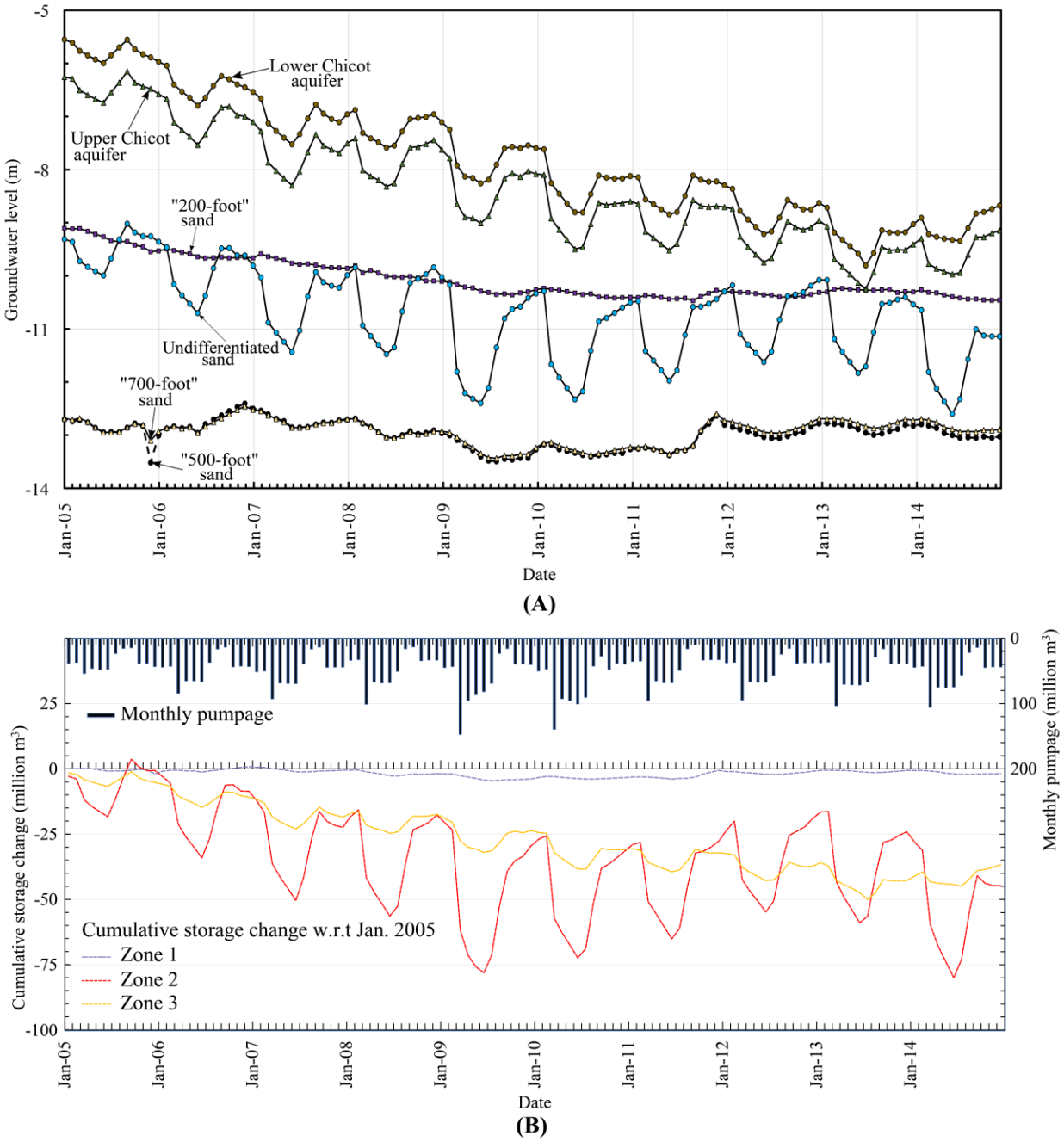

Figure 3.14. (A) Mean monthly groundwater level (m) in different sands of the Chicot aquifer system from January 2005 to December 2014. The groundwater level datum is NAVD 88, and **(B)** estimated cumulative groundwater storage change (million m^3) with respect to January 2005 for Zone 1, 2, and 3, and monthly pumpage (million m^3).

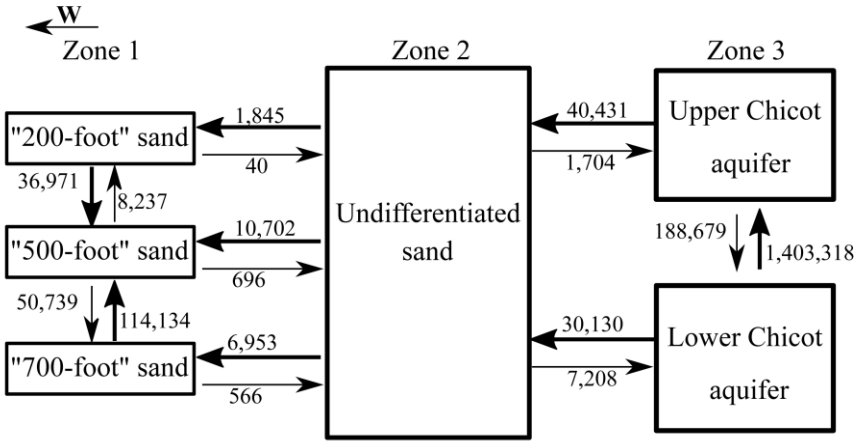

Figure 3.15. Flow directions and mean flow rates (m^3/day) in 2005-2014 between different sands in the Chicot aquifer system.

The intra-annual monthly average groundwater levels in different sands are shown in Figure 3.16. The average groundwater levels drop in the Undifferentiated sand, Upper Chicot aquifer and Lower Chicot aquifer during the rice irrigation season, which accords with the fact that most of the wells in these sands are for rice irrigation. However, the relatively stable average monthly groundwater levels in the "200-foot" sand, the "500-foot" sand, and the "700-foot" sand were due to the year-round continuous groundwater pumping by the industries.

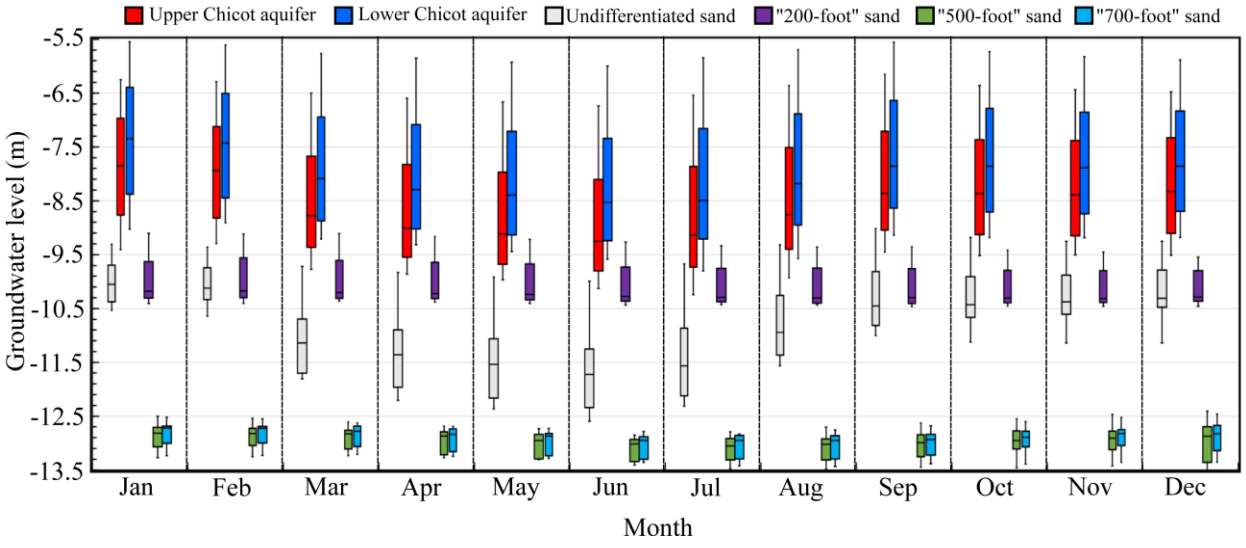

Figure 3.16. Intra-annual monthly groundwater level variation for different sands in the Chicot aquifer system from 2005 to 2014. The groundwater level datum is NAVD 88.

3.5. Conclusions

The methodology in this study can consider structural dip information, build realistic groundwater models using big well log datasets and reveal aquifer complexity. The methodology was successfully applied to discovering Chicot aquifer complexity and developing a detailed Chicot groundwater model for the agriculture-intensive southwestern Louisiana, where the Chicot aquifer system is under high stress by irrigation pumping. More than 29,000 well logs in Southwest Louisiana were interpreted and prioritized. Prioritizing electrical logs, well screens, and drillers' logs in this order helps reduce errors in the lithofacies modeling as electrical logs have better quality than drillers' logs. The developed Chicot model is one of few models that reveals hydrogeological complexity in the Coastal Lowlands aquifer system.

The Chicot stratigraphy model reveals that the aquifer system consists of highly interconnected sand units and outcrops in the north. Central and southern areas are covered by clays thickening toward the Gulf. Sand units are relatively thin in the north and are frequently interbedded by clays. Sand units are thick in the central and southern areas. The Upper Chicot aquifer and the Lower Chicot aquifer are interconnected in the east. The "200-foot" sand, the "500-foot" sand, and "700-foot" sand are interconnected in the west. The Undifferentiated sand is thick in the central area. These aquifers are laterally connected.

The groundwater modeling result shows that the storage loss due to groundwater pumping in the Chicot aquifer system is offset by inflows from surficial recharge, rivers and boundaries. The two large cones of depression created by the agricultural pumping in the east and by the industrial pumping in the west represent the key feature in the Chicot aquifer system. The storage loss occurs during the rice irrigation season. The aquifer system can be quickly replenished by the

inflows during the non-irrigation season. The storage of the Chicot aquifer system was estimated to slightly increase during the period 2005-2014.

The groundwater model shows that groundwater levels in the Lower Chicot aquifer, the Upper Chicot aquifer, the Undifferentiated sand are heavily impacted by the seasonal irrigation activities and result in groundwater storge depletion. On the contrary, groundwater levels in the "200-foot" sand, the "500-foot" sand, and "700-foot" sand have less variability. In other words, groundwater levels in the west are not heavily impacted by the irrigation activities.

The groundwater model indicates large amounts of upward vertical flows from the Lower Chicot aquifer to the Upper Chicot aquifer and from the "700-foot" sand to the "500-foot" sand. As salt water was reported at the base of the Chicot aquifer system, potential saltwater intrusion due to vertical saltwater migration from the deeper sands is likely to occur in the future.

Chapter 4. Multi-Objective Aquifer Storage and Recovery Operation Optimization with Surrogate Modeling under Uncertainty

4.1. Introduction

Aquifer storage and recovery (ASR) is a method to store excess water into aquifers via artificial recharge (Forghani, 2018). The recharge can be through a mechanism such as injection wells, infiltration basins, galleries for reclaimed water and stormwater, and water from other aquifer systems (Sheng, 2005; Dillon et al., 2009). There are major phases in ASR operations: 1) storage phase, and 2) recovery phase. The ASR can be classified as a category of managed aquifer recharge (MAR) (Maliva, 2014). What differentiates the ASR from other MAR is the recovery phase when the mixed recharged water and native water is extracted from aquifer. For ASR, a recharge (injection) period is normally followed by a recovery (extraction) period. This study focuses on an ASR operation where the storage phase and recovery phase are designed through injection of non-native water into the aquifer and extraction of groundwater from the aquifer using an ASR operation well. Figure 4.1 shows an ASR operation well for one injection season (Figure 4.1.a) followed by one pumping season (Figure 4.1.b). The process of water injection raises the groundwater level at the injection point and around the well. The groundwater level (pressure head) rise leads to an outward gradient from the ASR well. This mechanism can be used to force away brackish/saline water in aquifers which have saltwater encroachment problem (Shammas, 2008; Pyne, 2015). The rise in groundwater level may also help to alleviate land subsidence in coastal area where land loss is a core issue (Lu et al., 2011). In addition to acting as a hydraulic barrier, an ASR well is mostly used for storing surface water into aquifers in a wet season and pumping water in a following dry season (Forghani and Peralta, 2017). There may be other benefits from an ASR project such as agricultural water supply, restoration of groundwater levels, and reduction of environmental effects of streamflow diversions (Pyne, 1995; Khan et al., 2008).

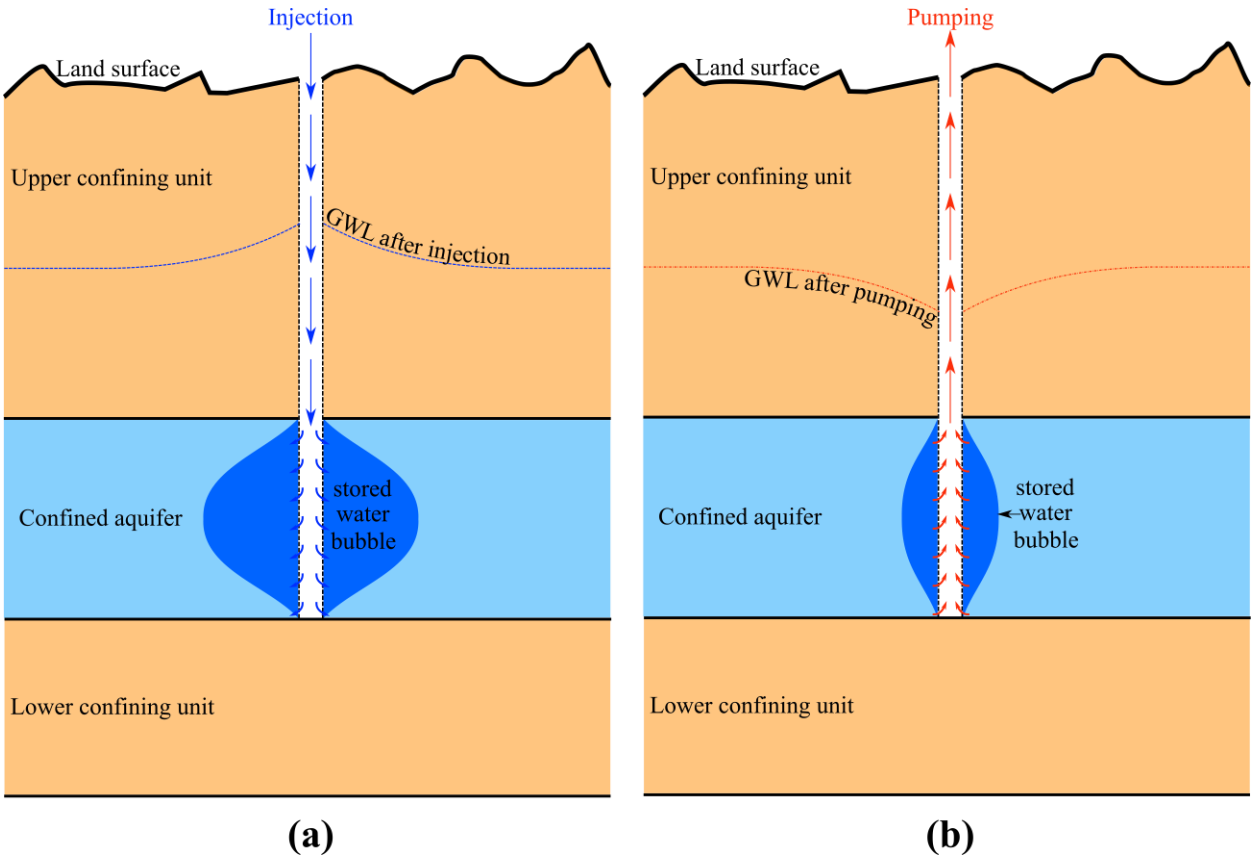

Figure 4.1. A schematic view of an ASR operation for one ASR cycle in **(a):** injection season, and **(b):** in pumping season. The groundwater level and ASR operation in the injection season and pumping season are designated by blue color and red color, respectively. GWL: groundwater level.

Planning and design of ASR operations normally include the amount of stored water and amount of withdrawn water (Uddameri, 2007). The optimal costs of ASR operations also have gained attention. Although there may be many components to an ASR operation in terms of capital costs and maintenance/operation costs (Almulla et al., 2005), the costs of ASR operation may include the pumping cost, injection cost, and surface water treatment which will be recharged into the aquifer (Triki et al., 2019). The ASR operations may also be designed through multiple wells (Merritt, 1986). The wells may either be single-purpose wells, where the water is solely injected into the aquifer or solely pumped out of the aquifer, or dual-purpose wells, used for both injection and pumping (Zuurbier et al., 2014; Sultana et al., 2015). One of the aspects which has been less

paid attention to is the scheduling of injection period and pumping period. The concept of an ASR cycle can be used for scheduling injection and pumping activities (Merritt, 1986). The performance of an ASR cycle can be quantitatively evaluated through the established concept of recovery efficiency (Lowry and Anderson, 2006; Ward et al., 2009; Lu et al., 2011; Guo et al., 2015; Forghani and Peralta, 2017).

Recovery efficiency is the fraction of injected water (injectate) being extracted out of an aquifer during the pumping period. To calculate recovery efficiency, injectate needs to be tracked during the ASR cycle. Solute transport models are normally coupled with groundwater flow models to track injectate (Lowry and Anderson, 2006). The basic assumption in this approach is to assume a non-zero solute concentration for injectate while considering a zero concentration for native water in the aquifer (Forghani and Peralta, 2018). Previous studies have shown that the density effect (buoyancy effect) can be ignored as long as dispersive mixing is dominant and difference between injectate and native water is not high (Pavelic et al., 2006; Ward et al., 2007; Ward et al., 2009; Minsley et al., 2011). Hence, groundwater flow modeling with constant fluid density is suitable for the ASR operation assessments.

Hydrogeological parameters in groundwater flow models and dispersion parameters in solute transport models introduce uncertainty into recovery efficiency calculation. It is a common practice to generate parameter realizations based on probability distribution of parameters and conduct statistical analysis of model outputs in evaluating uncertainties (Fu and Gómez-Hernández, 2009; Refsgaard et al., 2012). However, groundwater flow models and transport models are often computationally expensive. Uncertainty quantification can become intractable without the aid of techniques such as surrogate modeling which mimics the behavior of flow and transport models (Keating et al., 2010; Razavi et al., 2012). Artificial neural networks (ANN)

based surrogates have been demonstrated to be a powerful substitute for groundwater flow and transport models (Yan and Minsker, 2006; Yan and Minsker, 2011; Luo and Lu, 2014).

This study introduces a supervised learning method with an evolutionary optimization algorithm to optimize an ASR operation under parameter uncertainty. Objectives in the ASR operation are to maximize the amount of injectate into the aquifer during the injection season and to maximize the recovery efficiency during the pumping season. Uncertainty of the Pareto front of the two objectives comes from uncertainty of hydrogeological and dispersion parameters. To facilitate ASR operation optimization under uncertainty, a supervised artificial neural network (ANN) method is employed to substitute the groundwater model and the transport model. This study is organized as follows. Section 2 introduces the methodology including uncertainty assessment and application of a supervised ANN in optimization as well as formulation of the optimization problem. Section 3 introduces the study area. Section 4 explains how to build groundwater flow model, transport model, and ANN model. Section 5 discusses the results. Section 6 concludes this study.

4.2. Methodology

4.2.1. Formulation of ASR operation optimization

Performance of an ASR well is evaluated in one ASR cycle which includes one injection season and one pumping season. Figure 4.2 shows one ASR cycle. The injection season starts at t_0 and ends at t_1. The pumping season immediately follows the injection season and ends at t_2. The injection rates are constrained between $I_{\min}$ and $I_{\max}$, and pumping rates are constrained between $Q_{\min}$ and $Q_{\max}$. The ASR well is allowed to be inactive (injection rate or pumping rate to be zero). The bi-objective ASR operation optimization are defined as follows

$$\max \quad f_1 = \sum_{t=1}^{t_1} \Delta_t u_t I_t \tag{4-1}$$

$$\max \quad f_2 = \frac{\sum_{t=t_1+1}^{t_2} \Delta_t v_t Q_t C_t}{\sum_{t=0}^{t_1} \Delta_t u_t I_t C^0} \tag{4-2}$$

Subject to

$$I_t = \begin{cases} I_t, \text{ if } h_{t-1} < h_{\max} \\ 0, \text{ otherwise} \end{cases} \tag{4-3}$$

$$Q_t = \begin{cases} Q_t, \text{ if } h_{t-1} > h_{\min} \\ 0, \text{ otherwise} \end{cases} \tag{4-4}$$

$$I_{\min} \le I_t \le I_{\max} \tag{4-5}$$

$$Q_{\min} \le Q_t \le Q_{\max} \tag{4-6}$$

$$\sum_{t=t_0}^{t_1} u_t \ge 1 \qquad \sum_{t=t_1+1}^{t_2} v_t \ge 1 \qquad \forall u_t, v_t \in \{0,1\} \tag{4-7}$$

where Δ_t is the time interval of stress period *t* (day). I_t and Q_t denote the injection rate (m^3/day), the pumping rate (m^3/day) at stress period *t*, respectively. C_t is the concentration of injectate at the end of stress period *t*, respectively. C^0 is the concentration of injectate during the injection period. h_t is the groundwater level (m) at the end of stress period *t*. u_t and v_t are binary variables to indicate activeness of injection rates and pumping rates, respectively. When u_t is 1, injection is permitted, and injection is prohibited when u_t is 0. When v_t is 1, pumping is allowed, and pumping is prohibited when v_t is 0.

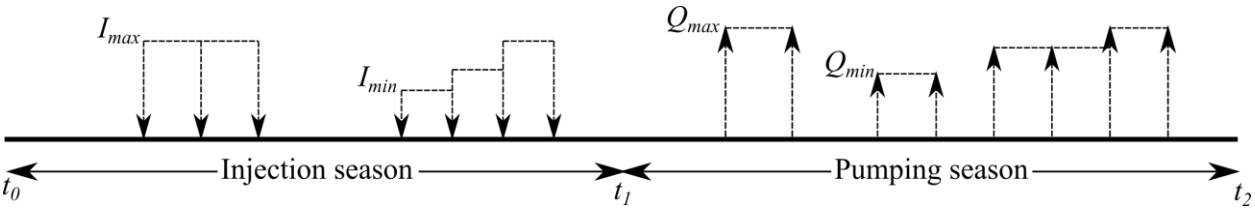

Figure 4.2. A conceptual schedule for one ASR cycle including one injection season and one pumping season.

The first objective (Eq. 4-1) maximizes the amount of injectate in the aquifer during the injection season. The second objective (Eq. 4-2) maximizes the injectate recovery efficiency during the pumping season (Forghani and Peralta, 2018). The two objectives are conflicting to each other. In other words, an increase in the amount of injectate leads to a decrease in the recovery efficiency. Eq. 4-3 and Eq. 4-4 are the managerial constraints where the injection is not allowed when the groundwater level is above a threshold $h_{\max}$ and pumping is prohibited when the groundwater level is below a threshold $h_{\min}$. Eq. 4-5 and Eq. 4-6 are bound constraints for injection rates and pumping rates, respectively, when they are active. Eq. 4-7 guarantees that at least one injection operation happens in the injection season and at least one pumping operation occurs in the pumping season. Calculation of groundwater levels and concentrations can be achieved by solving a groundwater flow equation and a solute transport equation as follows.

$$S_s \frac{\partial h}{\partial t} = \nabla \bullet \left(K \nabla h \right) + I\delta\left(\mathbf{x} - \mathbf{x}_{ASR} \right) - Q\delta\left(\mathbf{x} - \mathbf{x}_{ASR} \right) \tag{4-8}$$

$$\frac{\partial C}{\partial t} = \nabla \bullet \left(\bar{\mathbf{V}} C \right) - \nabla \bullet \left(\mathbf{D} \nabla C \right) + C^0 I\delta\left(\mathbf{x} - \mathbf{x}_{ASR} \right) - CQ\delta\left(\mathbf{x} - \mathbf{x}_{ASR} \right) \tag{4-9}$$

where S_s is the specific storage (m^{-1}), K is the hydraulic conductivity (m/day), $\delta\left(\mathbf{x} - \mathbf{x}_{ASR} \right)$ is the Kronecker delta, $\mathbf{x}$ is the coordinate vector (m), $\mathbf{x}_{ASR}$ is the location of the ASR well (m), $\mathbf{V}$ is the seepage velocity vector (m/day), $\mathbf{D}$ is the dispersion coefficient tensor (m^2/day), and ∇ is

the gradient operator. Since the ASR site is usually small, this study assumes constant hydraulic conductivity and porosity. The seepage velocity vector and the dispersion tensor are following

$$\vec{\mathbf{V}} = -\frac{K}{n}\nabla h \tag{4-10}$$

$$D_{ij} = \alpha_T \left|\vec{\mathbf{V}}\right| \delta_{ij} + \left(\alpha_L - \alpha_T\right) \frac{V_i V_j}{\left|\vec{\mathbf{V}}\right|} + D^* \delta_{ij} \quad , i = x, y, z;\ j = x, y, z \tag{4-11}$$

where n is the porosity, α_L is the longitudinal dispersivity (m), α_T is the transverse dispersivity (m), V_i is the seepage velocity in i direction, $\left|\vec{\mathbf{V}}\right| = \sqrt{V_x^2 + V_y^2 + V_z^2}$ is the velocity magnitude, D^* is the molecular diffusion coefficient (m^2/day), and δ_{ij} is the Kronecker delta,. This study assumed that molecular diffusion is negligible in the ASR operation.

The ASR operation optimization problem contains both continuous variables and integer variables. Consider one ASR cycle is a year with 12 monthly stress periods. The first 6 months are the injection season. The last 6 months are the pumping season. As shown in Figure 4.3, there are 12 binary variables (u_t, v_t) by which the schedule is determined. There are also 12 continuous variables (I_t, Q_t) where the injection rates and pumping rates are assigned. The multiplication of the binary variables and continuous variables results in injection rate or pumping rate for each stress period. Owing to the non-linear objective functions, the optimization problem becomes a mixed integer non-linear programming (MINLP). The non-dominated sorting genetic algorithm (NSGA-II) (Deb et al., 2002) has been shown to be promising for solving this type of problem (Pasandideh et al., 2015; Rabbani et al., 2019, Yin et al. 2020, Chen et al. 2021).

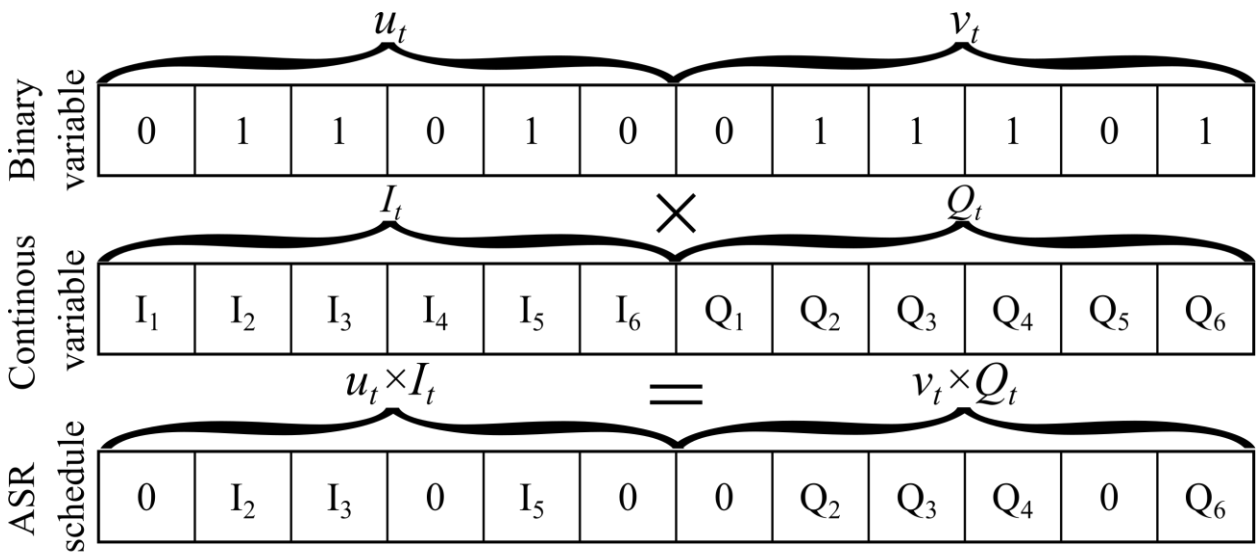

Figure 4.3. Relationship between decision variables in one ASR cycle. The schedule is built by multiplication of binary variables and corresponding injection/pumping rates.

4.2.2. Uncertainty in model parameters and LHS sampling

It is well understood the optimized ASR operations can be impacted by model uncertainty that can include a wide range of model parameters and model structure. Nevertheless, this study specifically targets uncertainty in hydraulic conductivity in the groundwater flow equation and dispersivity in the solution transpose equation to demonstrate the methodology because the plume of injectate is sensitive to these two model parameters.

This study adopts the Latin hypercube sampling (LHS) to generate realizations of hydraulic conductivity and dispersivity to address the uncertainty issue. As we know that the core to a successful Monte-Carlo simulation is the sampling method (Doucet et al., 2006). The better exploration of the parameter space, the more thorough the uncertainty assessment. Lack of a robust sampling method could introduce computational curse (Janssen, 2013). Stratified sampling where different parts of a population is proportionally represented is necessary for a thorough probe of

the sampling space (Neyman, 1992; Imbens and Lancaster, 1996). Latin hypercube sampling (LHS) as a stratified sampling has gained popularity because of its efficient stratification properties.

Assume that the parameter space consists of N parameters to be sampled. The LHS method divides the range of each parameter into *M* disjoint equiprobable intervals (Iman and Conover, 1982; Helton and Davis, 2003). A sampled parameter value D_j in each interval for a model parameter is drawn according to

$$D_{ij} = F_i^{-1}(R_j) \quad , i = 1, 2, ..., N; j = 1, 2, ..., M \tag{4-12}$$

where D_{ij} is the sampled value of parameter *i* in interval *j*, F_i^{-1} is the inverse cumulative probability distribution (cdf) function of parameter *i*, and R_j is the identically independently distributed (iid) random number within the range $\left[(j-1)/M,\ j/M\right]$ of the interval *j*. Figure 4.4 illustrates an LHS process for sampling two parameters (*N*=2). Figure 4.4.a shows the cdf of a uniform distribution. Figure 4.4.b shows the cdf of a Gaussian distribution. Both figures have 5 equiprobable intervals (*M*=5) with interval probability of 0.2. Each distribution function produces 5 random numbers within their corresponding intervals and corresponding parameter values. Figure 4.4.c shows 5 parameter sets resulted from one combination of the parameter values in Figure 4.4.a and Figure 4.4.b. LHS is complemented by a sampling strategy (Razavi and Gupta, 2016) to complete the exploration of the parameter space. As shown in Figure 4.5, more discrete parameter sets are made through each parameter set. Each parameter is discretized based on a predefined resolution (ΔU for variable *U* and ΔN for variable *N*). Given E discrete values for each parameter, the total number of discrete parameter sets is N×M×(E-1)+M.

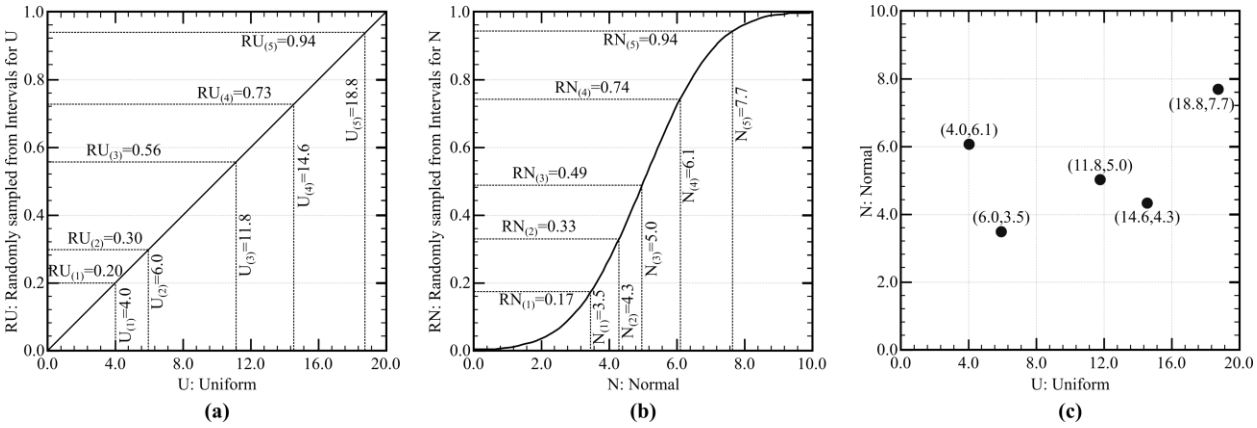

Figure 4.4. An LHS process for parameters space [U,N]. **(a)** Sampling for the first component with uniform distribution, variable U varying between [0 20]. **(b)** Sampling for the second component with normal distribution, variable N varying between [0 10]. **(c)** A sample for [U,N].

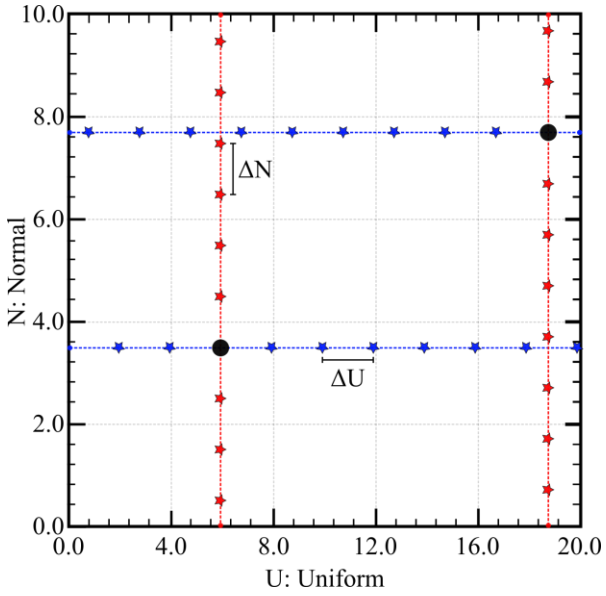

Figure 4.5. Star-sampling for two points in the parameters space [U,N].

4.2.3. Supervised learning-based surrogate modeling

Calculating groundwater level h_t and concentration C_t at the end of each stress period for the ASR operation optimization problem can be intractable if the groundwater flow equation and solution transport equations directly involved. Instead, the computational issue can be resolved by

using surrogate models to efficiently produce groundwater levels and concentrations in the optimization framework.

As response surface surrogates (a.k.a. data-driven surrogates) ANNs are trained based on a set of inputs and outputs from complex groundwater model/solute transport model (Razavi et al., 2012). Figure 4.6 illustrates a neural network. An artificial neuron is the building block of an ANN and has two major roles of combining inputs (operator Σ) and comparing the combined input with a given threshold (operator θ). The input to a neuron is weighted and added a bias term. The output from a neuron is produced after this weighed and biased term compared with a threshold. This entire unit, from input to output, is called perceptron. The most well-known ANN is the feedforward network or multilayer perceptron network which includes layers of parallel perceptrons. The network shown in Figure 4.6 has 3 layers with 3 perceptrons in the first layer (input layer), two perceptrons in the second layer (a.k.a. hidden layer), and 1 perceptron in the last layer (output layer). This network is named after the number of perceptrons in its different layers as 3-2-1 feedforward network. Since backward connections are not allowed in the networks, it is called feedforward. The mathematical formulation of the network shown in Figure 4.6 is as follows:

$$I_{3\times 2} = IW'_{3\times 2}\, X_{3\times 1} + IB_{2\times 1} \tag{4-13}$$

$$X = \begin{bmatrix} x_1 \\ x_2 \\ x_3 \end{bmatrix} \qquad IW = \begin{bmatrix} w_{11}\ w_{12} \\ w_{21}\ w_{22} \\ w_{31}\ w_{32} \end{bmatrix} \qquad IB = \begin{bmatrix} b_1 \\ b_2 \end{bmatrix}$$

where the input into the hidden layer (I) is obtained through multiplication of the model input (X) and weights into the hidden layer (IW) plus biases into the hidden layer (IB). Similarly, the inputs to the output layer are produced:

$$I^O_{1\times 1} = W'^O_{2\times 1}\, F(I)_{2\times 1} + B^O_{1\times 1} \tag{4-14}$$

$$W^O = \begin{bmatrix} w_{11}^o \\ w_{21}^o \end{bmatrix} \qquad B^O = b^o$$

where W^O and B^O are the weight matrix into the output layer and bias into the into the output layer, respectively. The function matrix F represents "transfer functions" of the hidden layer which indeed includes both Σ and θ operations. Finally, the outputs are computed based on the input into the output layer (I) and "transfer functions" of the output layer:

$$Y_{1\times1} = G(I^O)_{1\times1} \tag{4-15}$$

The details of calculating weights and different transfer functions can be found in Araghinejad (2013). In this study feedforward ANN is used to predict values of groundwater levels and concentrations in an ASR cycle (output Y) using the decision variables injection rates and pumping rates (output X).

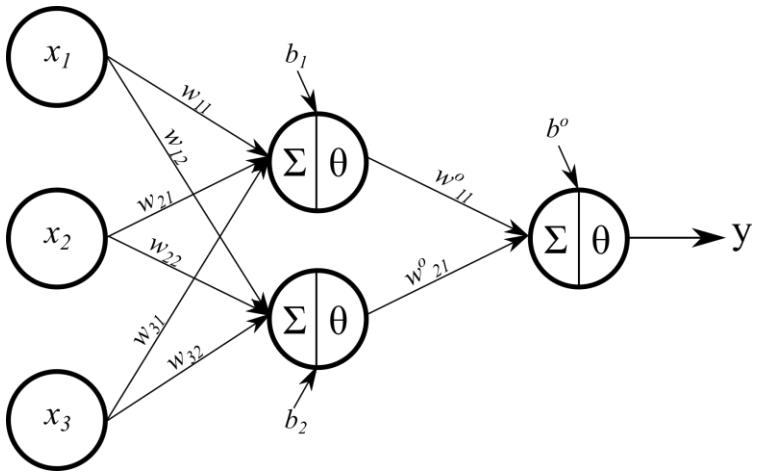

Figure 4.6. A feedforward 3-2-1 network.

4.3. ASR preliminary study in Southwest Louisiana

Up-to-date there is no actual ASR site in Louisiana. However, the concept of ASR operations is relevant to the Louisiana's coastal zone, which is prone to salinization. Although counteracting the effect of saltwater intrusion is one of the ASR purposes, the extent of saltwater

intrusion in the study region is insignificant. Hence, this ASR study does not aim to resolve the problem of saltwater intrusion. The selection of a potential ASR operation site in this work was based on the site selection suitability analysis in Southwest Louisiana conducted by LaHaye et al. (2021). The easy access to surface freshwater through local streams and suitable hydrogeologic characteristics of the underlying aquifer are the keys to make a suitable ASR operation site. Figure 4.7.a shows the location of the study area in the north of Vermillion parish, Louisiana. The model domain is 4 km by 4 km. The surface water source for the ASR operation may come from the Bayou Grand Marais. Figure 4.7.b illustrates the north-south cross section passing through the location of ASR well. The study area is covered by clay at the top as thick as 27 m and is underlain by the thick Undifferentiated sand of the Chicot aquifer system (Vahdat-Aboueshagh and Tsai, 2021). The Undifferentiated sand is heavily pumped for the agricultural purpose, where a large cone of depression has been created in the region (Fendick and Nyman, 1987; Lovelace et al., 2004). The adjacency to the Gulf of Mexico makes this region prone to saltwater encroachment.

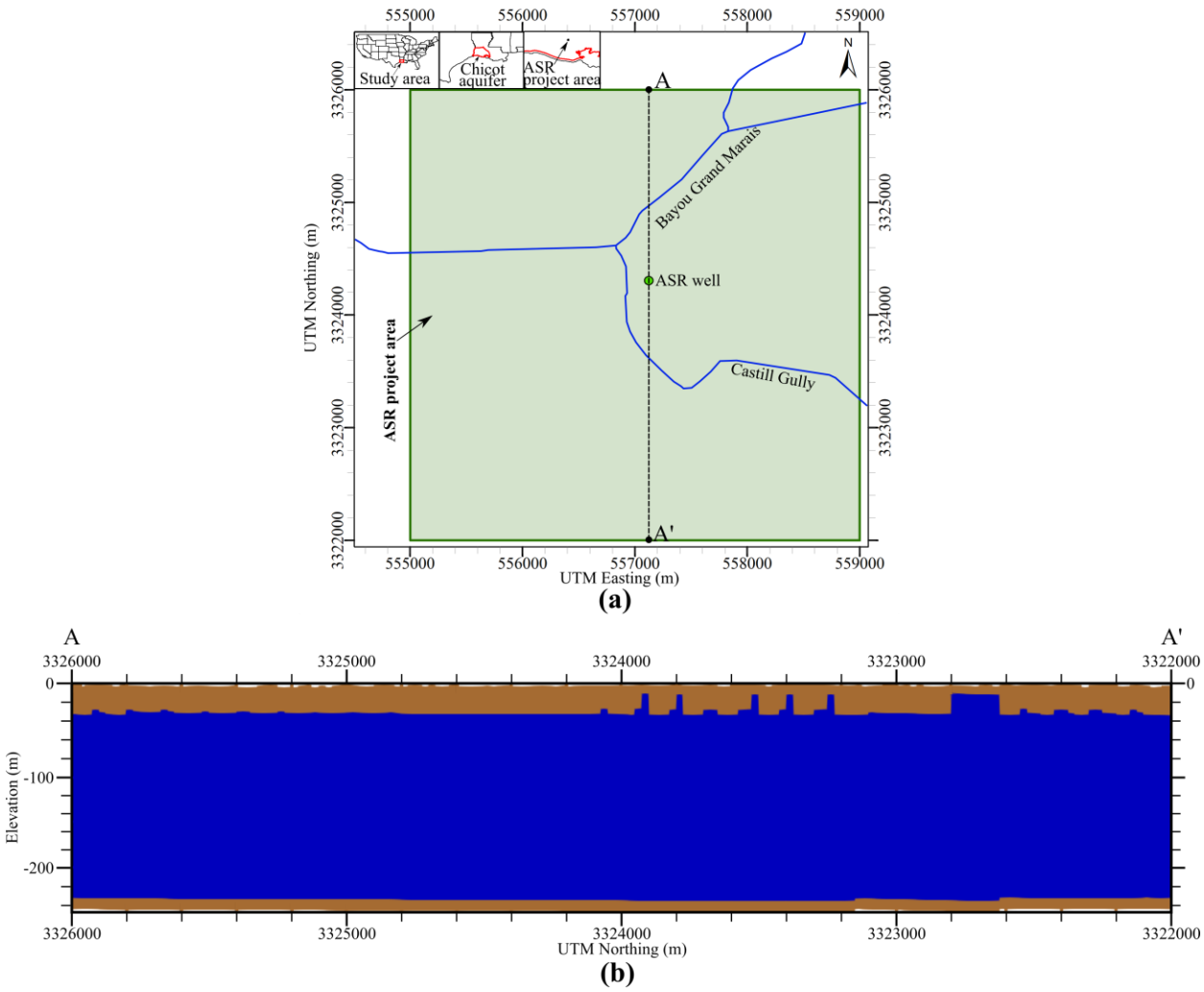

Figure 4.7. (a) Study area for the ASR project in north of Vermilion parish Louisiana, and (b) north-south cross section passing through the location of ASR well. Blue and brown represent sand and clay, respectively. The coordinates are in NAD83/ UTM zone 15N.

4.4. Modeling setup

4.4.1. Groundwater flow model

A MODFLOW groundwater model (Harbaugh, 2005) for the study area was developed based on the hydrogeological information from the region-scale groundwater model developed (Vahdat-Aboueshagh et al. 2021). The model horizontal extent is 4 km by 4 km, and the vertical

extent is from land surface around 1 m above mean sea level (MSL) down to 260 m below MSL. The horizontal cells size is 25 m. The model constitutes 24 layers with non-uniform thickness. The first layer and the last layer are confining layers. For year of 2015, groundwater level of -9 m MSL was used as the constant-head boundary condition. The initial groundwater level was -8.70 m MSL. 12 monthly stress periods were used for one ASR cycle. The ASR well screen was assumed to fully penetrate from elevation of -129 m to -140 m MSL in the aquifer.

Hydrogeologic properties of sand and clay were assumed to be homogeneous and isotropic. The specific storage of sand and clay is 1.9×10-5 1/m and 1.0×10-3 1/m, respectively. The hydraulic conductivity of sand and clay is 45.6 m/day and 1.0×10-4 m/day, respectively. This study involves uncertainty in sand hydraulic conductivity. Previous studies suggested that natural logarithm of hydraulic conductivity, ln(K), for an aquifer follows a normal distribution (Benson, 1993; Yeh and Liu, 2000; Zhao and Illman, 2021). Vahdat-Aboueshagh et al. (2021) derived the mean and standard deviation for ln(K) to be 3.82 and 0.74, respectively for the study after their model calibration.

4.4.2. Transport model

This study employed the MT3DMS (Zheng and Wang, 1999) to track the injectate inside the aquifer during the ASR cycle. To distinguish injectate from native groundwater, the injected water is presumed to contain an imaginary conservative solute (Forghani and Peralta, 2017). The concentration of injectate is assumed to be 1000 mg/l as Missimer et al. (2002) suggested values less than 20,000 mg/l for a successful ASR model and Brown et al. (2016) considered a cap of 10,000 mg/l.

Both advection and dispersion are required for more accurate results of concentrations (Lowry and Anderson, 2006; Forghani and Peralta, 2017). Probably the most challenging and complicated parameter in the MT3DMS models is the dispersivity (Burnett and Frind, 1987a, Burnett and Frind, 1987b). Due to very stochastic nature of dispersivity (Frind et al., 1987) and unknown field values of the parameter, the longitudinal dispersivity is considered as an uncertain parameter in the MT3DMS. Longitudinal dispersivity is assumed to be constant and follow a uniform probability distribution in this study with a lower bound and an upper bound of 0.05 m and 100 m, respectively (Xu and Eckstein, 1995; Schulze-Makuch, 2005). Lower values of the longitudinal dispersivity leads to an advection dominant behavior while the higher values cause a dispersivity dominant behavior (Konikow, 2011). With a constant grid resolution, the values of grid Peclet number changes based on values of longitudinal dispersivity (Zheng and Wang, 1999). The advection package is set in a way that the solution scheme is chosen based on the Peclet number.

4.4.3. Setting model parameters based on sampled values

The parameter space, including hydraulic conductivity and longitudinal dispersivity, was sampled. Using the LHS, 20 values of hydraulic conductivity were randomly selected from 20 equiprobable intervals of normal distribution and 20 values of longitudinal dispersivity were randomly selected from 20 equiprobable intervals of uniform distribution. 20 pairs were randomly produced by mixing the sampled values of hydraulic conductivity and longitudinal dispersivity. Given a pair, 3 parameter values were determined for each parameter. As a result, 100 samples ($2\times20\times(3-1)+20$) of hydraulic conductivity and longitudinal dispersivity were generated.

Every sample point was used to build a groundwater flow model and a solute transport model. 1000 random combinations of injection rates and pumping rates for a single ASR cycle

were produces. The combinations were employed to develop the well package in the groundwater flow model. The 1000 groundwater models sequenced by solute transport models were run to measure groundwater level at the end of each stress period in one ASR cycle as well as concentration at the end of pumping stress periods. Each set of a MODFLOW model followed by an MT3DMS model took approximately 5 minutes to run. All the 105 models were run on 100 processers parallelly on a supercomputer. The outputs were used to build the ANN models.

4.4.4. ANN models development

The ANN models are developed for every sampled point in the parameter space. There is one ANN model for predicting groundwater level at the end of each stress period and one ANN model for predicting concentration at the end of each pumping stress period. Therefore, there are 1800 ANN models in total. The developed ANNs are feedforward network with a single hidden layer. The training of the ANNs were performed in the parallel mode. The Levenberg-Marquardt (LM) algorithm was utilized to minimize the mean square error (MSE) cost function of the network (Ampazis and Perantonis, 2000; Singh et al., 2007).

4.4.5. Optimization model

To solve the bi-objective MINLP problem defined in Eq. 4-1- Eq. 4-7, the NSGA-II algorithm was utilized. Two scenarios were defined based on maximum and minimum groundwater level constraints. In the first scenario, the $h_{\max}$ and $h_{\min}$ were considered as 2 m above and 2 m below the initial groundwater head in the aquifer, respectively. In the second scenario the maximum and minimum groundwater levels were relaxed to 5 m above and below the initial groundwater head, respectively. The minimum injection rate and minimum pumping rate were set equally to 4,000 m3/day (roughly 1 million gallons per day). The maximum injection rate and

maximum pumping rate were set equally to 40,000 m^3/day (roughly 10 million gallons per day). The population size of 120, fivefold under of decision variables, and generation size of 480 were set up for the NSGA-II algorithm. The optimization problem was solved for aquifer setups defined based on sample points (100 pairs of hydraulic conductivity and longitudinal dispersivity). Parallel computations were performed to solve the optimization problem.

4.5. Results and discussion

4.5.1. Validity of MODFLOW-MT3DMS models

In order to make sure that the results of the ASR operation are reliable, the groundwater flow model and solute transport model were evaluated based on literature. The sequence of MODFLOW model and the corresponding MT3DMS model were run for highest and lowest amounts of parameters under investigation for uncertainty, which are hydraulic conductivity and longitudinal dispersivity. Figure 4.8 demonstrates the non-native water distribution in the aquifer after a hypothetical injection period with maximum injection I_{max} and pumping period with maximum pumping Q_{max} at all stress periods. Comparing Figure 4.8.a and Figure 4.8d with Figure 4.8.b and Figure 4.8.c reveals that the plume spread, which represents freshwater in this study, becomes limited in radius as longitudinal dispersivity lowers. The sharper and denser plume due to low longitudinal dispersivity, as seen in Figure 4.8.a, has also been reported in Minsley et al. (2011). The plume interface also moves vertically due to convection forces (Ward et al., 2007) which create the freshwater bubble around the injection well. As studied by Merritt (1986), the higher values of aquifer permeability, compare Figure 4.8.b to Figure 4.8.c, leads to rapid buoyancy of the stored water which in return may cause lower ASR efficiency.

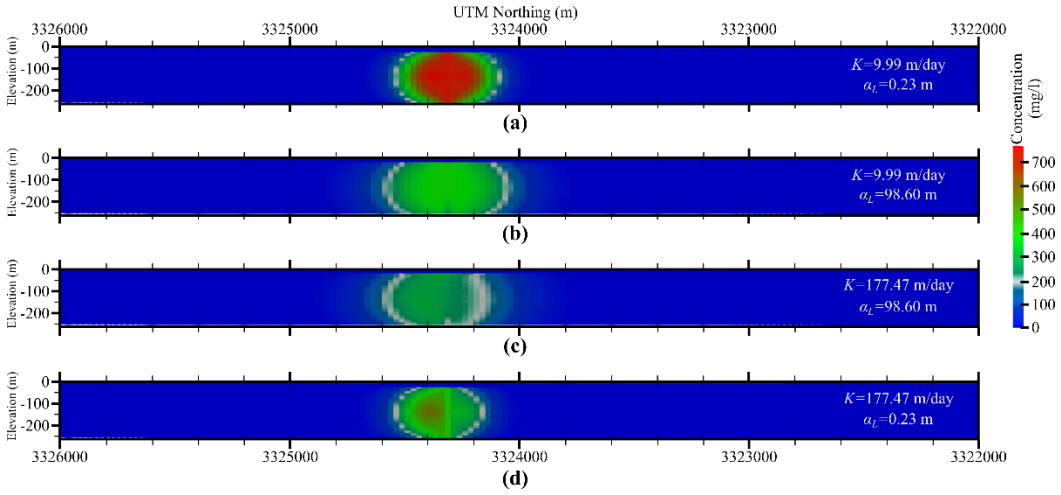

Figure 4.8. Freshwater distribution at and of an ASR cycle caused by maximum injections in injection season and maximum pumping rates in pumping season. The coordinates are in NAD83 / UTM zone 15N.

4.5.2. Performance of ANN models

The suitable data proportions for ANN models and data structure are determined through trial and error (Razavi et al., 2012). The proportions of training data, testing data, and validation data turned out to be 70%, 15%, and 15% which are in accordance with numbers reported in previous studies (Bowden et al., 2002; Shahin et al., 2004). The number of neurons in the hidden layer turned out to be 5. Figure 4.9 shows the error histograms of groundwater levels and concentrations for different datasets of ANN model. The error for groundwater level is almost zero for all the datasets. The great performance of the ANN on groundwater level prediction has been reported frequently and very small errors are not sign of overtraining (Nourani et al., 2008; Trichakis et al., 2011). The average error on concentration for all the datasets reduces continuously from 19 ml/l for the first stress period in the pumping season to 7 ml/l for the last stress period in the pumping season. The higher value of error for the first stress periods is due probably to the complex behavior of the aquifer during the shift between injection to pumping. However, the

values of error for concentration are still very satisfactory compared to the maximum concentration of the 1000 ml/l.

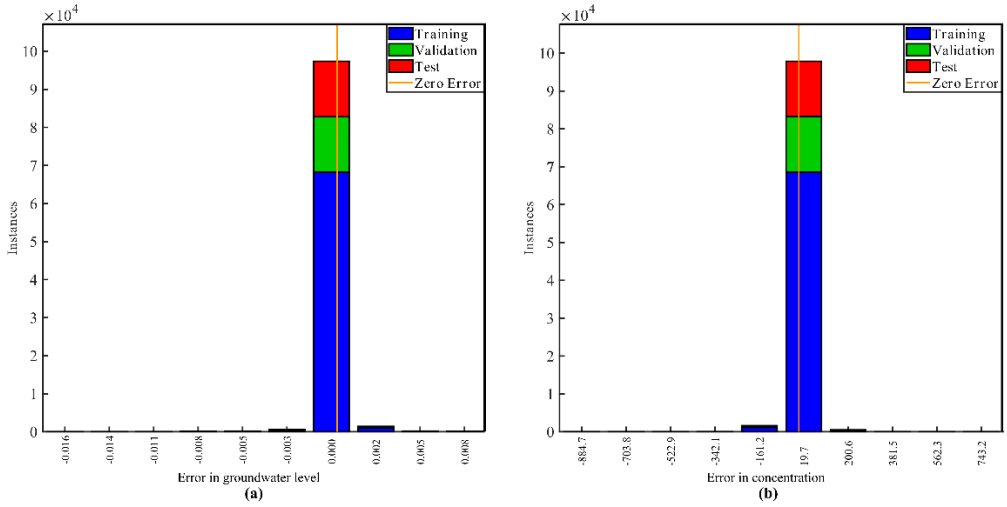

Figure 4.9. Error histograms for groundwater level prediction at end of every stress period and concentration prediction at end of every stress period in pumping season.

4.5.3. Optimum solutions under uncertainty

The results of optimization model for 100 aquifer model setups, different sets of hydraulic conductivity and longitudinal dispersivity, are shown in form of Pareto fronts in Figure 4.10. Clear concave fronts are recognized for every aquifer model setup. Every solution point on a Pareto is a trade-off between two conflicting objectives of maximizing the total amount of injection, f_1, the aquifer and maximizing the ASR efficiency, f_2. The maximum amount of both f_1 and f_2 increases for most of the models as h_{max} increases to 5 m above initial groundwater level and h_{min} decreases to 5m below initial groundwater level. The aquifer characteristics affect the limits of the objective functions in an ASR operation.

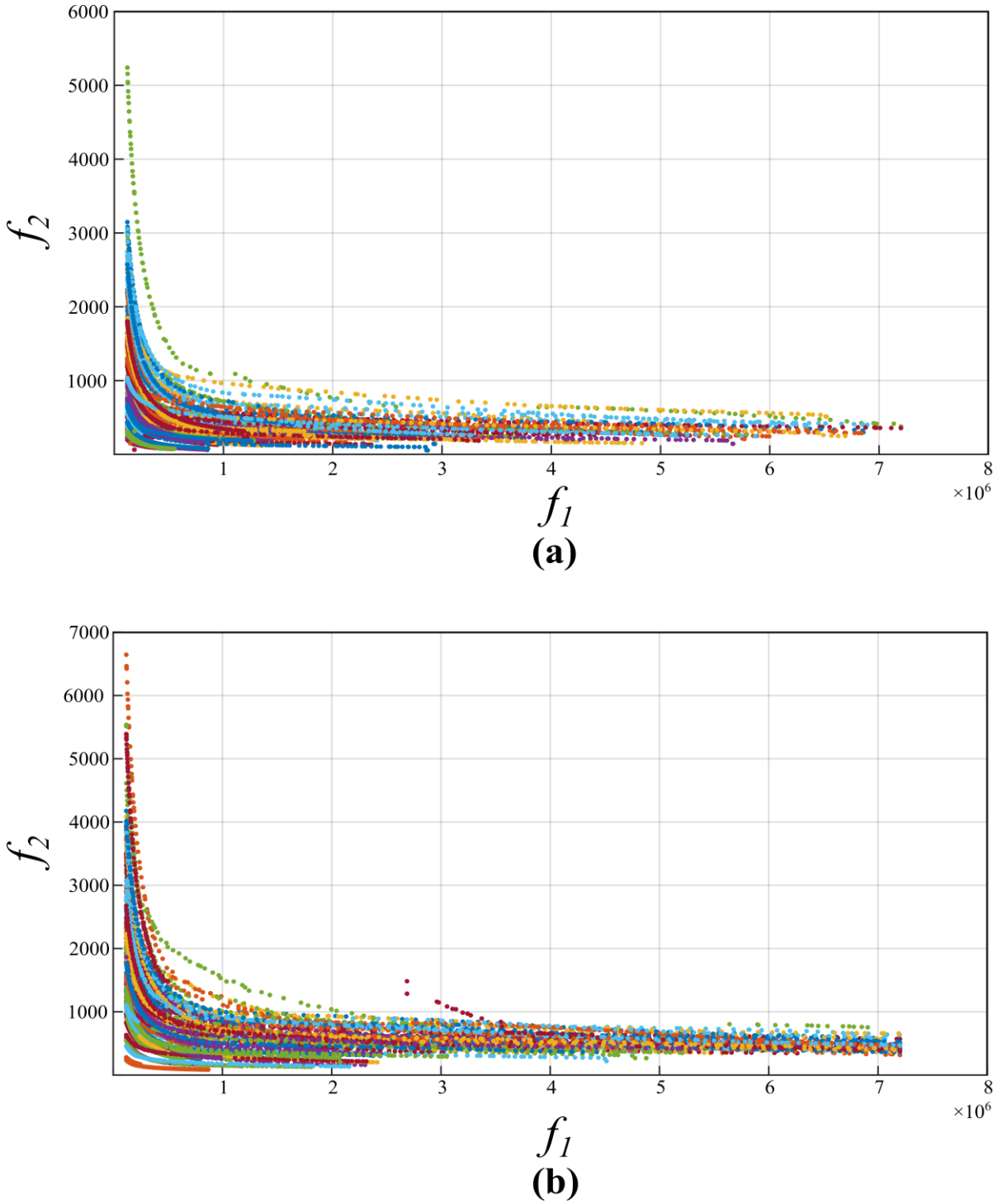

Figure 4.10. Pareto solutions for 100 groundwater models under **(a)**: the first scenario with the h_I^{max} and h_Q^{min} 2m below and 2m above the initial groundwater head and **(b)**: the second scenario with the h_I^{max} and h_Q^{min} 5m below and 5m above the initial groundwater head. Every color represents solution for an aquifer model with a specific set of hydraulic conductivity and longitudinal dispersivity.

To investigate the effect of hydraulic conductivity on the ASR operation, the maximum values of the first objective function was plotted versus their corresponding hydraulic conductivity values. Figure 4.11.a shows a clear positive relationship between *Max* f_1 and *K*. The relationship is in accordance with hydraulics of the confined aquifer systems because higher hydraulic conductivity of an aquifer means the lower fluctuation of groundwater level and as a result the higher injection may be allowed without exceeding the $h_{\max}$. On the other hand, Figure 4.11.b demonstrates a negative relationship between *Max* f_2 and the ratio of α_L/K. This pattern can be justified by this fact that the higher values of longitudinal dispersivity cause substantial loss of recovery efficiency (Merritt, 1986).

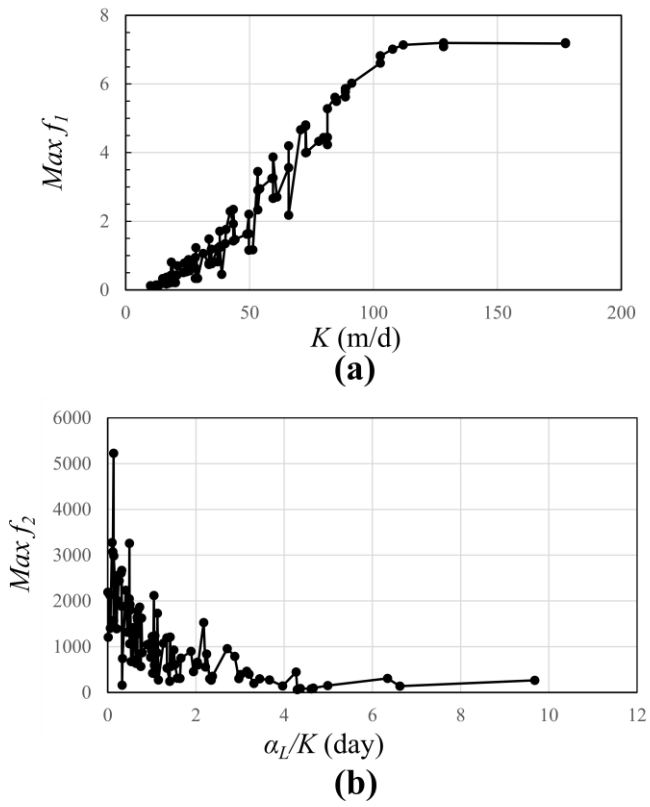

Figure 4.11. Significant parameters in objective functions **(a)**: variation of maximum of the first objective function versus the hydraulic conductivity for the first scenario. (**b)**: variation of maximum of the second objective function versus the ration of longitudinal dispersivity to hydraulic conductivity for the first scenario.

Further analysis on the schedule of all Pareto point models shows that the probability of having either injection operation or pumping operation increases later on in final stress periods of the season. Figure 4.12 illustrates the probability of having operation for every stress period based on 12,000 models of the Pareto front. The probability at the second half of the injection season and the second half of the pumping season is higher than their first halves. Another analysis on how ASR scheduling may be influenced by the aquifer characteristics proves that the higher the hydraulic conductivity of the aquifer system, the higher number of operations in an ASR cycle. As the Figure 4.13 shows the aquifers with lower values of *K* require less number of injection/pumping operations in an ASR cycle. This is because the freshwater bubble formed in the low *K* aquifer is smaller and recovery from the same bubble requires less amount of operation (Merritt, 1986; Ward et al., 2007).

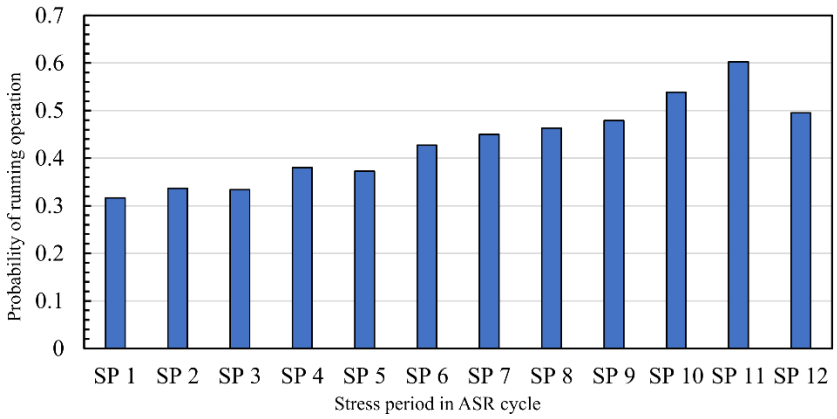

Figure 4.12. Probability of running operation in a certain ASR stress period based on all the Pareto front solutions.

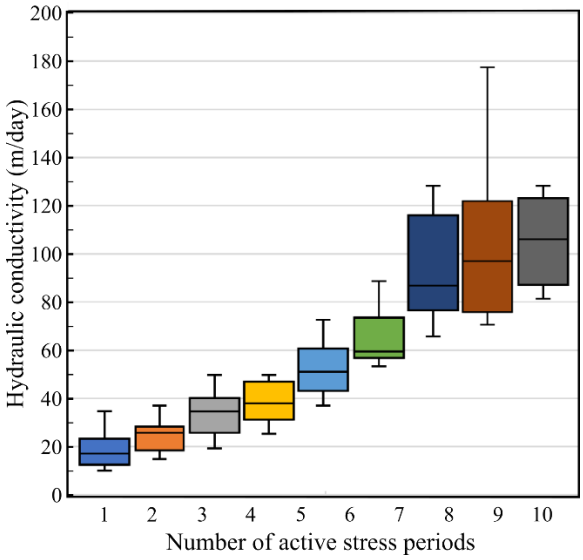

Figure 4.13. The effect of hydraulic conductivity of the aquifer on the number of active periods in ASR operation.

4.6. Conclusions

This study integrates a supervised learning-based surrogate method with a mixed integer non-linear programming (MINLP) to obtain optimal schedule for aquifer storage and recovery (ASR) operation. With the aid of the surrogate modeling the uncertainty propagated into the Pareto solution due to uncertainty in hydrogeological parameters such as hydraulic conductivity as well as longitudinal dispersivity is addressed. The following remarks can be made in this study:

- The combination of the LHS method and star-based sampling sufficiently probes the parameter space for uncertainty analysis. The simplicity and computational effectiveness are two major characteristics which make this approach a popular Monte-Carlo method.
- The feedforward artificial neural network (ANN) is a promising tool in surrogate modeling for predicting groundwater level and concentration in ASR operations. The integration of NSGA-II optimization method and surrogate modeling

adequately addressed the parameter uncertainty through obtaining a family of Pareto fronts.

- The amount of injectate into the aquifer system during the injection season is heavily affected by the permeability of the aquifer system. The higher the permeability, the lower the groundwater fluctuation in the ASR well after injection.
- The ratio of longitudinal dispersivity to the hydraulic conductivity in an aquifer system adversely affects the ASR efficiency.

The method proposed in this study can be used to study ASR operations with more than one cycle. A future research topic could be the study of multi-well ASR operation where the objectives may be defined differently for each operating well. The combination of optimum well configuration and objective functions also may be of interest for a future work.

Chapter 5. Summary and Concluding Remarks

This dissertation aims to study complex groundwater systems, ranging from a large-scale to a small scale, by developing models which sufficiently address the complexities in hydrostratigraphy structures. To do so, statewide-scale, regional-scale, and local-scale projects were defined and studied. The results of the studies can be summarized as follows.

Firstly, this study developed and examined a method for building hydrostratigraphy architectures. The methodology is based upon tessellation of the study domain into set of tiles considering the geological complexities and employment of a big well log dataset. Due to its unique geology and availability of a sizable well log dataset, the state of Louisiana was picked as a case study to validate the methodology. The tessellation in Louisiana area was performed based on the dip direction variation, from Sabine uplift in northwest to homoclines of the Gulf Coast in south, and traces of Baton Rouge fault system in southeast. The geological feature of angular unconformity between alluviums of the Mississippi River and the Red River was also modeled through vertical splitting of tiles in the alluvial areas. Integration of well logs from three sources of drillers' logs, geotechnical borings, and wireline electric logs yielded a dataset of more than 114000 well logs.

The developed hydrostratigraphy model for the state of Louisiana could successfully identify hydrogeological characteristics such as recharges zones, connections between aquifer systems, connection between the Mississippi River and the Red River and their alluviums, accessibility to aquifers, link between surface streams and lakes and shallow aquifer sands. The results also demonstrated that sand formations in southeastern Louisiana have two different patterns. The closely interbedded deposit of sand and clay is identified to the north of the Baton Rouge fault while the sand formations to the south of the fault are continuous. The modeled

difference between these two patterns of sand formations corresponds well with the hypothesis of multi-axis depositional patterns of the ancestral Mississippi River and Tennessee River. The close interbedding has also been confirmed through the studies on the Citronelle Formation in southeastern Louisiana.

Secondly, the developed methodology was utilized to create a complex groundwater flow model for the Chicot aquifer system which is a part of the Coastal Lowland Aquifer System. The goal of the groundwater study of the Chicot aquifer was to advance hydrogeological knowledge in the Gulf of Mexico region and other coastal areas. The aquifer system is the most heavily pumped aquifer in Louisiana and its complex aquifer structure is largely ignored. More than 29,000 well logs were integrated to construct the stratigraphy model for the Chicot aquifer. The recharge data and observation data together with pumping data were collected and processed to inform the groundwater model. Model calibration was conducted using the CMA-ES method with aid of parallel computing.

The Chicot stratigraphy model demonstrated that the aquifer system consists of highly interconnected sand units and outcrops in the north. Central and southern areas are covered by clays thickening toward the Gulf. Sand units are relatively thin in the north and are frequently interbedded by clays which adds to complexity of the aquifer system. Sand units are thick in the central and southern areas. The developed groundwater flow model results show that the storage loss due to groundwater pumping in the Chicot aquifer system is counterbalanced by inflows from surficial recharge, rivers and boundaries. The two large cones of depression created by the agricultural pumping in the east and by the industrial pumping in the west represent the key feature in the Chicot aquifer system. The groundwater storage loss in agriculture area occurs during the rice irrigation season. The aquifer system can be quickly replenished by the inflows during the

non-irrigation season. The groundwater levels in the Lower Chicot aquifer, the Upper Chicot aquifer, the Undifferentiated sand are heavily impacted by the seasonal irrigation activities and result in groundwater storge depletion. On the contrary, groundwater levels in the "200-foot" sand, the "500-foot" sand, and "700-foot" sand have less variability. In other words, groundwater levels in the west are not heavily impacted by the irrigation activities. Furthermore, large amounts of upward vertical flows from the Lower Chicot aquifer to the Upper Chicot aquifer and from the "700-foot" sand to the "500-foot" sand were observed through the groundwater model. As salt water was reported at the base of the Chicot aquifer system, potential saltwater intrusion due to vertical saltwater migration from the deeper sands is likely to occur in the future.

As the final goal in this dissertation, an ASR operation was studied in south part of the Chicot aquifer system. The focus of the ASR project was on an optimal scheduling during an ASR cycle where an injection season is immediately followed by a pumping season. The ASR operations may be intended for storing surface water into aquifer during a wet season or combating saltwater intrusion in coastal areas. This study used a supervised learning method to overcome the computationally intensive process of simulation-optimization and address parameter uncertainty. The groundwater flow model and solute transport model were built using the Chicot aquifer groundwater model. A LHS sampling technique was utilized to sample parameter values for hydraulic conductivity and longitudinal dispersivity. ANN models were build using the groundwater model and solute transport model to predict groundwater level and distribution of the non-native groundwater during an ASR operation. The ANN surrogates together with NSGA-II were employed to maximize the amount of the injectate into the aquifer and to maximize the ASR operation efficiency.

The initial results show that the feedforward ANN is a promising tool in surrogate modeling for predicting groundwater level and concentration in ASR projects. The integration of NSGA-II optimization method and surrogate modeling adequately addressed the parameter uncertainty through obtaining a family of Pareto fronts. Further analysis demonstrates that the amount of injectate into the aquifer system during the injection season is heavily affected by the hydraulic conductivity of the aquifer system. The higher the permeability, the lower the groundwater fluctuation in the ASR well after injection. The ratio of longitudinal dispersivity to the hydraulic conductivity in an aquifer system adversely affect the ASR efficiency.

Based on the so-far results from three groundwater studies in this dissertation in three different scales, the following suggestions may be made for prospective research:

- The hydrostratigraphy model for the state of Louisiana may be used to develop a statewide groundwater model. This requires a tremendous effort to collect and process the hydrological data as well as groundwater. The hydrostratigraphy model may be improved through including more data and further processing of data to a higher accuracy.
- The method proposed for hydrostratigraphy modeling may be utilized for larger scale areas and to discover both geological and hydrogeological characteristics of the area under investigation.
- The groundwater flow model developed for the Chicot aquifer could be further employed for agricultural management policy studies. This is an important topic since the Undifferentiated sand, Upper Chicot and Lower Chicot aquifers in the Chicot aquifer system are exploited for agriculture sector.

- Furthermore, the groundwater flow model may be used to develop a solute transport model in southwest Louisiana and evaluate the possibility and details of the saltwater intrusion from the Gulf of Mexico.
- The method explained for the ASR project may be extended for more than one ASR cycle and for configuration with more than one well.

Appendix. Copyright Information

Permission for Chapter 2

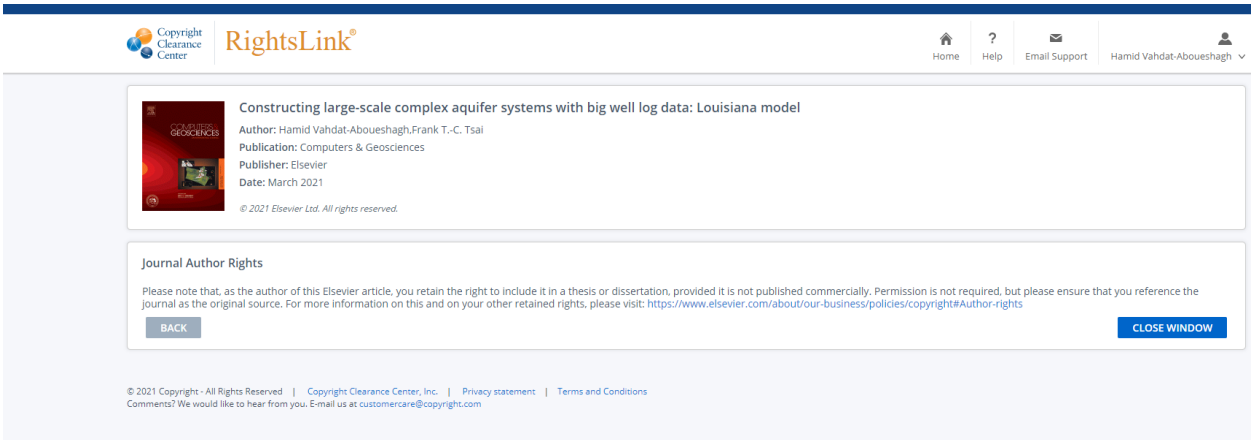

Permission for Chapter 3

ORIGINAL RESEARCH article
Front. Water, 06 April 2021 | https://doi.org/10.3389/frwa.2021.623476

Irrigation-Intensive Groundwater Modeling of Complex Aquifer Systems Through Integration of Big Geological Data

Hamid Vahdat-Abouesh agh[1], Frank T.-C. Tsai[2*], Dependra Bhatta[3] and Krishna P. Paudel[3]

[1]Department of Civil and Environmental Engineering, Louisiana State University, Baton Rouge, LA, United States
[2]Department of Civil and Environmental Engineering, Patrick F. Taylor Hall, Louisiana State University, Baton Rouge, LA, United States
[3]Department of Agricultural Economics and Agribusiness, Louisiana State University and LSU Agricultural Center, Baton Rouge, LA, United States

This study identifies hydrogeologic characteristics of complex aquifers based on constructing stratigraphic structure with large, non-uniform well log data. The approach was validated through a modeling study of the irrigation-intensive Chicot aquifer system, which is an important Pleistocene-Holocene aquifer of the Coastal Lowlands aquifer system in the southwestern Louisiana. Various well log types were unified into the same data structure, prioritized based on data sources, and interpolated to generate a detailed stratigraphic structure. More than 29,000 well logs were integrated to construct a stratigraphy model of 56 model layers for the Chicot aquifer system. The stratigraphy model revealed interconnections of various sands in the system, where 90% of the model domain is covered by fine-grained sediments. Although the groundwater model estimated a slight groundwater storage gain during 2005–2014 for the entire region, groundwater storage in the agricultural area was depleted. Nevertheless, the quick groundwater storage recovery during the non-irrigation seasons suggests that the Chicot aquifer system is a prolific aquifer system. The groundwater modeling result shows that the gulfward groundwater flow direction prior to pumping has been reversed toward inland pumping areas. The large upward vertical flow from the deeper sands indicates potential saltwater migration from the base of the Chicot aquifer system.

References

Aarts, E.H., van Laarhoven, P.J., 1987. Simulated annealing: a pedestrian review of the theory and some applications. In: Devijver P.A., Kittler J. (eds.) Pattern Recognition Theory and Applications. NATO ASI Series (Series F: Computer and Systems Sciences), Vol. 30. Springer, Berlin, Heidelberg. https://doi.org/10.1007/978-3-642-83069-3_15.

Abd-Elhamid, H.F., Javadi, A.A., 2011. A cost-effective method to control seawater intrusion in coastal aquifers. Water Resources Management, 25(11), pp. 2755-2780. https://doi.org/10.1007/s11269-011-9837-7.

Ackerman, D. J., 1989. Hydrology of the Mississippi River Valley alluvial aquifer, south-central United States; a preliminary assessment of the regional flow system, Water-Resources Investigations Report 88-4028. US Geological Survey, 74 pp. https://doi.org/10.3133/wri884028.

Agassi, M., Kirsten, W.F.A., Loock, A.H., Fine, P., 1998. Percolation and leachate composition in a disturbed soil layer mulched with sewage biosolids. Soil and Tillage Research, 45(3-4), pp. 359-372. https://doi.org/10.1016/S0933-3630(97)00028-7.

Alley, W.M., Healy, R.W., LaBaugh, J.W., Reilly, T.E., 2002. Flow and storage in groundwater systems. Science, 296(5575), pp. 1985-1990. https://doi.org/10.1126/science.1067123.

Alley, W.M., Leake, S.A., 2004. The journey from safe yield to sustainability. Groundwater, 42(1), pp. 12-16. https://doi.org/10.1111/j.1745-6584.2004.tb02446.x.

Almulla, A., Hamad, A., Gadalla, M., 2005. Aquifer storage and recovery (ASR): A strategic cost-effective facility to balance water production and demand for Sharjah. Desalination, 174(2), pp.193-204. https://doi.org/10.1016/j.desal.2004.08.042.

Ampazis, N., Perantonis, S. J., 2000. Levenberg-Marquardt algorithm with adaptive momentum for the efficient training of feedforward networks. In Proceedings of the IEEE-INNS-ENNS International Joint Conference on Neural Networks. IJCNN 2000. Neural Computing: New Challenges and Perspectives for the New Millennium, 1, pp. 126-131. DOI: 10.1109/IJCNN.2000.857825.

Araghinejad, S., 2013. *Data-driven modeling: using MATLAB® in water resources and environmental engineering* (Vol. 67). Springer Science & Business Media.

Archie, G.E., 1942. The electrical resistivity log as an aid in determining some reservoir characteristics. Transactions of the AIME, 146(01), pp. 54-62. https://doi.org/10.2118/942054-G.

ASTM (American Society for Testing and Materials), 2017. D2487-17: Standard Practice for Classification of Soils for Engineering Purposes (Unified Soil Classification System). ASTM International, West Conshohocken, PA. https://doi.org/10.1520/D2487-17.

Azizi, F., Vadiati, M., Moghaddam, A.A., Nazemi, A., Adamowski, J., 2019. A hydrogeological-

based multi-criteria method for assessing the vulnerability of coastal aquifers to saltwater intrusion. Environmental Earth Sciences, 78(17), p. 548. https://doi.org/10.1007/s12665-019-8556-x.

Barlow, P.M., Reichard, E.G., 2010. Saltwater intrusion in coastal regions of North America. Hydrogeology Journal, 18(1), pp. 247-260. https://doi.org/10.1007/s10040-009-0514-3.

Benson, C. H., 1993. Probability distributions for hydraulic conductivity of compacted soil liners. Journal of geotechnical engineering, 119(3), pp.471-486. https://doi.org/10.1061/(ASCE)0733-9410(1993)119:3(471).

Bentley Sr., S. J., Blum, M. D., Maloney, J., Pond, L., Paulsell, R., 2016. The Mississippi River source-to-sink system: Perspectives on tectonic, climatic, and anthropogenic influences, Miocene to Anthropocene. Earth-Science Reviews, 153, pp.139-174. https://doi.org/10.1016/j.earscirev.2015.11.001.

Berg, S.J., Illman, W.A., 2015. Comparison of hydraulic tomography with traditional methods at a highly heterogeneous site. Groundwater, 53(1), pp. 71-89. https://doi.org/10.1111/gwat.12159.

Bocanegra, E., Da Silva, G.C., Custodio, E., Manzano, M., Montenegro, S., 2010. State of knowledge of coastal aquifer management in South America. Hydrogeology Journal, 18(1), pp. 261-267. https://doi.org/10.1007/s10040-009-0520-5.

Boissonnat, J. D., Cazals, F., 2002. Smooth surface reconstruction via natural neighbour interpolation of distance functions. Computational Geometry, 22(1-3), pp.185-203. https://doi.org/10.1016/S0925-7721(01)00048-7.

Borrok, D.M., Broussard III, W.P., 2016. Long-term geochemical evaluation of the coastal Chicot aquifer system, Louisiana, USA. Journal of Hydrology, 533, pp. 320-331. https://doi.org/10.1016/j.jhydrol.2015.12.022.

Bowden, G.J., Maier, H.R. and Dandy, G.C., 2002. Optimal division of data for neural network models in water resources applications. Water Resources Research, 38(2), pp.2-1. https://doi.org/10.1029/2001WR000266.

Bredehoeft, J.D., 2002. The water budget myth revisited: why hydrogeologists model. Groundwater, 40(4), pp. 340-345. https://doi.org/10.1111/j.1745-6584.2002.tb02511.x.

Brown, C. J., Ward, J., Mirecki, J., 2016. A revised brackish water aquifer storage and recovery (ASR) site selection index for water resources management. Water resources management, 30(7), pp.2465-2481. https://doi.org/10.1007/s11269-016-1297-7.

Buono, A., 1983. The Southern Hills regional aquifer system of southeastern Louisiana and southwestern Mississippi, Water-Resources Investigations Report 83-4189. US Geological Survey. 43 pp. https://doi.org/10.3133/wri834189.

Burnett, R. D. and Frind, E. O., 1987a. Simulation of contaminant transport in three dimensions: 1. The alternating direction Galerkin technique. Water Resources Research, 23(4), pp.683-694. https://doi.org/10.1029/WR023i004p00683.

Burnett, R. D. and Frind, E. O., 1987b. Simulation of contaminant transport in three dimensions: 2. Dimensionality effects. Water Resources Research, 23(4), pp.695-705. https://doi.org/10.1029/WR023i004p00695.

Byrne, J. V., LeRoy, D. O., Riley, C. M., 1959. The Chenier plain and its stratigraphy, southwestern Louisiana. Gulf Coast Association of Geological Societies Transactions, 9: 237-260.

Cao, G., Zheng, C., Scanlon, B.R., Liu, J., Li, W., 2013. Use of flow modeling to assess sustainability of groundwater resources in the North China Plain. Water Resources Research, 49(1), pp. 159-175. https://doi.org/10.1029/2012WR011899.

Catuneanu, O., 2019. Model-independent sequence stratigraphy. Earth-Science Reviews, 188, pp. 312-388. https://doi.org/10.1016/j.earscirev.2018.09.017.

Catuneanu, O., Galloway, W.E., Kendall, C.G.S.C., Miall, A.D., Posamentier, H.W., Strasser, A., Tucker, M.E., 2011. Sequence stratigraphy: Methodology and nomenclature. Newsletters on Stratigraphy, 44(3), pp.173-245. https://dx.doi.org/10.1127/0078-0421/2011/0011.

Caumon, G., Collon-Drouaillet, P. L. C. D., De Veslud, C. L. C., Viseur, S., Sausse, J., 2009. Surface-based 3D modeling of geological structures. Mathematical Geosciences, 41(8), pp.927-945. https://doi.org/10.1007/s11004-009-9244-2.

Chai, T., Draxler, R.R., 2014. Root mean square error (RMSE) or mean absolute error (MAE)? Arguments against avoiding RMSE in the literature. Geoscientific Model Development, 7(3), pp. 1247-1250. https://doi.org/10.5194/gmd-7-1247-2014.

Chang, Y. S., Park, H. D., 2004. Development of a web-based geographic information system for the management of borehole and geological data. Computers and Geosciences, 30(8), pp. 887-897. https://doi.org/10.1016/j.cageo.2004.07.006.

Chen, Y.-H., Tsai, F. T.-C., Jafari, N. H., 2021. Multi-objective Optimization of Relief Well Operations to Improve Levee Safety. Journal of Geotechnical and Geoenvironmental Engineering 147(7). https://doi.org/10.1061/(ASCE)GT.1943-5606.0002532.

Cheng, T., 2013. Accelerating universal Kriging interpolation algorithm using CUDA-enabled GPU. Computers and Geosciences, 54, pp. 178-183. https://doi.org/10.1016/j.cageo.2012.11.013.

Chesnaux, R., Lambert, M., Walter, J., Fillastre, U., Hay, M., Rouleau, A., Daigneault, R., Moisan, A., Germaneau, D., 2011. Building a geodatabase for mapping hydrogeological features and 3D modeling of groundwater systems: Application to the Saguenay–Lac-St.-Jean region, Canada. Computers and Geosciences, 37(11), pp. 1870-1882.

https://doi.org/10.1016/j.cageo.2011.04.013.

Chilès, J. P., Delfiner, P., 2009. Geostatistics: Modeling Spatial Uncertainty. John Wiley and Sons, 734 pp.

Christelis, V., Mantoglou, A., 2016. Coastal aquifer management based on the joint use of density-dependent and sharp interface models. Water Resources Management, 30(2), pp. 861-876. https://doi.org/10.1007/s11269-015-1195-4.

Clevis, Q., Tucker, G.E., Lancaster, S.T., Desitter, A., Gasparini, N., Lock, G., 2006. A simple algorithm for the mapping of TIN data onto a static grid: applied to the stratigraphic simulation of river meander deposits. Computers and geosciences, 32(6), pp. 749-766. https://doi.org/10.1016/j.cageo.2005.05.012.

Collier, A., Sargent, B. P., 2018. Water use in Louisiana, 2015. Water Resources Special Report 18, Louisiana Department of Transportation and Development, Baton Rouge, LA, 138 p.

Cousquer, Y., Pryet, A., Flipo, N., Delbart, C., Dupuy, A., 2017. Estimating river conductance from prior information to improve surface-subsurface model calibration. Groundwater, 55(3), pp. 408-418. https://doi.org/10.1111/gwat.12492.

Custodio, E., 2010. Coastal aquifers of Europe: an overview. Hydrogeology Journal, 18(1), pp. 269-280. https://doi.org/10.1007/s10040-009-0496-1.

D'Agnese, F. A., Faunt, C. C., Hill, M. C., Turner, A. K., 1999. Death Valley regional ground-water flow model calibration using optimal parameter estimation methods and geoscientific information systems. Advances in Water Resources 22(8), 777–790. https://doi.org/10.1016/S0309-1708(98)00053-0.

Daniel, D.E., 1984. Predicting hydraulic conductivity of clay liners. Journal of Geotechnical Engineering, 110(2), pp.285-300. https://doi.org/10.1061/(ASCE)0733-9410(1984)110:2(285).

Danielsen, J.E., Dahlin, T., Owen, R., Mangeya, P., Auken, E., 2007. Geophysical and hydrogeologic investigation of groundwater in the Karoo stratigraphic sequence at Sawmills in northern Matabeleland, Zimbabwe: a case history. Hydrogeology Journal, 15, pp. 945-960. https://doi.org/10.1007/s10040-007-0191-z.

de Graaf, I. E. M., Sutanudjaja, E. H., van Beek, L. P. H., Bierkens, M. F. P., 2015. A high-resolution global-scale groundwater model. Hydrology and Earth System Sciences 19, 823–837. https://doi.org/10.5194/hess-19-823-2015.

Deb, K., Pratap, A., Agarwal, S., Meyarivan, T. A. M. T., 2002. A fast and elitist multiobjective genetic algorithm: NSGA-II. IEEE transactions on evolutionary computation, 6(2), pp.182-197. DOI: 10.1109/4235.996017.

Dillon, P. J., Pavelic, P., Page, D., Beringen, H., Ward, J., 2009. Managed aquifer recharge. *An introduction waterlines report series, 13*, pp.1-64.

Doherty, J. E., M. N. Fienen, and R. J. Hunt. 2010. “Approaches to Highly Parameterized Inversion: Pilot-Point Theory, Guidelines, and Research Directions.” U.S. Geological Survey Scientific Investigations Report 2010–5168, 36 p.

Döll, P., Schmied, H. M., Schuh, C., Portmann, F. T., Eicker, A., 2014. Global-scale assessment of groundwater depletion and related groundwater abstractions: Combining hydrological modeling with information from well observations and GRACE satellites. Water Resources Research 50(7), 5698–5720. https://doi.org/10.1002/2014WR015595.

Dorigo, M., Di Caro, G., 1999. Ant colony optimization: a new meta-heuristic. In Proceedings of the 1999 congress on evolutionary computation-CEC99 (Cat. No. 99TH8406). IEEE, pp. 1470-1477. https://doi.org/10.1109/CEC.1999.782657.

Doucet, A., Briers, M., Sénécal, S., 2006. Efficient block sampling strategies for sequential Monte Carlo methods. Journal of Computational and Graphical Statistics, 15(3), pp.693-711. https://doi.org/10.1198/106186006X142744.

Dowd, P. A., 1991. A review of recent developments in geostatistics. Computers and Geosciences, 17(10), pp. 1481-1500. https://doi.org/10.1016/0098-3004(91)90009-3.

Eggleston, J., Pope, J., 2013. Land subsidence and relative sea-level rise in the southern Chesapeake Bay region. US Geological Survey Circular, 1392, p. 30. https://dx.doi.org/10.3133/cir1392.

Elshall, A.S., Pham, H.V., Tsai, F.T.-C., Yan, L., Ye, M., 2015. Parallel inverse modeling and uncertainty quantification for computationally demanding groundwater-flow models using covariance matrix adaptation. Journal of Hydrologic Engineering, 20(8): 04014087. http://dx.doi.org/10.1061/(ASCE)HE.1943-5584.0001126.

Elshall, A.S., Tsai, F.T.-C., Hanor, J.S., 2013. Indicator geostatistics for reconstructing Baton Rouge aquifer-fault hydrostratigraphy, Louisiana, USA. Hydrogeology Journal, 21(8), pp. 1731-1747. https://doi.org/10.1007/s10040-013-1037-5.

Ewing, T. E., 2009. The ups and downs of the Sabine Uplift and the northern Gulf of Mexico Basin: Jurassic basement blocks, Cretaceous thermal uplifts, and Cenozoic flexure. Gulf Coast Association of Geological Societies Transactions, 59, p. 253-269.

Fendick Jr., R.B., Nyman, D.J., 1987. Louisiana ground-water map no. 1: potentiometric surface, 1985, and water-level changes, 1983-85, of the Chicot aquifer in southwestern Louisiana, Water-Resources Investigations Report 86-4348. US Geological Survey. https://doi.org/10.3133/wri864348.

Forghani, A., 2018."Simulation and Optimization Models to Evaluate Performance of Aquifer Storage and Recovery Wells in Fresh Water Aquifers" *All Graduate Theses and Dissertations*. 6933. https://digitalcommons.usu.edu/etd/6933.

Forghani, A., Peralta, R. C., 2017. Transport modeling and multivariate adaptive regression splines for evaluating performance of ASR systems in freshwater aquifers. Journal of

Hydrology, 553, pp.540-548. https://doi.org/10.1016/j.jhydrol.2017.08.012.

Forghani, A., Peralta, R. C., 2018. Intelligent performance evaluation of aquifer storage and recovery systems in freshwater aquifers. Journal of Hydrology, 563, pp.599-608. https://doi.org/10.1016/j.jhydrol.2018.06.042.

Frind, E. O., Sudicky, E. A. and Schellenberg, S. L., 1987. Micro-scale modelling in the study of plume evolution in heterogeneous media. Stochastic hydrology and Hydraulics, 1(4), pp.263-279. https://doi.org/10.1007/BF01543098.

Fu, J., Gómez-Hernández, J. J., 2009. Uncertainty assessment and data worth in groundwater flow and mass transport modeling using a blocking Markov chain Monte Carlo method. Journal of Hydrology, 364(3-4), pp.328-341. https://doi.org/10.1016/j.jhydrol.2008.11.014.

Gallerini, G., De Donatis, M., 2009. 3D modeling using geognostic data: The case of the low valley of Foglia river (Italy). Computers and Geosciences, 35(1), pp. 146-164. https://doi.org/10.1016/j.cageo.2007.09.012.

Galloway, W. E., Whiteaker, T. L., Ganey-Curry, P., 2011. History of Cenozoic North American drainage basin evolution, sediment yield, and accumulation in the Gulf of Mexico basin. Geosphere, 7(4), pp. 938-973. https://doi.org/10.1130/GES00647.1.

Galloway, W.E., 1977. Catahoula Formation of the Texas Coastal Plain: depositional systems, composition, structural development, ground-water flow history, and uranium distribution, Report of Investigations No. 87. Bureau of Economic Geology, The University of Texas at Austin.

Goderniaux, P., Brouyère, S., Fowler, H. J., Blenkinsop, S., Therrien, R., Orban, P., Dassargues, A., 2009. Large scale surface–subsurface hydrological model to assess climate change impacts on groundwater reserves. Journal of Hydrology, 373(1-2), pp.122-138. https://doi.org/10.1016/j.jhydrol.2009.04.017.

Granata, W. H., 1963. Cretaceous stratigraphy and structural development of the Sabine Uplift area, Texas and Louisiana. Shreveport Geological Society, 5, 84 pp.

Green, P.J., Sibson, R., 1978. Computing Dirichlet tessellations in plane. Computer Journal 21 (2), 168–173. https://doi.org/10.1093/comjnl/21.2.168.

Guo, H., Zhang, Z., Cheng, G., Li, W., Li, T. and Jiao, J.J., 2015. Groundwater-derived land subsidence in the North China Plain. Environmental Earth Sciences, 74(2), pp. 1415-1427. https://doi.org/10.1007/s12665-015-4131-2.

Guo, W., Coulibaly, K., Maliva, R. G., 2015. Simulated effects of aquifer heterogeneity on ASR system performance. Environmental Earth Sciences, 73(12), pp.7803-7809. https://doi.org/10.1007/s12665-014-3822-4.

Halbouty, M. T., Halbouty, J. J., 1982. Relationships between East Texas field region and

Sabine Uplift in Texas. The American Association of Petroleum Geologists Bulletin, 66(8), pp. 1042-1054.

Hansen, N., Müller, S.D., Koumoutsakos, P., 2003. Reducing the time complexity of the derandomized evolution strategy with covariance matrix adaptation (CMA-ES). Evolutionary Computation, 11(1), pp. 1-18. https://doi.org/10.1162/106365603321828970.

Haq, B. U., 1991. Sequence stratigraphy, sea-level change, and significance for the deep sea. In: Macdonald, D. I. M. (Ed) Sedimentation, Tectonics and Eustasy: Sea-Level Changes at Active Margins, Special Publications of The International Association of Sedimentologists, 12, pp. 3-39.

Harbaugh, A. W. (2005). "MODFLOW-2005, The U.S. Geological Survey Modular Ground-Water Model: the ground-water flow process," in: Modeling techniques, Book 6, section A, (Reston, VA US Geological Survey), 253. https://doi.org/10.3133/tm6A16.

Hartono, S., 2005. Spatial and temporal estimation of pumping and recharge in groundwater system analysis (Doctoral dissertation), Louisiana State University, Baton Rouge, Louisiana, US. https://digitalcommons.lsu.edu/gradschool_dissertations/309.

He, X., Koch, J., Sonnenborg, T. O., Jørgensen, F., Schamper, C., Refsgaard, J. C., 2014. Transition probability-based stochastic geological modeling using airborne geophysical data and borehole data. Water Resources Research, 50(4), pp.3147-3169. https://doi.org/10.1002/2013WR014593.

Heinrich, P. V., 2005. Distribution and Origin of Fault-Line Scarps of Southwest Louisiana, USA. Gulf Coast Association of Geological Societies Transactions, 55, pp. 284-293.

Helton, J. C. and Davis, F. J., 2003. Latin hypercube sampling and the propagation of uncertainty in analyses of complex systems. Reliability Engineering & System Safety, 81(1), pp.23-69. https://doi.org/10.1016/S0951-8320(03)00058-9.

Hilchie, D. W., (1982). Applied Openhole Log Interpretation for Geologists and Engineers (Revised). Douglas W. Hilchie Inc., Golden, Colorado.

Horton, J. D. The State Geologic Map Compilation (SGMC) geodatabase of the conterminous United States: U.S. Geological Survey data release, version 1.1, 2017. https://doi.org/10.5066/F7WH2N65.

Hosman, R. L., 1996. Regional stratigraphy and subsurface geology of Cenozoic deposits, Gulf Coastal Plain, south-central United States, Professional Paper 1416- G. US Geological Survey, 48 pp. https://doi.org/10.3133/pp1416G.

Hu, L. Y., Chugunova, T., 2008. Multiple-point geostatistics for modeling subsurface heterogeneity: A comprehensive review. Water Resources Research, 44(11). https://doi.org/10.1029/2008WR006993.

Iman, R. L., Conover, W. J., 1982. A distribution-free approach to inducing rank correlation among input variables. Communications in Statistics-Simulation and Computation, 11(3), pp.311-334. https://doi.org/10.1080/03610918208812265.

Imbens, G. W., Lancaster, T., 1996. Efficient estimation and stratified sampling. Journal of Econometrics, 74(2), pp.289-318. https://doi.org/10.1016/0304-4076(95)01756-9.

Janssen, H., 2013. Monte-Carlo based uncertainty analysis: Sampling efficiency and sampling convergence. Reliability Engineering & System Safety, 109, pp.123-132. https://doi.org/10.1016/j.ress.2012.08.003.

Jasechko, S., Perrone, D., Seybold, H., Fan, Y., Kirchner, J.W., 2020. Groundwater level observations in 250,000 coastal US wells reveal scope of potential seawater intrusion. Nature communications, 11(1), pp. 1-9. https://doi.org/10.1038/s41467-020-17038-2.

Johnson, A.I. 1967. Specific yield: Compilation of specific yields for various materials." U.S. Geological Survey, Water Supply Paper 1662-D. https://doi.org/10.3133/wsp1662D

Johnson, N. M., 1995. Characterization of alluvial hydrostratigraphy with indicator semivariograms. Water Resources Research, 31(12), pp.3217-3227. https://doi.org/10.1029/95WR02571.

Johnson, N. M., Dreiss, S. J., 1989. Hydrostratigraphic interpretation using indicator geostatistics. Water Resources Research, 25(12), pp.2501-2510. https://doi.org/10.1029/WR025i012p02501.

Johnson, N.M., Dreiss, S.J., 1989. Hydrostratigraphic interpretation using indicator geostatistics. Water Resources Research, 25(12), pp. 2501-2510. https://doi.org/10.1029/WR025i012p02501.

Jones, P. H., Hendricks, E. L., Irelan, B., 1956. Water resources of southwestern Louisiana, Water Supply Paper 1364. US Government Printing Office, 460 pp. https://doi.org/10.3133/wsp1364.

Jones, P. H., Hendricks, E. L., Irelan, B., 1956. Water resources of southwestern Louisiana, Water Supply Paper 1364. US Government Printing Office, 460 pp. https://pubs.er.usgs.gov/publication/wsp1364.

Jørgensen, F., Høyer, A. S., Sandersen, P. B., He, X., Foged, N., 2015. Combining 3D geological modelling techniques to address variations in geology, data type and density–An example from Southern Denmark. Computers and Geosciences, 81, pp. 53-63. https://doi.org/10.1016/j.cageo.2015.04.010.

Journel, A.G., Alabert, F., 1989. Non-Gaussian data expansion in the Earth Sciences. Terra Nova, 1(2), pp.123-134. https://doi.org/10.1111/j.1365-3121.1989.tb00344.x.

Katal, A., Wazid, M., Goudar, R. H., 2013. Big data: issues, challenges, tools and good practices. In: 2013 Sixth International Conference on Contemporary Computing (IC3). IEEE, pp.

404-409. https://doi.org/10.1109/IC3.2013.6612229.

Keating, E. H., Doherty, J., Vrugt, J. A., Kang, Q., 2010. Optimization and uncertainty assessment of strongly nonlinear groundwater models with high parameter dimensionality. Water Resources Research, 46(10). https://doi.org/10.1029/2009WR008584.

Khan, S., Mushtaq, S., Hanjra, M. A., Schaeffer, J., 2008. Estimating potential costs and gains from an aquifer storage and recovery program in Australia. Agricultural Water Management, 95(4), pp.477-488. https://doi.org/10.1016/j.agwat.2007.12.002.

Kindinger, J. L., Williams, S. J., Penland, S., Flocks, J. G., Connor, P., 1997. Holocene geologic framework of Lake Pontchartrain Basin and lakes of southeastern Louisiana. Gulf Coast Association of Geological Societies 47, pp. 635-638.

Konikow, L. F., 2011. The secret to successful solute-transport modeling. Groundwater, 49(2), pp.144-159. https://doi.org/10.1111/j.1745-6584.2010.00764.x.

Konikow, L.F., 2013. Groundwater depletion in the United States (1900−2008): U.S. Geological Survey Scientific Investigations Report 2013−5079, 63 p., http://pubs.usgs.gov/sir/2013/5079.

Kostic, B., Becht, A., Aigner, T., 2005. 3-D sedimentary architecture of a Quaternary gravel delta (SW-Germany): Implications for hydrostratigraphy. Sedimentary Geology, 181(3-4), pp. 147-171. https://doi.org/10.1016/j.sedgeo.2005.07.004.

Kumar, M., Husian, M., Upreti, N., Gupta, D., 2010. Genetic algorithm: Review and application. International Journal of Information Technology and Knowledge Management, 2(2), pp. 451-454.

LaHaye, O., Habib, E.H., Vahdat-Aboueshagh, H., Tsai, F.T.-C. and Borrok, D., 2021. Assessment of Aquifer Storage and Recovery Feasibility Using Numerical Modeling and Geospatial Analysis: Application in Louisiana. JAWRA Journal of the American Water Resources Association, 57(3), pp. 505-526. https://doi.org/10.1111/1752-1688.12923.

Lee, S. Y., Carle, S. F., Fogg, G. E., 2007. Geologic heterogeneity and a comparison of two geostatistical models: Sequential Gaussian and transition probability-based geostatistical simulation. Advances in Water Resources, 30(9), pp. 1914-1932. https://doi.org/10.1016/j.advwatres.2007.03.005.

Lemon, A. M. and Jones, N. L., 2003. Building solid models from boreholes and user-defined cross-sections. Computers and Geosciences, 29(5), pp. 547-555. https://doi.org/10.1016/S0098-3004(03)00051-7.

Lien, J-M, Liu, G., Langevin, C.D., 2015. GRIDGEN version 1.0: A computer program for generating unstructured finite-volume grids. U.S. Geological Survey Open-File Report 2014–1109, 26 p., https://dx.doi.org/10.3133/ofr20141109.

Liu, Y., Harding, A., Abriel, W., Strebelle, S., 2004. Multiple-point simulation integrating wells, three-dimensional seismic data, and geology. The American Association of Petroleum Geologists bulletin, 88(7), pp.905-921. https://doi.org/10.1306/02170403078.

Loucks, D.P., 2000. Sustainable water resources management. Water international, 25(1), pp. 3-10. https://doi.org/10.1080/02508060008686793.

Lovelace, J. K., Jared, W., Fontenot, C., Paul, F. (2004). Withdrawals, water levels, and specific conductance in the Chicot aquifer system in southwestern Louisiana, 2000-03, Scientific Investigations Report 2004-5212. U.S. Geol. Survey. https://doi.org/10.3133/sir20045212.

Lowry, C. S., Anderson, M. P., 2006. An assessment of aquifer storage recovery using ground water flow models. Groundwater, 44(5), pp.661-667. https://doi.org/10.1111/j.1745-6584.2006.00237.x.

Lu, C., Du, P., Chen, Y., Luo, J., 2011. Recovery efficiency of aquifer storage and recovery (ASR) with mass transfer limitation. Water Resources Research, 47(8). https://doi.org/10.1029/2011WR010605.

Luo, J., Lu, W., 2014. Comparison of surrogate models with different methods in groundwater remediation process. Journal of Earth System Science, 123(7), pp.1579-1589. https://doi.org/10.1007/s12040-014-0494-0.

MacCormack, K.E., Berg, R.C., Kessler, H., Russell, H.A.J., Thorleifson, L.H. (ed.), 2019. 2019 synopsis of current three-dimensional geological mapping and modelling in geological survey organizations; Alberta Energy Regulator / Alberta Geological Survey, AER/AGS Special Report 112, 307 p. https://ags.aer.ca/publications/SPE_112.html#summary.

Maliva, R. G., 2014. Economics of managed aquifer recharge. Water, *6*(5), pp.1257-1279. https://doi.org/10.3390/w6051257.

Mallet, J.L., 2004. Space–time mathematical framework for sedimentary geology. Mathematical geology, 36(1), pp.1-32. https://doi.org/10.1023/B:MATG.0000016228.75495.7c.

Mallet, J.L., 2014. Elements of Mathematical Sedimentary Geology: the GeoChron Model. European Association of Geoscientists and Engineers (EAGE) Publications, 374 pp.

Marinoni, O., 2003. Improving geological models using a combined ordinary–indicator kriging approach. Engineering Geology, 69(1-2), pp. 37-45. https://doi.org/10.1016/S0013-7952(02)00246-6.

Martin, A., Whiteman, C.D., 1989. Geohydrology and regional ground-water flow of the Coastal Lowlands aquifer system in parts of Louisiana, Mississippi, Alabama, and Florida--a preliminary analysis. Department of the Interior, US Geological Survey. Series number: 8-4100. https://doi.org/10.3133/wri884100.

Matson, G. C., 1916. The Pliocene Citronelle Formation of the Gulf Coastal Plain, Professional

Paper 98- L. US Government Printing Office. https://doi.org/10.3133/pp98L.

Maxwell, R. M., Condon, L. E., Kollet, S. J., 2015. A high-resolution simulation of groundwater and surface water over most of the continental US with the integrated hydrologic model ParFlow v3. Geoscientific Model Development 8, pp. 923–937. https://doi.org/10.5194/gmd-8-923-2015.

McCulloh R. P., Heinrich P. V., 2012. Surface faults of the south Louisiana growth-fault province. Geological Society of America Special Papers, 493, pp. 37–49. https://doi.org/10.1130/2012.2493(03).

Merritt, M. L., 1986. Recovering fresh water stored in saline limestone aquifers. Groundwater, 24(4), pp.516-529. https://doi.org/10.1111/j.1745-6584.1986.tb01031.x.

Minsley, B. J., Ajo-Franklin, J., Mukhopadhyay, A., Morgan, F. D., 2011. Hydrogeophysical methods for analyzing aquifer storage and recovery systems. Groundwater, 49(2), pp.250-269. https://doi.org/10.1111/j.1745-6584.2010.00676.x.

Missimer, T. M., Guo, W., Walker, C. W., Maliva, R. G., 2002. Hydraulic and density considerations in the design of aquifer storage and recovery systems. Florida Water Resources Journal, 55(2), pp.30-36.

Neyman, J., 1992. On the two different aspects of the representative method: the method of stratified sampling and the method of purposive selection. In *Breakthroughs in Statistics* (pp. 123-150). Springer, New York, NY. https://doi.org/10.1007/978-1-4612-4380-9_12.

Nourani, V., Mogaddam, A. A., Nadiri, A. O., 2008. An ANN-based model for spatiotemporal groundwater level forecasting. Hydrological Processes: An International Journal, 22(26), pp.5054-5066. https://doi.org/10.1002/hyp.7129.

Nyman, D.J., Halford, K.J., Martin Jr., A., 1990. Geohydrology and simulation of flow in the Chicot aquifer system of Southwest Louisiana, Water Resources Technical Report 50. Louisiana Department of Transportation and Development, 65 pp.

Owen, D. E., 2008. Geology of the Chenier Plain of Cameron Parish, southwestern Louisiana. In: Moore G. (Ed.) Geological Society of America Field Guide 14 2008 Joint Annual Meeting, Houston, Texas, 5–9 October 2008, The Geological Society of America. https://doi.org/10.1130/2008.fld014(02).

Pardo-Iguzquiza, E., Dowd, P.A., 1998. The second-order stationary universal kriging model revisited. Mathematical geology, 30(4), pp. 347-378. https://doi.org/10.1023/A:1021740123100.

Parizi, E., Hosseini, S.M., Ataie-Ashtiani, B., Simmons, C.T., 2019. Vulnerability mapping of coastal aquifers to seawater intrusion: review, development and application. Journal of hydrology, 570, pp. 555-573. https://doi.org/10.1016/j.jhydrol.2018.12.021.

Pasandideh, S. H. R., Niaki, S. T. A. and Asadi, K., 2015. Bi-objective optimization of a multi-product multi-period three-echelon supply chain problem under uncertain environments: NSGA-II and NRGA. Information Sciences, 292, pp.57-74. https://doi.org/10.1016/j.ins.2014.08.068.

Pavelic, P., Dillon, P. J. and Simmons, C. T., 2006. Multi-scale hydraulic characterization of a stratified aquifer used for ASR. Ground Water, 44(2), pp.155-164. https://doi.org/10.1111/j.1745-6584.2005.00135.x.

Pham, H. V., Tsai, F.T.-C., 2017. Modeling complex aquifer systems: a case study in Baton Rouge, Louisiana (USA). Hydrogeology Journal 25, pp. 601–615. https://doi.org/10.1007/s10040-016-1532-6.

Poli, R., Kennedy, J., Blackwell, T., 2007. Particle swarm optimization. Swarm intelligence, 1(1), pp. 33-57. https://doi.org/10.1007/s11721-007-0002-0.

Posamentier, H. W., Allen, G. P., 1993. Siliciclastic sequence stratigraphic patterns in foreland, ramp-type basins. Geology, 21(5), pp. 455-458. https://doi.org/10.1130/0091-7613(1993)021%3C0455:SSSPIF%3E2.3.CO;2.

Posamentier, H. W., James, D. P., 1993. An overview of sequence-stratigraphic concepts: uses and abuses. In: Posamentier, H. W., Summerhayes, C. P., Haq, B. U., Allen, G. P. (Eds) Sequence Stratigraphy and Facies Associations, Special Publications of The International Association of Sedimentologists, 18, pp. 3-18.

Pyne, R. D. G., 1995. Groundwater Recharge and Wells: A Guide to Aquifer Storage Recovery. Lewis Publishers, Boca Raton, FL.

Pyne, R. D. G., 2015. Aquifer storage recovery: An ASR solution to saltwater intrusion at Hilton Head Island, South Carolina, USA. Environmental Earth Sciences, 73(12), pp.7851-7859. https://doi.org/10.1007/s12665-014-3985-z.

Quintana, D.S.Z., Rentería, C.M.L., Vega, N.E.M., Peralta, J.E., Contreras, L.E.V., 2018. Sustainability strategies for coastal aquifers: A case study of the Hermosillo Coast aquifer. Journal of Cleaner Production, 195, pp. 1170-1182. https://doi.org/10.1016/j.jclepro.2018.05.191.

Rabbani, M., Heidari, R. and Yazdanparast, R., 2019. A stochastic multi-period industrial hazardous waste location-routing problem: Integrating NSGA-II and Monte Carlo simulation. European Journal of Operational Research, 272(3), pp.945-961. https://doi.org/10.1016/j.ejor.2018.07.024.

Rahman, A., Tsai, F.T.-C., White, C.D., Carlson, D.A., Willson, C.S., 2008. Geophysical data integration, stochastic simulation and significance analysis of groundwater responses using ANOVA in the Chicot Aquifer system, Louisiana, USA. Hydrogeology Journal, 16(4), pp. 749-764. https://doi.org/10.1007/s10040-007-0258-x.

Razavi, S., Gupta, H. V., 2016. A new framework for comprehensive, robust, and efficient global

sensitivity analysis: 1. Theory. Water Resources Research, 52(1), pp.423-439. https://doi.org/10.1002/2015WR017558.

Razavi, S., Tolson, B. A., Burn, D. H., 2012. Review of surrogate modeling in water resources. Water Resources Research, 48(7). https://doi.org/10.1029/2011WR011527.

Refsgaard, J. C., Christensen, S., Sonnenborg, T. O., Seifert, D., Højberg, A. L., Troldborg, L., 2012. Review of strategies for handling geological uncertainty in groundwater flow and transport modeling. Advances in Water Resources, 36, pp.36-50. https://doi.org/10.1016/j.advwatres.2011.04.006.

Reitz, M., Sanford, W.E., 2019a. Estimating quick-flow runoff at the monthly timescale for the conterminous United States. Journal of Hydrology, 573, pp. 841-854. https://doi.org/10.1016/j.jhydrol.2019.04.010.

Reitz, M., Sanford, W.E., 2019b. Modern monthly effective recharge maps for the conterminous U.S., 2003-2015. U.S. Geological Survey data release. https://doi.org/10.5066/P9NRVAQ5.

Renken, R. A., 1998. Ground Water Atlas of the United States: Segment 5, Arkansas, Louisiana, Mississippi, Hydrologic Atlas 730- F. US Geological Survey. 28 pp. https://doi.org/10.3133/ha730F.

Rios, L.M., Sahinidis, N.V., 2013. Derivative-free optimization: a review of algorithms and comparison of software implementations. Journal of Global Optimization, 56(3), pp. 1247-1293. https://doi.org/10.1007/s10898-012-9951-y.

Roberts, H.H., 1997. Dynamic changes of the Holocene Mississippi River delta plain: the delta cycle. Journal of Coastal Research 13(3), pp. 605-627.

Ross, M., Parent, M., Lefebvre, R., 2005. 3D geologic framework models for regional hydrogeology and land-use management: a case study from a Quaternary basin of southwestern Quebec, Canada. Hydrogeology Journal, 13(5-6), pp. 690-707. https://doi.org/10.1007/s10040-004-0365-x.

Royse, K. R., 2010. Combining numerical and cognitive 3D modelling approaches in order to determine the structure of the Chalk in the London Basin. Computers and Geosciences, 36(4), pp. 500-511. https://doi.org/10.1016/j.cageo.2009.10.001.

Ryals, G. N., 1982. Regional Geohydrology of the Northern Louisiana Salt-dome Basin: Part I, Conceptual Model and Data Needs, Open-File Report 82-343. US Geological Survey, 27 pp. https://doi.org/10.3133/ofr82343.

Sargent, B.P., 2004. Thickness of the Chicot aquifer system surficial confining unit and location of Shallow sands, Southwestern Louisiana. Louisiana Department of Transportation and Development, Water Resources Technical Report 73. 34 pp.

Sargent, B. P., 2011. Water use in Louisiana, 2010. Louisiana Department of Transportation and

Development. 136 pp. (Revised December 2012)

Saucier, R. T., 1994. Geomorphology and Quarternary geologic history of the Lower Mississippi Valley. y: Vicksburg, Mississippi, Waterways Experiment Station, U.S. Army Corps of Engineers,. 417 pp.

Schulze-Makuch, D., 2005. Longitudinal dispersivity data and implications for scaling behavior. Groundwater, 43(3), pp.443-456. https://doi.org/10.1111/j.1745-6584.2005.0051.x.

Shahin, M. A., Maier, H. R., Jaksa, M. B., 2004. Data division for developing neural networks applied to geotechnical engineering. Journal of Computing in Civil Engineering, 18(2), pp.105-114. https://doi.org/10.1061/(ASCE)0887-3801(2004)18:2(105).

Shammas, M. I., 2008. The effectiveness of artificial recharge in combating seawater intrusion in Salalah coastal aquifer, Oman. Environmental geology, 55(1), pp.191-204. https://doi.org/10.1007/s00254-007-0975-4.

Sheng, Z., 2005. An aquifer storage and recovery system with reclaimed wastewater to preserve native groundwater resources in El Paso, Texas. Journal of environmental management, 75(4), pp.367-377. https://doi.org/10.1016/j.jenvman.2004.10.007.

Shields, M. D., Zhang, J., 2016. The generalization of Latin hypercube sampling. Reliability Engineering & System Safety, 148, pp.96-108. https://doi.org/10.1016/j.ress.2015.12.002.

Singh, V., Gupta, I., Gupta, H. O., 2007. ANN-based estimator for distillation using Levenberg–Marquardt approach. Engineering Applications of Artificial Intelligence, 20(2), pp.249-259. https://doi.org/10.1016/j.engappai.2006.06.017.

Sivarajah, U., Kamal, M. M., Irani, Z., Weerakkody, V., 2017. Critical analysis of Big Data challenges and analytical methods. Journal of Business Research, 70, pp. 263-286. https://doi.org/10.1016/j.jbusres.2016.08.001.

Smoot, C. W., 1986. Louisiana hydrologic atlas map no. 2: Areal extent of freshwater in major aquifers of Louisiana: U.S. Geological Survey Water-Resources Investigations Report 86-4150, 1 sheet. https://doi.org/10.3133/wri864150.

Soares, A., 1990. Geostatistical estimation of orebody geometry: morphological kriging. Mathematical Geology, 22(7), pp. 787-802. https://doi.org/10.1007/BF00890663.

Song, S., Hou, J., Dou, L., Song, Z., Sun, S., 2020. Geologist-level wireline log shape identification with recurrent neural networks. Computers & Geosciences, 134, p.104313. https://doi.org/10.1016/j.cageo.2019.104313.

Spiegel, M.R., 1986. Mathematical Handbook of Formulas and Tables., Schaum's Outline Series., McGraw-Hill Publishing Company, New York, 271pp.

Sreekanth, J., Datta, B., 2015. Simulation-optimization models for the management and monitoring of coastal aquifers. Hydrogeology Journal, 23(6), pp. 1155-1166. https://doi.org/10.1007/s10040-015-1272-z.

Strebelle, S., 2002. Conditional simulation of complex geological structures using multiple-point statistics. Mathematical geology, 34(1), pp.1-21. https://doi.org/10.1023/A:1014009426274.

Stuart, C. G., Knochenmus, D. D., McGee, B. D., 1994. Guide to Louisiana's Ground-water Resources (Vol. 94, No. 4085). U.S. Geological Survey, Water-Resources Investigations Report 94-4085. USGS Earth Science Information Center, Open-File Reports Section, 55 pp. https://doi.org/10.3133/wri944085.

Sukumar, N., Moran, B., Yu Semenov, A., Belikov, V.V., 2001. Natural neighbour Galerkin methods. International Journal for Numerical Methods in Engineering, 50(1), pp.1-27. https://doi.org/10.1002/1097-0207(20010110)50:1%3C1::AID-NME14%3E3.0.CO;2-P.

Sultana, S., Ahmed, K. M., Mahtab-Ul-Alam, S. M., Hasan, M., Tuinhof, A., Ghosh, S. K., Rahman, M. S., Ravenscroft, P., Zheng, Y., 2015. Low-cost aquifer storage and recovery: implications for improving drinking water access for rural communities in coastal Bangladesh. Journal of Hydrologic Engineering, 20(3), p.B5014007. https://doi.org/10.1061/(ASCE)HE.1943-5584.0001100.

Sutanudjaja, E. H., van Beek, L. P. H., de Jong, S. M., van Geer, F. C., Bierkens, M. F. P., 2011. Large-scale groundwater modeling using global datasets: a test case for the Rhine-Meuse basin. Hydrology and Earth System Sciences 15, 2913–2935. https://doi.org/10.5194/hess-15-2913-2011.

Tartakovsky, D.M., Wohlberg, B., Guadagnini, A., 2007. Nearest-neighbor classification for facies delineation. Water resources research, 43(7). https://doi.org/10.1029/2007WR005968.

Touch, S., Likitlersuang, S., Pipatpongsa, T., 2014. 3D geological modelling and geotechnical characteristics of Phnom Penh subsoils in Cambodia. Engineering geology, 178, pp.58-69. https://doi.org/10.1016/j.enggeo.2014.06.010.

Trichakis, I. C., Nikolos, I. K., Karatzas, G. P., 2011. Artificial neural network (ANN) based modeling for karstic groundwater level simulation. Water Resources Management, 25(4), pp.1143-1152. https://doi.org/10.1007/s11269-010-9628-6.

Triki, C., Zekri, S., Al-Maktoumi, A., Bazargan-Lari, M. R., 2019. Optimal location of wells for storage and recovery of surplus desalinated water in coastal aquifers. Groundwater, 58(5), pp.831-841. https://doi.org/10.1111/gwat.12951.

Tsai, F.T.-C., 2009. Indicator generalized parameterization for interpolation point selection in groundwater inverse modeling. Journal of Hydrologic Engineering, 14(3), pp. 233-242. https://doi.org/10.1061/(ASCE)1084-0699(2009)14:3(233).

Tsai, F.T.-C, Li, X. 2009. Conditional estimation of distributed hydraulic conductivity in groundwater inverse modeling: Indicator-generalized parameterization and natural neighbors. In: Abrahart, R.J., See, L.M., Solomatine, D.P. (eds) Practical Hydroinformatics. Water Science and Technology Library, vol 68. Springer, Berlin, Heidelberg. https://doi.org/10.1007/978-3-540-79881-1_18.

U.S. Census Bureau, 2010. State Area Measurements and Internal Point Coordinates. https://www.census.gov/geographies/reference-files/2010/geo/state-area.html (Access date: Jan. 11, 2020)

Uddameri, V., 2007. A dynamic programming model for optimal planning of aquifer storage and recovery facility operations. Environmental geology, 51(6), pp.953-962. https://doi.org/10.1007/s00254-006-0458-z.

USEPA, 2019, Overview of the Drinking Water Sole Source Aquifer Program. U.S. Environmental Protection Agency, Retrieved from: https://www.epa.gov/dwssa/overview-drinking-water-sole-source-aquifer-program#What_Is_SSA.

USGS, 2020. U.S. Geological Survey, Water Resources of Louisiana's Parishes. https://www.usgs.gov/centers/lmg-water/science/water-resources-louisiana-s-parishes?qt-science_center_objects=0#qt-science_center_objects (Access date: Jan. 2020)

Vahdat-Aboueshagh, H., Tsai, F. T.-C., 2021. Constructing large-scale complex aquifer systems with big well log data: Louisiana model. Computers & Geosciences, 148, p.104687. https://doi.org/10.1016/j.cageo.2021.104687.

Vahdat-Aboueshagh, H., Tsai, F. T.-C., Bhatta, D., Paudel, K. P., 2021. Irrigation-Intensive groundwater modeling of complex aquifer systems through integration of big geological data. Frontiers in Water, 3, p.29. https://doi.org/10.3389/frwa.2021.623476.

Wackernagel, H., 2013. Multivariate Geostatistics: An Introduction with Applications. Springer Science and Business Media, 292pp.

Ward, J. D., Simmons, C. T. and Dillon, P. J., 2007. A theoretical analysis of mixed convection in aquifer storage and recovery: how important are density effects? Journal of Hydrology, 343(3-4), pp.169-186. https://doi.org/10.1016/j.jhydrol.2007.06.011.

Ward, J. D., Simmons, C. T., Dillon, P. J., Pavelic, P., 2009. Integrated assessment of lateral flow, density effects and dispersion in aquifer storage and recovery. Journal of Hydrolody, 370(1-4), pp.83-99. https://doi.org/10.1016/j.jhydrol.2009.02.055.

Watson, D., 1999. The natural neighbor series manuals and source codes. Computers and Geosciences, 25(4), pp.463-466. https://doi.org/10.1016/S0098-3004(98)00150-2.

Weiss, J. S., 1990. Geohydrologic units of the coastal lowlands aquifer system, south-central United States, Open-File Report 90-173. Department of the Interior, U.S. Geological Survey; Books and Open-File Reports Section, 34 pp. https://doi.org/10.3133/ofr90173.

Weissmann, G. S., Carle, S. F., Fogg, G. E., 1999. Three-dimensional hydrofacies modeling based on soil surveys and transition probability geostatistics. Water Resources Research, 35(6), pp.1761-1770. https://doi.org/10.1029/1999WR900048.

Williams, C.B., Duex, T.W. (1995). A hydrogeological study of the Chicot aquifer in Lafayette Parish, Louisiana. Gulf Coast Association of Geological Societies Transactions, 45, pp. 165-172.

Wolock, D.M., 2003. Estimated mean annual natural ground-water recharge in the conterminous United States. U.S. Geological Survey, 2003-311. https://doi.org/10.3133/ofr03311.

Wu, Q., Xu, H., Zou, X., 2005. An effective method for 3D geological modeling with multi-source data integration. Computers and Geosciences, 31(1), pp.35-43. https://doi.org/10.1016/j.cageo.2004.09.005.

Wycisk, P., Hubert, T., Gossel, W., Neumann, C., 2009. High-resolution 3D spatial modelling of complex geological structures for an environmental risk assessment of abundant mining and industrial megasites. Computers and Geosciences, 35(1), pp. 165-182. https://doi.org/10.1016/j.cageo.2007.09.001.

Xu, M., Eckstein, Y., 1995. Use of weighted least-squares method in evaluation of the relationship between dispersivity and field scale. Groundwater, 33(6), pp.905-908. https://doi.org/10.1111/j.1745-6584.1995.tb00035.x.

Yan, S., Minsker, B., 2006. Optimal groundwater remediation design using an adaptive neural network genetic algorithm. Water Resources Research, 42(5). https://doi.org/10.1029/2005WR004303.

Yan, S., Minsker, B., 2011. Applying dynamic surrogate models in noisy genetic algorithms to optimize groundwater remediation designs. Journal of Water Resources Planning and Management, 137(3), pp.284-292. https://doi.org/10.1061/(ASCE)WR.1943-5452.0000106.

Yeh, T. C. J., Liu, S., 2000. Hydraulic tomography: Development of a new aquifer test method. Water Resources Research, 36(8), pp.2095-2105. https://doi.org/10.1029/2000WR900114.

Yin, J., Pham, H. V., Tsai, F. T.-C., 2020. Multi-objective Spatial Pumping Optimization for Groundwater Management in a Multi-Aquifer System. Journal of Water Resources Planning and Management, 146(4). https://doi.org/10.1061/(ASCE)WR.1943-5452.0001180.

Yoshida, S., Steel, R. J., Dalrymple, R. W., 2007. Changes in depositional processes—an ingredient in a new generation of sequence-stratigraphic models. Journal of Sedimentary Research, 77(6), pp. 447-460. https://doi.org/10.2110/jsr.2007.048.

Younger, P.L., 1993. Simple generalized methods for estimating aquifer storage parameters. Quarterly Journal of Engineering Geology and Hydrogeology, 26(2), pp. 127-135.

https://doi.org/10.1144/GSL.QJEG.1993.026.02.04.

Zhang, H., Harter, T., Sivakumar, B., 2006. Nonpoint source solute transport normal to aquifer bedding in heterogeneous, Markov chain random fields. Water Resources Research, 42(6). https://doi.org/10.1029/2004WR003808.

Zhao, Z., Illman, W. A., 2021. On the importance of considering specific storage heterogeneity in hydraulic tomography: Laboratory sandbox and synthetic studies. Journal of Hydrology, 593, p.125874. https://doi.org/10.1016/j.jhydrol.2020.125874.

Zheng, C., Wang, P. P., 1999. MT3DMS, A Modular Three-Dimensional Multispecies Transport Model for Simulation of Advection, Dispersion and Chemical Reactions of Contaminants in Groundwater Systems. Waterways Experiment Station, U.S. Army Corps of Engineers, Vicksburg, Mississippi.

Zhou, Y., 2009. A critical review of groundwater budget myth, safe yield and sustainability. Journal of Hydrology, 370(1-4), pp. 207-213. https://doi.org/10.1016/j.jhydrol.2009.03.009.

Zhu, L., Zhang, C., Li, M., Pan, X., Sun, J., 2012. Building 3D solid models of sedimentary stratigraphic systems from borehole data: An automatic method and case studies. Engineering Geology, 127, pp. 1-13. https://doi.org/10.1016/j.enggeo.2011.12.001.

Zuurbier, K. G., Zaadnoordijk, W. J., Stuyfzand, P. J., 2014. How multiple partially penetrating wells improve the freshwater recovery of coastal aquifer storage and recovery (ASR) systems: A field and modeling study. Journal of Hydrology, 509, pp.430-441. https://doi.org/10.1016/j.jhydrol.2013.11.057.

Vita

Hamid Vahdat-Aboueshagh was born in Tehran, Iran. He graduated from the University of Tabriz with a Bachelor's degree in Civil Engineering. He moved back to Tehran where he received a Master's degree from the University of Tehran in Water Resources Engineering. He moved to the Louisiana State University to earn a Graduate degree in Water Resources Engineering. He is currently a candidate for the degree of Doctor of Philosophy in Civil Engineering.